

Charged lepton flavour violation from inverse seesaw with flavour and CP symmetries

F. P. Di Meglio and C. Hagedorn

Instituto de Física Corpuscular, Universidad de Valencia and CSIC, Edificio Institutos Investigación, Catedrático José Beltrán 2, 46980 Paterna, Spain

E-mail: francescopaolo.dimeglio@ific.uv.es, claudia.hagedorn@ific.uv.es

Abstract

We study charged lepton flavour violation in a scenario in which light neutrino masses are generated via the inverse seesaw mechanism with 3+3 gauge singlet fermions, N_i and S_j , $i, j = 1, 2, 3$. Lepton mixing is predicted with the help of the flavour symmetries $\Delta(3n^2)$ and $\Delta(6n^2)$ combined with CP. In the neutral lepton sector, the non-trivial flavour structure is only encoded in the Dirac neutrino Yukawa matrix (the coupling relating left-handed lepton doublets and gauge singlets N_i). Current experimental bounds on the processes $\mu \rightarrow e\gamma$, $\mu \rightarrow 3e$, $\mu - e$ conversion in nuclei and the tau lepton decays $\tau \rightarrow \ell\gamma$ and $\tau \rightarrow 3\ell$, $\ell = e, \mu$, do not constrain the considered parameter space of this scenario. Prospective limits on the decay $\mu \rightarrow 3e$ and $\mu - e$ conversion in aluminium instead can markedly reduce the available parameter space. We also comment on the effects of the heavy sterile states on light neutrino masses and lepton mixing.

1 Introduction

The Standard Model (SM) successfully describes many experimental results. However, important observations such as the smallness of neutrino masses and the peculiar flavour structure in the lepton and quark sectors remain unexplained.

Many extensions of the SM offer a generation mechanism for neutrino masses. Among these are the well-known type-I [1–5], type-II [6–11] and type-III seesaw mechanisms [12] which typically require new particles with masses much larger than the electroweak scale, if couplings are of order one. Alternatives such as the inverse seesaw (ISS) mechanism [13–16] can reconcile new particles with masses in the TeV-range with not too small couplings, while the smallness of neutrino masses is due to a small breaking of lepton number (in the form of a Majorana mass term for the gauge singlets).

The organising principle of the flavour sector responsible for the observed pattern of fermion masses and mixing is yet to be found. Nevertheless, discrete flavour symmetries, especially when combined with CP, that are broken in a certain way among e.g. charged leptons and neutral states are promising candidates for correctly describing the observed lepton mixing angles and making testable predictions for the leptonic CP phases [17–19] (for earlier works see [20–25]); reviews can be found, for example, in [26–30]. In this work, we employ the series of discrete groups $\Delta(3n^2)$ and $\Delta(6n^2)$, n integer, [31, 32] and CP symmetries, which correspond to automorphisms of these [17–19]. As is known [33], four different types of lepton mixing patterns are found, called Case 1), Case 2), Case 3 a) and Case 3 b.1), if the flavour symmetry G_f and CP are broken to a residual Z_3 symmetry among charged leptons and to $Z_2 \times CP$ among the neutral states. For further studies of lepton mixing from the groups $\Delta(3n^2)$ and $\Delta(6n^2)$ and CP, see e.g. [34–44].

In the current study, we analyse a scenario in which light neutrino masses are generated by the ISS mechanism with 3+3 gauge singlet fermions and the flavour symmetries $\Delta(3n^2)$ and $\Delta(6n^2)$ and CP are broken non-trivially.¹ Concretely, the non-trivial flavour structure among the neutral states is encoded in the Dirac neutrino Yukawa matrix, while the mass matrices (Dirac and Majorana) of the gauge singlet fermions do neither break G_f nor CP. This possibility has been called option 2 in [45]. We scrutinise analytically and numerically the Pontecorvo-Maki-Nakagawa-Sakata (PMNS) mixing matrix and different charged lepton flavour violating (cLFV) processes for Case 1) through Case 3 b.1). The main findings are that the effects of non-unitarity of the PMNS mixing matrix induced by the existence of the heavy sterile states have a more general form than those found in the scenario analysed in [45] (called option 1) and that signals of cLFV $\mu - e$ transitions can be sizeable in the studied parameter space, while those involving the tau lepton are more suppressed.

The remainder of the paper is organised as follows: in section 2 we outline the scenario, show the form of the different mass and coupling matrices, comment on the masses of the different neutral states, discuss the mixing matrices and the effects of the heavy sterile states on the light neutrinos. Section 3 contains information on lepton mixing including the characteristics of the mixing patterns of Case 1) through Case 3 b.1) and the effects of non-unitarity due to the mixing of the light neutrinos and the heavy sterile states. In section 4 we present analytic estimates as well as numerical results for the branching ratios (BRs) $BR(\mu \rightarrow e\gamma)$ and $BR(\mu \rightarrow 3e)$ and the $\mu - e$ conversion rate (CR) in aluminium, $CR(\mu - e, Al)$, for examples of all cases, Case 1) through Case 3 b.1). We comment on the expected size of the signals of the cLFV tau lepton decays $\tau \rightarrow \mu\gamma$, $\tau \rightarrow e\gamma$, $\tau \rightarrow 3\mu$ and $\tau \rightarrow 3e$ in section 5 and summarise in section 6. In appendix A basics of the group theory of $\Delta(3n^2)$ and $\Delta(6n^2)$ can be found, while we collect the form of different relevant matrices in appendix B. Appendix C comprises a concise description of the numerical scan and supplementary plots displaying results of the studied $\mu - e$ transitions for Case 3 b.1) are given in appendix D.

¹We do not specify the breaking mechanism here.

2 Scenario

In the following, we focus on the lepton sector. We add 3+3 gauge singlet fermions N_i and S_j , $i, j = 1, 2, 3$, to the SM in order to generate light neutrino masses via the ISS mechanism.

The flavour structure of the scenario is controlled by a flavour and a CP symmetry that are assumed to be broken to different non-trivial subgroups in the charged lepton, G_e , and in the neutral lepton sectors, G_ν , respectively. As flavour symmetry we choose one of the groups $\Delta(3n^2)$ and $\Delta(6n^2)$ with $n \geq 2$, see appendix A for relevant details of these groups. The CP symmetry corresponds to an automorphism of the flavour group and is selected according to the findings of [33].

Left-handed (LH) lepton doublets L_α , $\alpha = e, \mu, \tau$, are assigned to a triplet **3**. This representation is taken to be irreducible, faithful and complex. The gauge singlets N_i and S_j instead each transform as an irreducible, unfaithful, real triplet **3'**. The existence of such a representation requires that the flavour group has an even index n . On the contrary, right-handed (RH) charged leptons $\ell_{\alpha R}$ are singlets, all in **1**, under the flavour group. In order to distinguish these, we employ an additional Z_3 symmetry $Z_3^{(\text{aux})}$, i.e. $\ell_{eR} \sim 1$, $\ell_{\mu R} \sim \omega$ and $\ell_{\tau R} \sim \omega^2$ with $\omega = e^{\frac{2\pi i}{3}}$. LH lepton doublets and the gauge singlets are neutral under this additional group.

The group G_e determines the structure of the charged lepton mass matrix m_ℓ . We use a residual Z_3 symmetry that is a diagonal subgroup of the Z_3 symmetry, generated by the generator a of the flavour group (which is represented by a diagonal matrix in the chosen basis, compare appendix A), and the additional Z_3 symmetry $Z_3^{(\text{aux})}$. Consequently, m_ℓ is diagonal and contains three free parameters corresponding to the masses of the electron, muon and tau lepton. We take these to be ordered canonically such that the contribution U_ℓ to lepton mixing is $U_\ell = \mathbb{1}$.

The masses of the neutral states arise from the terms²

$$-(y_D)_{\alpha i} \bar{L}_\alpha^c H N_i^c - (M_{NS})_{ij} \bar{N}_i S_j - \frac{1}{2} (\mu_S)_{kl} \bar{S}_k^c S_l + \text{h.c.} \quad (1)$$

with H being the Higgs field, y_D the Dirac neutrino Yukawa matrix, M_{NS} the matrix connecting the gauge singlets N_i and S_j and μ_S the Majorana mass matrix of the singlets S_i . From eq. (1), we can define the Dirac neutrino mass matrix m_D as $m_D = y_D \langle H \rangle$ with $\langle H \rangle$ being the vacuum expectation value (VEV) of the Higgs, $\langle H \rangle \approx 174 \text{ GeV}$. The masses of all neutral states, light and heavy ones, come from the nine-by-nine mass matrix

$$\mathcal{M}_{\text{Maj}} = \begin{pmatrix} 0 & m_D & 0 \\ m_D^T & 0 & M_{NS} \\ 0 & M_{NS}^T & \mu_S \end{pmatrix}, \quad (2)$$

which is given in the basis $(\nu_{\alpha L}, N_i^c, S_j)$. This matrix can be diagonalised as

$$\mathcal{U}^T \mathcal{M}_{\text{Maj}} \mathcal{U} = \mathcal{M}_{\text{Maj}}^{\text{diag}} \quad (3)$$

with

$$\mathcal{U} = \begin{pmatrix} \tilde{U}_\nu & S \\ T & V \end{pmatrix} \text{ and } \mathcal{M}_{\text{Maj}}^{\text{diag}} = \text{diag}(m_1, m_2, m_3, m_4, \dots, m_9), \quad (4)$$

where \tilde{U}_ν is a three-by-three, S a three-by-six, T a six-by-three and V a six-by-six matrix. The masses $m_{1,2,3}$ are the light neutrino masses and m_4 to m_9 those of the heavy states. The matrix \mathcal{U} is unitary, while none of the matrices \tilde{U}_ν , S , T and V has this property. We assume in the following $|\mu_S| \ll |m_D| \ll |M_{NS}|$. As shown in [46], the light neutrino mass matrix at leading, m_ν , and at sub-leading order, m_ν^1 , in $(|m_D|/|M_{NS}|)^2$ read

$$m_\nu = m_D \left(M_{NS}^{-1} \right)^T \mu_S M_{NS}^{-1} m_D^T \quad (5)$$

²For simplicity, we do not take into account a possible coupling between LH lepton doublets and the gauge singlets S_j nor do we consider a Majorana mass term for the singlets N_i . Additional symmetries and/or an extension of the gauge group can motivate this choice.

and

$$\begin{aligned} m_\nu^1 &= -\frac{1}{2} m_D \left(M_{NS}^{-1} \right)^T \left(\mu_S M_{NS}^{-1} m_D^T m_D^* \left(M_{NS}^{-1} \right)^\dagger + \left(M_{NS}^{-1} \right)^* m_D^\dagger m_D \left(M_{NS}^{-1} \right)^T \mu_S \right) M_{NS}^{-1} m_D^T \\ &= -(m_\nu \eta + \eta^* m_\nu) , \end{aligned} \quad (6)$$

using the matrix η defined in eq. (10). The matrix m_ν is (approximately) diagonalised by \tilde{U}_ν ,

$$\tilde{U}_\nu^T m_\nu \tilde{U}_\nu \approx \text{diag}(m_1, m_2, m_3) . \quad (7)$$

We can define the (non-unitary) lepton mixing matrix

$$\tilde{U}_{\text{PMNS}} = U_\ell^\dagger \tilde{U}_\nu = \tilde{U}_\nu , \quad (8)$$

where the second equality takes into account that $U_\ell = \mathbb{1}$ in the chosen basis. This non-unitarity is due to the mixing of the light neutrinos with the heavy states and it can be encoded in the hermitean matrix η ,

$$\tilde{U}_{\text{PMNS}} = (\mathbb{1} - \eta) U_0 \quad (9)$$

with U_0 being unitary. Note that in the chosen basis eq. (9) also holds for \tilde{U}_ν . The form of the matrix η is at leading order given by

$$\eta = \frac{1}{2} m_D^* \left(M_{NS}^{-1} \right)^\dagger M_{NS}^{-1} m_D^T . \quad (10)$$

As N_i and S_j transform both as the real representation $\mathbf{3}'$, the matrices M_{NS} and μ_S are non-vanishing in the limit of unbroken flavour and CP symmetries. In particular, using the basis given in appendix A, the form of the matrices is

$$M_{NS} = M_0 \begin{pmatrix} 1 & 0 & 0 \\ 0 & 1 & 0 \\ 0 & 0 & 1 \end{pmatrix} \quad \text{and} \quad \mu_S = \mu_0 \begin{pmatrix} 1 & 0 & 0 \\ 0 & 0 & 1 \\ 0 & 1 & 0 \end{pmatrix} \quad (11)$$

with M_0 and μ_0 being positive and having dimension of mass. The non-trivial flavour information is encoded in the Dirac neutrino Yukawa matrix y_D whose form is determined by the following equations

$$Z(\mathbf{3})^T y_D Z(\mathbf{3}')^* = y_D \quad \text{and} \quad X(\mathbf{3}) y_D X(\mathbf{3}')^* = y_D^* , \quad (12)$$

where the matrices $Z(\mathbf{3})$ and $Z(\mathbf{3}')$ are the representation matrices of the generator of the preserved Z_2 group, belonging to the residual symmetry G_ν , in the representations $\mathbf{3}$ (for the LH lepton doublets) and $\mathbf{3}'$ (for the gauge singlets N_i), respectively. The matrices $X(\mathbf{3})$ and $X(\mathbf{3}')$ represent the CP transformation in these representations that also belongs to the group G_ν . The explicit form of these matrices can be found in [47]. As a result, the matrix y_D depends on five real parameters in total: three Yukawa couplings, y_1 , y_2 and y_3 , and two angles, called θ_L and θ_R . Its form is

$$y_D = \Omega(\mathbf{3})^* R_{ij}(\theta_L) \text{diag}(y_1, y_2, y_3) P_{kl}^{ij} R_{kl}(-\theta_R) \Omega(\mathbf{3}')^T . \quad (13)$$

The different matrices are fixed as follows: the unitary matrices $\Omega(\mathbf{3})$ and $\Omega(\mathbf{3}')$ are determined by the form of the matrices $X(\mathbf{3})$ and $X(\mathbf{3}')$, respectively,

$$\Omega(\mathbf{3}) \Omega(\mathbf{3})^T = X(\mathbf{3}) \quad \text{and} \quad \Omega(\mathbf{3}') \Omega(\mathbf{3}')^T = X(\mathbf{3}') , \quad (14)$$

the planes of the rotation matrices $R_{ij}(\theta_L)$ and $R_{kl}(\theta_R)$ are given by the plane of the two degenerate eigenvalues of the matrices $Z(\mathbf{3})$ and $Z(\mathbf{3}')$ in the basis transformed by $\Omega(\mathbf{3})$ and $\Omega(\mathbf{3}')$, respectively. If these two planes do not coincide, the permutation matrix P_{kl}^{ij} is necessary. The form of these matrices depends on the mixing pattern which we consider, i.e. Case 1) through Case 3 b.1). It can be found in [47] and is repeated for convenience in appendix B. This scenario has been first mentioned in the context of the ISS mechanism in [45] and called option 2. However, neither the

results for fermion masses and mixing nor for the signal strength of different cLFV processes have been discussed there. This analysis is performed in the current study.

With the given information, we can compute both the masses of the neutral states as well as their mixing. We begin with the mass matrix of the heavy states and their mass spectrum, since this structure is very simple. It can be derived (to very good approximation) from the matrix

$$\begin{pmatrix} \emptyset & M_{NS} \\ M_{NS}^T & \mu_S \end{pmatrix} \quad (15)$$

which is (approximately) diagonalised by the six-by-six matrix V , i.e.

$$V^T \begin{pmatrix} \emptyset & M_{NS} \\ M_{NS}^T & \mu_S \end{pmatrix} V \approx \text{diag}(m_4, \dots, m_9) . \quad (16)$$

For M_{NS} and μ_S as in eq. (11), one finds for the masses of the heavy states that these are all degenerate to very high degree and form three pairs of pseudo-Dirac neutrinos, splitted by μ_0 ,

$$m_4 \approx m_5 \approx m_6 \approx M_0 - \frac{\mu_0}{2} \quad \text{and} \quad m_7 \approx m_8 \approx m_9 \approx M_0 + \frac{\mu_0}{2} , \quad (17)$$

as well as the approximate form of V

$$V = \frac{1}{\sqrt{2}} \begin{pmatrix} i U_S^* & U_S^* \\ -i U_S & U_S \end{pmatrix} \quad (18)$$

with U_S being chosen as

$$U_S = \frac{1}{\sqrt{2}} \begin{pmatrix} \sqrt{2} & 0 & 0 \\ 0 & 1 & i \\ 0 & 1 & -i \end{pmatrix} \quad (19)$$

such that

$$U_S^T \mu_S U_S = \mu_0 \begin{pmatrix} 1 & 0 & 0 \\ 0 & 1 & 0 \\ 0 & 0 & 1 \end{pmatrix} , \quad (20)$$

compare [45, 47]. The approximate form of the matrix S is related to the form of V , i.e.

$$S = \left(\emptyset , \quad m_D^* \left(M_{NS}^{-1} \right)^\dagger \right) V = \frac{\langle H \rangle}{\sqrt{2} M_0} \left(-i y_D^* U_S , \quad y_D^* U_S \right) , \quad (21)$$

see also [45, 46].

Using the general formulae, found in [45, 46], we see that the light neutrino mass matrix m_ν at leading order is of the form

$$\begin{aligned} m_\nu &= \left(\frac{\mu_0 \langle H \rangle^2}{M_0^2} \right) U_0(\theta_L)^* \text{diag}(y_1, y_2, y_3) \\ &\quad \times \left[P_{kl}^{ij} R_{kl}(-\theta_R) \Omega(\mathbf{3}')^T \begin{pmatrix} 1 & 0 & 0 \\ 0 & 0 & 1 \\ 0 & 1 & 0 \end{pmatrix} \Omega(\mathbf{3}') R_{kl}(\theta_R) (P_{kl}^{ij})^T \right] \\ &\quad \times \text{diag}(y_1, y_2, y_3) U_0(\theta_L)^\dagger \end{aligned} \quad (22)$$

with the definition of the unitary matrix $U_0(\theta)$

$$U_0(\theta) = \Omega(\mathbf{3}) R_{ij}(\theta) \quad (23)$$

and the form of the hermitean matrix η given by

$$\eta = \eta'_0 U_0(\theta_L) \text{diag}(y_1^2, y_2^2, y_3^2) U_0(\theta_L)^\dagger \quad \text{with} \quad \eta'_0 = \frac{\langle H \rangle^2}{2 M_0^2} . \quad (24)$$

The quantity η'_0 is similar to the quantity η_0 defined in [45].

In order to continue we have to have knowledge about the form of the matrix combination in square brackets in eq. (22). Indeed, it is known [47] that this expression³ is either diagonal or has a block-diagonal form that can be diagonalised by a rotation in the (ij) -plane, i.e. the same plane in which the rotation $R_{ij}(\theta_L)$ acts. In the following, we first discuss the situation in which this expression is diagonal and then turn to the instance in which an additional rotation is necessary.

If the expression is diagonal, we find that the matrix diagonalising m_ν at leading order is of the form

$$\tilde{U}_\nu \approx U_0(\theta_L) K_\nu = \Omega(\mathbf{3}) R_{ij}(\theta_L) K_\nu , \quad (25)$$

where the role of K_ν is to ensure that the light neutrino masses are positive semi-definite.⁴ Interestingly, then the leading order values of the light neutrino masses m_f are simply given by

$$m_f = \left(\frac{\mu_0 \langle H \rangle^2}{M_0^2} \right) y_f^2 \quad \text{with} \quad f = 1, 2, 3 \quad (26)$$

for Case 1) through Case 3 a), whereas for Case 3 b.1) we have to take into account an additional permutation P among the light neutrino masses in order to produce the corresponding mixing pattern, i.e.

$$m_1 = \left(\frac{\mu_0 \langle H \rangle^2}{M_0^2} \right) y_3^2 , \quad m_2 = \left(\frac{\mu_0 \langle H \rangle^2}{M_0^2} \right) y_1^2 , \quad m_3 = \left(\frac{\mu_0 \langle H \rangle^2}{M_0^2} \right) y_2^2 \quad (27)$$

and thus

$$\tilde{U}_\nu \approx U_0(\theta_L) P K_\nu = \Omega(\mathbf{3}) R_{ij}(\theta_L) P K_\nu \quad \text{with} \quad P = \begin{pmatrix} 0 & 1 & 0 \\ 0 & 0 & 1 \\ 1 & 0 & 0 \end{pmatrix} , \quad (28)$$

see e.g. [47]. Furthermore, we can express η in terms of \tilde{U}_ν and the light neutrino masses m_f

$$\eta \approx \frac{1}{2\mu_0} \tilde{U}_\nu \text{diag}(m_1, m_2, m_3) \tilde{U}_\nu^\dagger . \quad (29)$$

This has two immediate consequences: firstly, the matrix m_ν^1 is diagonalised by the same matrix as the leading order term m_ν , since we can write the expression in the second line of eq. (6) as

$$m_\nu^1 \approx -\frac{1}{\mu_0} \tilde{U}_\nu^* \text{diag}(m_1^2, m_2^2, m_3^2) \tilde{U}_\nu^\dagger . \quad (30)$$

Consequently, lepton mixing is not influenced by this sub-leading term, while the light neutrino masses are (slightly) corrected. Secondly, we can estimate the effect of non-unitarity of the lepton mixing matrix using eq. (9)

$$\tilde{U}_\nu = U_0(\theta_L) (\mathbb{1} - \eta'_0 \text{diag}(y_1^2, y_2^2, y_3^2)) \quad \text{and} \quad \tilde{U}_\nu = U_0(\theta_L) P (\mathbb{1} - \eta'_0 \text{diag}(y_3^2, y_1^2, y_2^2)) \quad (31)$$

for Case 1) through Case 3 a) and Case 3 b.1), respectively. This can also be written in terms of the light neutrino masses m_f as

$$\tilde{U}_\nu = \tilde{U}_\nu^0 \left(\mathbb{1} - \frac{1}{2\mu_0} \text{diag}(m_1, m_2, m_3) \right) , \quad (32)$$

where \tilde{U}_ν^0 indicates the unitary matrix in eq. (25) and (28) for Case 1) through Case 3 a) and Case 3 b.1), respectively. A suppression of the columns of the PMNS mixing matrix is induced that is in general different for the different columns, since it depends on the Yukawa couplings y_f /the light neutrino masses m_f . In particular, in case of strong normal ordering (NO) or strong inverted

³In [47], the complex conjugate of this matrix combination is found.

⁴We set K_ν to the identity matrix in analytic results, but take it properly into account in the numerical study.

ordering (IO), i.e. the lightest neutrino mass m_0 vanishes, one of the columns remains unaffected. This is slightly more general than the effect observed in [45], where a common suppression factor for all entries of the mixing matrix is encountered. We discuss the effect of the suppression in eq. (31) in more detail in section 3.

In case the expression in square brackets in eq. (22) is not diagonal, we have to take into account an additional rotation through an angle determined by the Yukawa couplings y_f and the angle θ_R occurring in the (ij) -plane such that the angle θ_L becomes replaced by an effective angle $\bar{\theta}_L$,⁵ i.e. (disregarding the matrix K_ν)

$$\tilde{U}_\nu \approx U_0(\bar{\theta}_L) = \Omega(\mathbf{3}) R_{ij}(\bar{\theta}_L) . \quad (33)$$

Only one of the three light neutrino masses, m_k with $k \neq i$ and $k \neq j$, depends on a single Yukawa coupling, as shown in eq. (26), while the others are determined by the remaining Yukawa couplings and the angle θ_R , e.g. for Case 1) (and independent of the choice of the parameter s , see section 3) we have

$$m_2 = \left(\frac{\mu_0 \langle H \rangle^2}{M_0^2} \right) y_2^2 , \quad m_{1,3} = \left(\frac{\mu_0 \langle H \rangle^2}{2 M_0^2} \right) \left| (y_1^2 - y_3^2) \cos 2 \theta_R \pm \sqrt{4 y_1^2 y_3^2 + (y_1^2 - y_3^2)^2 \cos^2 2 \theta_R} \right| , \quad (34)$$

which in the case of strong NO ($m_1 = 0$) is reduced to

$$m_1 = 0 , \quad m_2 = \left(\frac{\mu_0 \langle H \rangle^2}{M_0^2} \right) y_2^2 , \quad m_3 = \left(\frac{\mu_0 \langle H \rangle^2}{M_0^2} \right) y_3^2 |\cos 2 \theta_R| , \quad (35)$$

and for strong IO ($m_3 = 0$) to

$$m_1 = \left(\frac{\mu_0 \langle H \rangle^2}{M_0^2} \right) y_1^2 |\cos 2 \theta_R| , \quad m_2 = \left(\frac{\mu_0 \langle H \rangle^2}{M_0^2} \right) y_2^2 , \quad m_3 = 0 . \quad (36)$$

The form of the matrix η in eq. (24) does not change, but we can no longer identify $U_0(\theta_L)$ with \tilde{U}_ν . Instead we have

$$\eta \approx \eta'_0 \tilde{U}_\nu R_{ij}(\Delta\theta) \text{diag}(y_1^2, y_2^2, y_3^2) R_{ij}(-\Delta\theta) \tilde{U}_\nu^\dagger , \quad (37)$$

using the definition of $U_0(\theta)$ in eq. (23) and setting $\Delta\theta = \theta_L - \bar{\theta}_L$. Regarding the form of the sub-leading term m_ν^1 we note that it can be written as

$$\begin{aligned} m_\nu^1 &\approx -\eta'_0 \tilde{U}_\nu^\star [\text{diag}(m_1, m_2, m_3) R_{ij}(\Delta\theta) \text{diag}(y_1^2, y_2^2, y_3^2) R_{ij}(-\Delta\theta) \\ &\quad + R_{ij}(\Delta\theta) \text{diag}(y_1^2, y_2^2, y_3^2) R_{ij}(-\Delta\theta) \text{diag}(m_1, m_2, m_3)] \tilde{U}_\nu^\dagger . \end{aligned} \quad (38)$$

Hence, this sub-leading term is not diagonalised by \tilde{U}_ν (the matrix that diagonalises the leading term m_ν), but induces a (small) additional rotation in the (ij) -plane. Also, the light neutrino masses get slightly shifted. For the effects of non-unitarity of lepton mixing, we have in this case

$$\tilde{U}_\nu = U_0(\bar{\theta}_L) (\mathbb{1} - \eta'_0 R_{ij}(\Delta\theta) \text{diag}(y_1^2, y_2^2, y_3^2) R_{ij}(-\Delta\theta)) . \quad (39)$$

Thus, only one column receives a common suppression determined by one of the light neutrino masses, while the effects on the other two are more involved, see discussion in section 3. We note that the formulae given here are valid for Case 1) through Case 3 a), while for Case 3 b.1) the permutation P has to be taken into account which slightly complicates the expressions.

3 Lepton mixing

In this section, we comment on the results for the lepton mixing parameters derived from the different cases, Case 1) through Case 3 b.1), and how these are affected by the presence of the heavy sterile

⁵The effective angle $\bar{\theta}_L$ is denoted by $\tilde{\theta}_L$ in [47].

states. There are two effects, already mentioned in section 2: the sub-leading contribution m_ν^1 can lead to deviations from the results, determined by the flavour and CP symmetries, and the non-unitarity of the lepton mixing matrix, induced through the heavy sterile states.

Whether the sub-leading contribution m_ν^1 gives rise to deviations from the lepton mixing obtained at leading order or not depends on whether the expression in square brackets in eq. (22) is diagonal or not. If it is diagonal, then the lepton mixing parameters remain unaltered. Otherwise, the form of m_ν^1 leads to an additional rotation, compare eq. (38), whose effect is suppressed by η'_0 . The typical size of η'_0 is expected to be of the order of the experimental bounds on the entries of the matrix η , $|\eta_{\alpha\beta}| < 1.0 \times 10^{-5} \div 1.4 \times 10^{-3}$ depending on the flavours α and β [48]. This effect is, thus, in general small.

In order to analyse the non-unitarity of the lepton mixing matrix, we extract the lepton mixing angles and CP invariants J_{CP} , I_1 and I_2 from a three-by-three mixing matrix U with elements $U_{\alpha i}$, $\alpha = e, \mu, \tau$ and $i = 1, 2, 3$, as follows

$$\begin{aligned} \sin^2 \theta_{13} &= |U_{e3}|^2, \quad \sin^2 \theta_{12} = \frac{|U_{e2}|^2}{1 - |U_{e3}|^2}, \quad \sin^2 \theta_{23} = \frac{|U_{\mu 3}|^2}{1 - |U_{e3}|^2}, \\ J_{\text{CP}} &= \text{Im} (U_{e1} U_{e3}^* U_{\tau 1}^* U_{\tau 3}) = \frac{1}{8} \sin(2\theta_{12}) \sin(2\theta_{23}) \sin(2\theta_{13}) \cos\theta_{13} \sin\delta, \\ I_1 &= \text{Im} (U_{e2}^2 (U_{e1}^*)^2) = \frac{1}{4} \sin^2(2\theta_{12}) \cos^4 \theta_{13} \sin\alpha, \\ I_2 &= \text{Im} (U_{e3}^2 (U_{e1}^*)^2) = \frac{1}{4} \sin^2(2\theta_{13}) \cos^2 \theta_{12} \sin\beta. \end{aligned} \quad (40)$$

The size of these effects crucially depends on the parameter η'_0 , the Yukawa couplings y_f and potentially also the angle θ_R (i.e. the difference between the angles θ_L and $\bar{\theta}_L$).

Before commenting on the results for the different cases, we discuss the generic effects using as form of the lepton mixing matrix either the one in eq. (31) or (39), depending on whether the matrix in square brackets in eq. (22) is diagonal or not. We define the deviations of the lepton mixing angles and CP invariants in the ISS framework as

$$\Delta \sin^2 \theta_{ij} = \frac{(\sin^2 \theta_{ij})_{\text{ISS}} - (\sin^2 \theta_{ij})_{\text{FCS}}}{(\sin^2 \theta_{ij})_{\text{FCS}}}, \quad \Delta J_{\text{CP}} = \frac{(J_{\text{CP}})_{\text{ISS}} - (J_{\text{CP}})_{\text{FCS}}}{(J_{\text{CP}})_{\text{FCS}}}, \quad \Delta I_i = \frac{(I_i)_{\text{ISS}} - (I_i)_{\text{FCS}}}{(I_i)_{\text{FCS}}}, \quad (41)$$

as long as the result obtained from the flavour and CP symmetries (FCS) is non-vanishing; this definition is identical to the one used in [45].

As already mentioned in section 2, from eq. (31) follows that the elements of one column are suppressed by the same factor. We always observe a suppression, since $\eta'_0 y_f^2$ is positive semi-definite. Using eq. (40) and the result for Case 1) through Case 3 a) in eq. (31), the explicit dependence on η'_0 and y_f of these deviations is

$$\begin{aligned} \Delta \sin^2 \theta_{13} &\approx -2\eta'_0 y_3^2, \quad \Delta \sin^2 \theta_{12} \approx -2\eta'_0 y_2^2, \quad \Delta \sin^2 \theta_{23} \approx -2\eta'_0 y_3^2, \\ \Delta J_{\text{CP}} &\approx -2\eta'_0 (y_1^2 + y_3^2), \quad \Delta I_1 \approx -2\eta'_0 (y_1^2 + y_2^2), \quad \Delta I_2 \approx -2\eta'_0 (y_1^2 + y_3^2). \end{aligned} \quad (42)$$

In these approximations, we only take into account the leading order in η'_0 and neglect terms of order $|U_{e3}|^2$ or smaller. Since $\eta'_0 y_f^2 \geq 0$, all deviations are negative or zero. Given that experimental data are compatible with at most one vanishing light neutrino mass, only one of the couplings y_f can be zero. We comment on the consequences below. Obviously, in the (unrealistic) limit in which y_f are equal, we end up with the same expressions as in [45].

If the matrix in square brackets in eq. (22) is not diagonal, we encounter as form of the non-unitarity lepton mixing matrix the one mentioned in eq. (39), at least for Case 1) through Case 3 a). Then, the deviations of the lepton mixing angles and the CP invariants in the ISS framework also depend on the difference, $\Delta\theta$, between the angles θ_L and $\bar{\theta}_L$, where the latter depends on the Yukawa couplings y_f and the free angle θ_R . For example for $(ij) = (13)$, i.e. the additional rotation diagonalising the matrix in square brackets in eq. (22) acts in the (13)-plane, we find at linear order

in η'_0 and $|U_{e3}|$

$$\begin{aligned}\Delta \sin^2 \theta_{13} &\approx \eta'_0 \left(\frac{\operatorname{Re}(U_{e1}^* U_{e3})}{|U_{e3}|^2} (y_1^2 - y_3^2) \sin 2 \Delta\theta - 2 (y_1^2 \sin^2 \Delta\theta + y_3^2 \cos^2 \Delta\theta) \right), \\ \Delta \sin^2 \theta_{12} &\approx \eta'_0 (-2 y_2^2 + \operatorname{Re}(U_{e1}^* U_{e3}) (y_1^2 - y_3^2) \sin 2 \Delta\theta), \\ \Delta \sin^2 \theta_{23} &\approx \eta'_0 \left(-2 (y_1^2 \sin^2 \Delta\theta + y_3^2 \cos^2 \Delta\theta) + \operatorname{Re} \left(U_{e1}^* U_{e3} + \frac{U_{\mu 1}^* U_{\mu 3}}{|U_{\mu 3}|^2} \right) (y_1^2 - y_3^2) \sin 2 \Delta\theta \right)\end{aligned}\quad (43)$$

as well as

$$\begin{aligned}\Delta J_{\text{CP}} &\approx -2 \eta'_0 (y_1^2 + y_3^2) \\ &+ \eta'_0 (y_1^2 - y_3^2) \frac{((|U_{e1}|^2 + |U_{e3}|^2) \operatorname{Im}(U_{\tau 1}^* U_{\tau 3}) + (|U_{\tau 1}|^2 + |U_{\tau 3}|^2) \operatorname{Im}(U_{e1} U_{e3}^*))}{2 \operatorname{Im}(U_{e1} U_{e3}^* U_{\tau 1}^* U_{\tau 3})} \sin 2 \Delta\theta, \\ \Delta I_1 &\approx -2 \eta'_0 (y_1^2 \cos^2 \Delta\theta + y_2^2 + y_3^2 \sin^2 \Delta\theta) + \eta'_0 (y_1^2 - y_3^2) \frac{\operatorname{Im}(U_{e2}^2 U_{e1}^* U_{e3}^*)}{\operatorname{Im}(U_{e2}^2 (U_{e1}^*)^2)} \sin 2 \Delta\theta, \\ \Delta I_2 &\approx -2 \eta'_0 (y_1^2 + y_3^2) + \eta'_0 (y_1^2 - y_3^2) \frac{(|U_{e1}|^2 + |U_{e3}|^2)}{2 \operatorname{Re}(U_{e1}^* U_{e3})} \sin 2 \Delta\theta,\end{aligned}\quad (44)$$

where we refer with $U_{\alpha i}$ to the elements of the unitary matrix, i.e. the one obtained from flavour and CP symmetries. Clearly, in the limit in which θ_L and $\bar{\theta}_L$ coincide, $\Delta\theta = 0$, we recover the formulae found in eq. (42). Given the more general form of the deviation it is possible that the non-unitary lepton mixing matrix leads to non-trivial CP violation, although flavour and CP symmetries predict certain CP phases to be trivial.

Case 1) As has been shown in [33], the choice of residual symmetries is described by one integer, called s , varying between 0 and $n - 1$, which corresponds to the employed CP symmetry. Two of the three CP phases, β and δ , are trivial in this case, i.e. $I_2 = 0$ and $J_{\text{CP}} = 0$, while the third one, the Majorana phase α , is determined by the choice of the CP symmetry, $|\sin \alpha| = |\sin 6\phi_s|$ with $\phi_s = \frac{\pi s}{n}$.⁶ In contrast to this, the three lepton mixing angles are independent of this choice and only depend on the free angle θ_L (or in case the matrix combination in square brackets in eq. (22) is not diagonal this angle is given by $\bar{\theta}_L$). This angle is adjusted such that the reactor mixing angle is very close to its experimental best-fit value [49] and, consequently, the solar and atmospheric mixing angle are given by $\sin^2 \theta_{12} \approx 0.341$ and $\sin^2 \theta_{23} \approx 0.604(5)$ for light neutrino masses with NO (IO).

As has been analysed in [47], only for $y_1 = 0$ or $y_3 = 0$ or θ_R chosen such that $\sin 2 \theta_R = 0$, the matrix combination in square brackets in eq. (22) is diagonal. Then, we can apply the results found in eq. (42). In particular, we see that in the case of light neutrino masses with strong NO ($y_1 = 0$) the deviations of the CP invariants also only depend on one coupling y_f , while for strong IO ($y_3 = 0$) the deviations of both the reactor and the atmospheric mixing angle are suppressed. Otherwise, we can use the formulae in eqs. (43) and (44), since the rotation always occurs in the (13)-plane in this case. Although one may presume that one can achieve non-trivial CP phases δ and β then, this does not happen, as can be checked by explicit computation.

Case 2) From [33] it is known that the CP symmetry is fixed by two integer parameters, s and t , ranging from 0 to $n - 1$. Alternatively, one can define the combinations u and v as

$$u = 2s - t \quad \text{and} \quad v = 3t. \quad (45)$$

The smallness of the reactor mixing angle can be achieved for $\frac{u}{n}$ ($\phi_u = \frac{\pi u}{n}$) being small, $-0.1 \lesssim \frac{u}{n} \lesssim 0.12$ ($-0.31 \lesssim \phi_u \lesssim 0.37$), and the free angle, appearing in the lepton mixing matrix, close to zero or π , see [33, 47]. The solar mixing angle is, similar to Case 1), constrained to fulfil $\sin^2 \theta_{12} \gtrsim \frac{1}{3}$,

⁶The sign in the relation for the Majorana phase α depends on the explicit form of the matrix K_ν .

while the atmospheric mixing angle can lie in its experimentally preferred 3σ range [49]. Valid choices of u and n can be found in section 4.4, where the numerical results are presented, as well as in e.g. [33, 45, 47]. While the Dirac phase δ and the Majorana phase β depend like the lepton mixing angles on the parameter u and the free angle, the Majorana phase α is (mainly) determined by the parameter v and to very good approximation it holds $|\sin \alpha| \approx |\sin \phi_v|$ with $\phi_v = \frac{\pi v}{n}$.⁷

In [47] it has been found that for t even the matrix combination in square brackets in eq. (22) is always diagonal, while for t odd this only occurs for $y_1 = 0$ or $y_3 = 0$ or θ_R chosen such that $\cos 2\theta_R = 0$. We, thus, can apply in these situations the results given in eq. (42). Like for Case 1), we can consider light neutrino masses with strong NO ($y_1 = 0$) or strong IO ($y_3 = 0$) and arrive at the same conclusions. Note that setting y_2 to zero does not lead to a viable light neutrino mass spectrum, since y_2 is always associated with the light neutrino mass m_2 , compare eq. (26). For t odd in general, a rotation in the (13)-plane is necessary in order to diagonalise the matrix combination in square brackets in eq. (22). Consequently, we can apply the formulae in eqs. (43) and (44). As has been shown in [33], for the free angle being zero, one can accommodate the lepton mixing angles well for $\frac{u}{n} \approx 0.12$, while both J_{CP} and I_2 vanish. Taking into account the effects of non-unitarity, we see that for $\sin 2\Delta\theta \neq 0$ J_{CP} as well as I_2 can be non-zero. On the other hand, for $u = 0$ the CP invariant I_2 is zero and the inclusion of the effects of non-unitarity does not change this result.

Case 3 a) In this case the residual Z_2 symmetry is characterised by the parameter m which can take values between 0 and $n - 1$, while the CP symmetry is fixed by one integer parameter s , also varying between 0 and $n - 1$. For Case 3 a) the ratio $\frac{m}{n}$ has to be either close to zero or to one (or equivalently ϕ_m , $\phi_m = \frac{\pi m}{n}$, small or close to π) in order to accommodate well the reactor mixing angle. For this reason, n should be at least 16 and, consequently, $m = 1$ or $m = 15$.⁸ At the same time, fixing this ratio determines the value of the atmospheric mixing angle. The free angle, contained in the lepton mixing matrix, can take, depending on the choice of s ($\phi_s = \frac{\pi s}{n}$), up to two distinct values that allow for a good fit of the solar mixing angle. Further details can be found in [33, 45, 47] as well as in section 4.5. The three CP phases are in general non-trivial; numerical values and analytic estimates are given in the cited works.

Using the results of [47] we know that for the parameters m and s both even or both odd the matrix combination in square brackets in eq. (22) is diagonal and the formulae in eq. (42) can be used. In contrast, for m even and s odd or vice versa this matrix combination is only diagonal for $y_1 = 0$ or $\sin 2\theta_R = 0$. For $y_1 = 0$ we encounter the same situation as for Case 1) and Case 2), since light neutrino masses then follow strong NO and all deviations only depend on one Yukawa coupling y_f . If both parameters m and s are even or both are odd, setting $y_3 = 0$ permits us to suppress the deviations of the reactor and the atmospheric mixing angle, compare eq. (42). In case the matrix combination in square brackets in eq. (22) is not diagonal, it is diagonalised by a rotation in the (12)-plane. For this situation similar formulae as those in eqs. (43) and (44) can be derived.

Case 3 b.1) Like for Case 3 a), the integer parameters m and s with $0 \leq m, s \leq n - 1$ describe the residual Z_2 symmetry and the CP symmetry, respectively. From [33], we know that the requirement to accommodate the solar mixing angle well constrains the parameter m to be close to $\frac{n}{2}$. The free angle, appearing in the lepton mixing matrix, has to be close to $\frac{\pi}{2}$ such that the reactor mixing angle can be fitted well. For $\frac{m}{n} = \frac{1}{2}$, usually two such values exist. Otherwise, it depends on the choice of m and s how many distinct values of the free angle admit a good fit to the experimental data of the lepton mixing angles. The atmospheric mixing angle also depends on the parameter s . Likewise, all CP phases are determined by the actual values of the ratios $\frac{m}{n}$ and $\frac{s}{n}$ as well as the free angle. More information, in particular about analytical estimates and numerical values of the CP phases, is given in [33, 45, 47]. Explicit choices of m and s are discussed in section 4.6.

⁷As for Case 1), the sign in this relation depends on K_ν .

⁸Since the index n has to be even in the current scenario, $n = 17$ and $m = 1$ (or $m = 16$) is not eligible, but very similar results can be obtained for $n = 34$ and $m = 2$ (or $m = 32$), see [47]. This choice also permits to study even values of m .

Whether or not the matrix combination in square brackets in eq. (22) is diagonal is subject to very similar constraints as for Case 3 a). The only difference is due to the fact that the light neutrino masses are assigned differently in Case 3 b.1) than Case 3 a), compare eqs. (27) and (26), i.e. in order to have a diagonal matrix combination for m even and s odd or vice versa we have to set $y_2 = 0$ which corresponds to light neutrino masses with strong IO. For Case 3 b.1) the relevant rotation effectively appears in the (23)-plane and expressions equivalent to those in eqs. (43) and (44) can be obtained.

4 $\mu - e$ transitions

In the discussion of cLFV processes, we focus on different $\mu - e$ transitions, since they are subject to the strongest experimental bounds. As we show in the following, current experimental limits do not constrain the considered parameter space of this scenario, while prospective bounds, in particular on $\mu - e$ conversion in aluminium, turn out to be very constraining in general.

4.1 Prerequisites

We first list the experimental inputs and constraints we apply. Furthermore, we outline the parameter space of the scenario that we scan for viable choices of the group theory parameters (depending on the case) in terms of the free angle θ_R and the two mass scales μ_0 and M_0 . The angle θ_L is determined by the requirement to accommodate the measured lepton mixing angles well and the couplings y_f are fixed by the light neutrino mass spectrum, i.e. the value of the lightest neutrino mass m_0 and the mass ordering, either NO or IO.

4.1.1 Experimental inputs and constraints

The lepton mixing angles are constrained by the global fits found in [49] (version 5.3).⁹ Since the experimental preference for a certain value of the Dirac phase δ is still rather weak, we do not include this information here, when fitting the angle θ_L in order to accommodate well the lepton mixing parameters.

Taking into account the experimental information on neutrino masses, in particular the results for the mass squared differences from neutrino oscillations [49] and the bound on the sum of the light neutrino masses, derived from cosmology [50], we use the following benchmark values for the lightest neutrino mass m_0 : either $m_0 = 0$ (strong NO or strong IO) or

$$m_0 = 0.03 \text{ eV for NO and } m_0 = 0.015 \text{ eV for IO.} \quad (46)$$

The mass squared differences Δm_{sol}^2 and Δm_{atm}^2 are defined as

$$\Delta m_{\text{sol}}^2 = m_2^2 - m_1^2 \text{ and } \Delta m_{\text{atm}}^2 = \begin{cases} m_3^2 - m_1^2 & (\text{NO}) \\ m_3^2 - m_2^2 & (\text{IO}) \end{cases}. \quad (47)$$

These are always fixed to their experimental best-fit values [49]. The light neutrino masses for NO are given by

$$m_1 = m_0, \quad m_2 = \sqrt{m_1^2 + \Delta m_{\text{sol}}^2}, \quad m_3 = \sqrt{m_1^2 + \Delta m_{\text{atm}}^2}, \quad (48)$$

and for IO they read

$$m_1 = \sqrt{m_0^2 + |\Delta m_{\text{atm}}^2| - \Delta m_{\text{sol}}^2}, \quad m_2 = \sqrt{m_0^2 + |\Delta m_{\text{atm}}^2|}, \quad m_3 = m_0. \quad (49)$$

As experimental bounds on the parameters $\eta_{\alpha\beta}$, $\alpha, \beta = e, \mu, \tau$, we use [48]

$$|\eta_{\alpha\beta}| < \begin{pmatrix} 1.3(1.4) \times 10^{-3} & 1.2 \times 10^{-5} & 9.0(8.0) \times 10^{-4} \\ 1.2 \times 10^{-5} & 1.1(1.0) \times 10^{-5} & 5.7(1.8) \times 10^{-5} \\ 9.0(8.0) \times 10^{-4} & 5.7(1.8) \times 10^{-5} & 1.0(0.81) \times 10^{-3} \end{pmatrix} \text{ at 95\% C.L.} \quad (50)$$

⁹In the numerical analysis we use version 5.2, but check that the fitted lepton mixing angles are also compatible with the results given in version 5.3.

for light neutrino masses with NO (IO). Additionally, the trace of η is constrained by

$$\text{tr}(\eta) < 1.9 (1.5) \times 10^{-3} \text{ at 95\% C.L.} \quad (51)$$

for NO (IO).

Furthermore, we employ as current bounds on the BRs of the cLFV decays $\mu \rightarrow e\gamma$ and $\mu \rightarrow 3e$

$$\begin{aligned} \text{BR}(\mu \rightarrow e\gamma) &< 3.1 \times 10^{-13} \text{ at 90\% C.L. (MEG II [51]) ,} \\ \text{BR}(\mu \rightarrow 3e) &< 1.0 \times 10^{-12} \text{ at 90\% C.L. (SINDRUM [52]) ,} \end{aligned} \quad (52)$$

as well as on the CR of $\mu - e$ conversion in gold and titanium

$$\begin{aligned} \text{CR}(\mu - e, \text{Au}) &< 7.0 \times 10^{-13} \text{ at 90\% C.L. (SINDRUMII [53]) ,} \\ \text{CR}(\mu - e, \text{Ti}) &< 6.1 \times 10^{-13} \text{ at 90\% C.L. (SINDRUMII [54]) .} \end{aligned} \quad (53)$$

Future bounds on the first two processes are

$$\begin{aligned} \text{BR}(\mu \rightarrow e\gamma) &< 6 \times 10^{-14} \text{ (MEG II [55]) ,} \\ \text{BR}(\mu \rightarrow 3e) &< 20 (1) \times 10^{-16} \text{ (Phase 1(2) of Mu3E [56]) ,} \end{aligned} \quad (54)$$

and for the CR of $\mu - e$ conversion in aluminium we expect

$$\begin{aligned} \text{CR}(\mu - e, \text{Al}) &< 2.6 \times 10^{-17} \text{ (COMET [57]) ,} \\ \text{CR}(\mu - e, \text{Al}) &< 2.9 \times 10^{-17} \text{ (Mu2e [58]) .} \end{aligned} \quad (55)$$

4.1.2 Parameter space

The parameter space of this scenario is spanned by the following quantities: the group theory parameters which depend on the considered case (n and s for Case 1), n , s and t (or u and v) for Case 2), n , m and s for Case 3 a) and Case 3 b.1)), the free angles θ_L and θ_R , the three couplings y_f and the two scales μ_0 and M_0 , appearing in the matrices y_D , μ_S and M_{NS} , see eqs. (13) and (11), respectively. The group theory parameters are fixed to certain values that have been shown to lead to lepton mixing angles that agree well with the experimental data, see [33, 45, 47]. The angle θ_R can be chosen freely and different values are explored. In general, it is linearly varied in the interval

$$0 \leq \theta_R \leq 2\pi. \quad (56)$$

In several of the following figures, see e.g. figs. 1, 6 and 22, we only display results for values of θ_R that lie in the range $0 \leq \theta_R \leq \frac{\pi}{4}$. Nevertheless, we have checked that we obtain the same results for values outside this range. The angle θ_L , on the other hand, is determined by fitting the measured values of the lepton mixing angles as best as possible. Depending on the case, Case 1) through Case 3 b.1), we find one or two such values for θ_L , see section 3. The couplings y_f are fixed such that the neutrino masses m_i , $i = 1, 2, 3$, are correctly reproduced, while still being perturbative, i.e. $y_f \leq \sqrt{8\pi}$ [59]. Indeed, in the presented scans these range in the interval $4 \times 10^{-5} \lesssim y_f \lesssim 1.2$, independent of the ordering of the light neutrino masses. We choose the signs of y_f to be positive. The scales μ_0 and M_0 are varied in certain ranges. In particular, we take the lepton number violating parameter μ_0 to be much smaller than the electroweak scale, as expected in the ISS framework, and vary it logarithmically as follows

$$100 \text{ eV} \leq \mu_0 \leq 100 \text{ keV ,} \quad (57)$$

while the scale M_0 is in the range

$$150 \text{ GeV} \leq M_0 \leq 10 \text{ TeV .} \quad (58)$$

Heavy sterile states in such a mass range can have different observational imprints, see e.g. [60–69]. In order to optimise the exploration of this range of M_0 , we divide it into three intervals, i.e. a lower mass interval, $150 \text{ GeV} \leq M_0 \leq 1 \text{ TeV}$, an intermediate mass interval, $1 \text{ TeV} \leq M_0 \leq 5 \text{ TeV}$, and a higher mass interval, $5 \text{ TeV} \leq M_0 \leq 10 \text{ TeV}$. In each of these intervals we vary M_0 uniformly and logarithmically. A concise description of the numerical scan is found in appendix C.

4.2 Analytical considerations

In this subsection, we remark features of the discussed BRs and CR that are common to all cases. In the following, we use the formulae found in [70, 71]. These can be simplified by taking into account the mass spectrum of the neutral states and the fact that the heavy sterile states form three pairs of pseudo-Dirac neutrinos, compare eqs. (18) and (21), see details in [45]. For the radiative cLFV decays $\ell_\beta \rightarrow \ell_\alpha \gamma$, we have

$$\text{BR}(\ell_\beta \rightarrow \ell_\alpha \gamma) \approx \frac{\alpha_w^3 s_w^2}{64 \pi^2} \frac{m_\beta^4}{M_W^4} \frac{m_\beta}{\Gamma_\beta} |\eta_{\alpha\beta}|^2 G_\gamma(x_0)^2, \quad (59)$$

where $\alpha_w = \frac{g_w^2}{4\pi}$ is the weak coupling, s_w the sine of the weak mixing angle, M_W the mass of the W boson, m_β the mass of the charged lepton of flavour β and Γ_β the corresponding total decay width as well as $G_\gamma(x)$ the relevant loop function with the limit $G_\gamma(x) \approx \frac{1}{2}$ for $x \gg 1$ and $x_0 = \left(\frac{M_0}{M_W}\right)^2$. Similarly, we get for the BR of the tri-lepton decays $\ell_\beta \rightarrow 3\ell_\alpha$

$$\begin{aligned} \text{BR}(\ell_\beta \rightarrow 3\ell_\alpha) = & \frac{\alpha_w^4}{24576 \pi^3} \frac{m_\beta^4}{M_W^4} \frac{m_\beta}{\Gamma_\beta} \left(2 \left| \frac{1}{2} F_{\text{box}}^{\beta 3\alpha} + F_Z^{\beta\alpha} - 2 s_w^2 (F_Z^{\beta\alpha} - F_\gamma^{\beta\alpha}) \right|^2 \right. \\ & + 4 s_w^4 |F_Z^{\beta\alpha} - F_\gamma^{\beta\alpha}|^2 + 16 s_w^2 \text{Re} \left((F_Z^{\beta\alpha} - \frac{1}{2} F_{\text{box}}^{\beta 3\alpha}) (G_\gamma^{\beta\alpha})^* \right) \\ & \left. - 48 s_w^4 \text{Re} \left((F_Z^{\beta\alpha} - F_\gamma^{\beta\alpha}) (G_\gamma^{\beta\alpha})^* \right) + 32 s_w^4 |G_\gamma^{\beta\alpha}|^2 \left(\log \frac{m_\beta^2}{m_\alpha^2} - \frac{11}{4} \right) \right) \end{aligned} \quad (60)$$

with the form factors reading approximately

$$\begin{aligned} G_\gamma^{\beta\alpha} & \approx 2 \eta_{\alpha\beta} G_\gamma(x_0), \quad F_\gamma^{\beta\alpha} \approx 2 \eta_{\alpha\beta} F_\gamma(x_0), \\ F_Z^{\beta\alpha} & \approx 2 \eta_{\alpha\beta} F_Z(x_0) + 4 (\eta_{\alpha\beta} - 2 \eta_{\alpha\beta}^2) G_Z(x_0, 0) + 4 \eta_{\alpha\beta}^2 G_Z(x_0, x_0), \\ F_{\text{box}}^{\beta 3\alpha} & \approx -4 (\eta_{\alpha\beta} - 2 \eta_{\alpha\alpha} \eta_{\alpha\beta}) - 8 \eta_{\alpha\alpha} \eta_{\alpha\beta} F_{\text{Xbox}}(x_0, x_0) \end{aligned} \quad (61)$$

with the limits for $x \gg 1$ being $F_\gamma(x) \approx -\frac{7}{12} - \frac{1}{6} \log x$, $F_Z(x) \approx \frac{5}{2} - \frac{5}{2} \log x$, $G_Z(x, 0) = G_Z(0, x) \approx \frac{1}{2} \log x$, $G_Z(x, x) \approx -\frac{x}{2} - \frac{x \log x}{1-x}$ and $F_{\text{Xbox}}(x, x) \approx -\frac{x}{4} + \frac{1}{4} (13 - 6 \log x)$. Furthermore, the CR for $\mu - e$ conversion in nuclei is

$$\text{CR}(\mu - e, \text{N}) = \frac{2 G_F^2 \alpha_w^2 m_\mu^5}{(4\pi)^2 \Gamma_{\text{capt}}} \left| 4 V^{(p)} \left(2 \tilde{F}_u^{\mu e} + \tilde{F}_d^{\mu e} \right) + 4 V^{(n)} \left(\tilde{F}_u^{\mu e} + 2 \tilde{F}_d^{\mu e} \right) + s_w^2 \frac{G_\gamma^{\mu e} D}{2e} \right|^2, \quad (62)$$

where G_F is the Fermi constant, Γ_{capt} the muon capture rate and D , $V^{(p)}$ and $V^{(n)}$ are nuclear form factors. The expressions for the form factors are

$$\begin{aligned} \tilde{F}_d^{\mu e} & = -\frac{1}{3} s_w^2 F_\gamma^{\mu e} - \left(\frac{1}{4} - \frac{1}{3} s_w^2 \right) F_Z^{\mu e} + \frac{1}{4} F_{\text{box}}^{\mu e dd}, \\ \tilde{F}_u^{\mu e} & = \frac{2}{3} s_w^2 F_\gamma^{\mu e} + \left(\frac{1}{4} - \frac{2}{3} s_w^2 \right) F_Z^{\mu e} + \frac{1}{4} F_{\text{box}}^{\mu e uu} \end{aligned} \quad (63)$$

with $F_\gamma^{\mu e}$ and $F_Z^{\mu e}$ found in eq. (61), and

$$F_{\text{box}}^{\mu e dd} \approx 2 \eta_{e\mu} \quad \text{and} \quad F_{\text{box}}^{\mu e uu} \approx -8 \eta_{e\mu} \quad (64)$$

in the limit $x_0 \gg 1$. Moreover, one makes use of the unitarity of the quark mixing matrix and takes into account the smallness of $|V_{td}|$. These formulae can be used to show the following three statements: all these observables are mostly proportional to $|\eta_{\alpha\beta}|^2$, both the tri-lepton decays and $\mu - e$ conversion in nuclei are dominated by the contribution due to the Z penguin (in particular for larger values of x_0), see also [72, 73], as well as $\text{CR}(\mu - e, \text{N})$ is very suppressed for a specific value of

M_0 which depends on the actual nucleus N. In the case of aluminium and using the (approximate) formula found in [70] together with the numerical values of the nuclear form factors D , $V^{(p)}$ and $V^{(n)}$, $D = 0.0362$, $V^{(p)} = 0.0161$, $V^{(n)} = 0.0173$, and the capture rate $\Gamma_{\text{capt}} = 0.7054 \times 10^6 \text{ s}^{-1}$, all given in [74], we arrive at

$$x_0 \approx 6470 \text{ corresponding to } M_0 \approx 6.5 \text{ TeV} \quad (65)$$

for $s_w^2 = 0.23$. This cancellation is clearly visible in e.g. fig. 2.

4.3 Results for Case 1)

We discuss in detail the results for Case 1). For this, we choose as exemplary values

$$n = 26 \text{ and } 0 \leq s \leq 25, \quad (66)$$

see also [45]. We inspect the form of the matrix $U_0(\theta)$ in eq. (23) for Case 1), using $\Omega(s)(3)$ as given in eq. (95) in appendix B and that the rotation is in the (13)-plane, and see that $U_0(\theta)$ can be written as

$$U_0(\theta) = U_0(\theta, s = 0) \text{diag}(e^{i\phi_s}, e^{-2i\phi_s}, e^{i\phi_s}), \quad (67)$$

where $U_0(\theta, s = 0)$ refers to the matrix $U_0(\theta)$ for $s = 0$. With this, it follows that the matrix η , see eq. (24), does not depend on the parameter s . Thus, we can set s without loss of generality to $s = 1$. We have also numerically studied the results for different values of s (both even and odd) and no dependence on this parameter is encountered.

A dependence of the size of $\text{BR}(\mu \rightarrow e\gamma)$, $\text{BR}(\mu \rightarrow 3e)$ and $\text{CR}(\mu - e, \text{Al})$ on the angle θ_R is in general expected, since the matrix combination in square brackets in eq. (22) is not diagonal and the light neutrino mass spectrum is either given by eq. (34), (35) or (36). We first explore the impact of this free angle by fixing the two scales μ_0 and M_0 to $\mu_0 = 1 \text{ keV}$ and $M_0 = 3 \text{ TeV}$. Light neutrino masses either follow NO or IO with the lightest neutrino mass being set to $m_0 = 0.03 \text{ eV}$ or $m_0 = 0.015 \text{ eV}$, respectively. The results for the BRs of $\mu \rightarrow e\gamma$ and $\mu \rightarrow 3e$ as well as the CR of $\mu - e$ conversion in aluminium are displayed in fig. 1 for different values of θ_R , as indicated by the different colours, and for both light neutrino mass orderings in the left and right plots, respectively. The small vertical coloured bands in the plots for $\text{CR}(\mu - e, \text{Al})$ show the interval of θ_L which leads to an acceptable fit of the lepton mixing angles with $\chi^2 \leq 27$, as defined in eq. (111) in appendix C. As mentioned, none of the current bounds on $\mu - e$ transitions can constrain the considered parameter space. Thus, we present in fig. 1 the exclusion due to the prospective limits as grey area, see eqs. (54) and (55); in darker and lighter grey in the case of Phase 1 and Phase 2 of the experiment Mu3E in the plots in the middle. The constraining power of the future bound on $\text{BR}(\mu \rightarrow e\gamma)$ is limited to the larger values of θ_R that are shown, while the bound on $\text{BR}(\mu \rightarrow 3e)$ expected from Phase 1 of Mu3E can exclude all used values apart from vanishing θ_R . Phase 2 of Mu3E and even more the prospective bound on $\text{CR}(\mu - e, \text{Al})$ have the potential to test all the displayed values of θ_R for $\mu_0 = 1 \text{ keV}$ and $M_0 = 3 \text{ TeV}$. We note that for these scales the obtained BRs and CR are for most of the studied values of θ_R slightly larger for light neutrino masses with IO than for a NO light neutrino mass spectrum. We can estimate their size easily for $\theta_R = 0$, since for this choice the matrix combination in square brackets in eq. (22) is automatically diagonal. We use that the BRs and CR are mainly proportional to $|\eta_{e\mu}|^2$, as argued in section 4.2. The quantity $\eta_{e\mu}$ is calculated from eq. (24). It turns out to depend on θ_L (which can be written in terms of $\sin \theta_{13}$, see [33]) as well as on the differences of the squares of the Yukawa couplings Δy_{ij}^2 , $\Delta y_{ij}^2 = y_i^2 - y_j^2$,

$$\eta'_{e\mu} = \frac{\eta_0'}{6} \left(2 \Delta y_{21}^2 - 3 (\sqrt{2 - 3 \sin^2 \theta_{13}} + \sin \theta_{13}) \sin \theta_{13} \Delta y_{31}^2 \right). \quad (68)$$

The differences Δy_{ij}^2 can be expressed as the differences of the light neutrino masses, i.e. $\Delta y_{ij}^2 = \left(\frac{M_0^2}{\mu_0 \langle H \rangle^2} \right) (m_i - m_j)$. With this information, we find

$$\text{BR}(\mu \rightarrow e\gamma) \approx 5.9 \times 10^{-15}, \quad \text{BR}(\mu \rightarrow 3e) \approx 9.5 \times 10^{-16}, \quad \text{CR}(\mu - e, \text{Al}) \approx 4.2 \times 10^{-16} \quad (69)$$

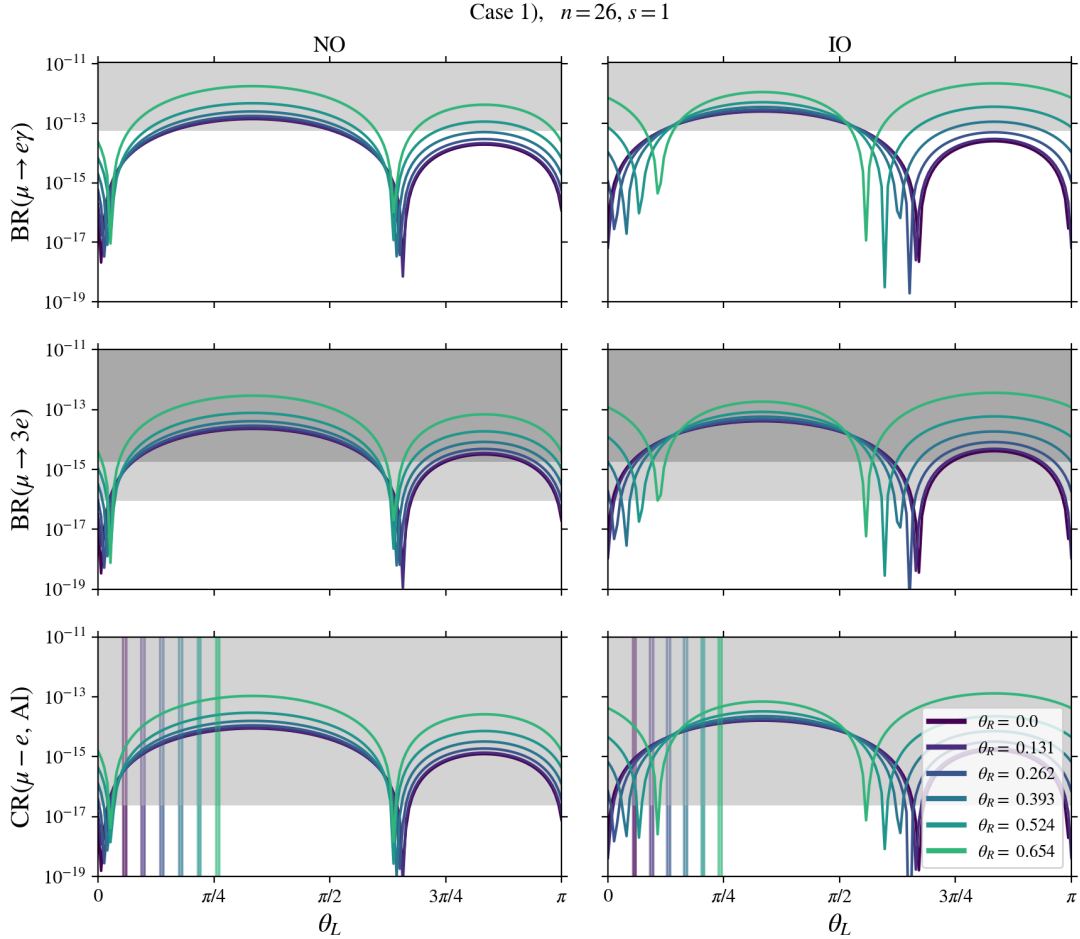


Figure 1: **Case 1).** Predictions for $\text{BR}(\mu \rightarrow e\gamma)$, $\text{BR}(\mu \rightarrow 3e)$ and $\text{CR}(\mu - e, \text{Al})$ as a function of the angle θ_L in the upper, middle and lower row. This angle is strongly constrained by the measured lepton mixing angles, compare the coloured bands in the plots for $\text{CR}(\mu - e, \text{Al})$. The index n of the flavour symmetry is fixed to $n = 26$ and the CP symmetry is chosen such that $s = 1$. However, the obtained results do not depend on s . Left (right) plots are for light neutrino masses with NO (IO) and $m_0 = 0.03$ (0.015) eV. Different values of the free angle θ_R , see the different colours, are explored. The scales μ_0 and M_0 are set to $\mu_0 = 1$ keV and $M_0 = 3$ TeV, respectively. Grey regions are excluded by the prospective bounds on the different BRs and CR with the darker (lighter) grey referring to Phase 1 (2) of Mu3E in the plots in the middle row.

for light neutrino masses with NO and $m_0 = 0.03$ eV as well as

$$\text{BR}(\mu \rightarrow e\gamma) \approx 1.4 \times 10^{-14}, \quad \text{BR}(\mu \rightarrow 3e) \approx 2.2 \times 10^{-15}, \quad \text{CR}(\mu - e, \text{Al}) \approx 9.9 \times 10^{-16} \quad (70)$$

for IO light neutrino masses with $m_0 = 0.015$ eV. As one can see, these estimates agree well with the numerical results displayed in fig. 1.

In fig. 2, we vary in addition to θ_R also the scale M_0 (up to 50 TeV), while still fixing $\mu_0 = 1$ keV. The value of θ_L is always fitted such that the lepton mixing angles are accommodated best. Furthermore, light neutrino masses are taken as in fig. 1. We observe that the smaller values of θ_R that we show give rise to smaller BRs and CR and that the dependence on the angle θ_R appears less pronounced for light neutrino masses with IO and than with NO. Furthermore, we see that for the larger values of θ_R slightly smaller values of the BRs and CR are achieved for light neutrino masses with IO. The dependence on M_0 is in general mild, in particular for $\text{BR}(\mu \rightarrow e\gamma)$, if not for the cancellation occurring in the CR, see comments in section 4.2. As already shown in fig. 1, the future bound on $\text{BR}(\mu \rightarrow e\gamma)$ is only effective for the larger values of θ_R , while the limit expected

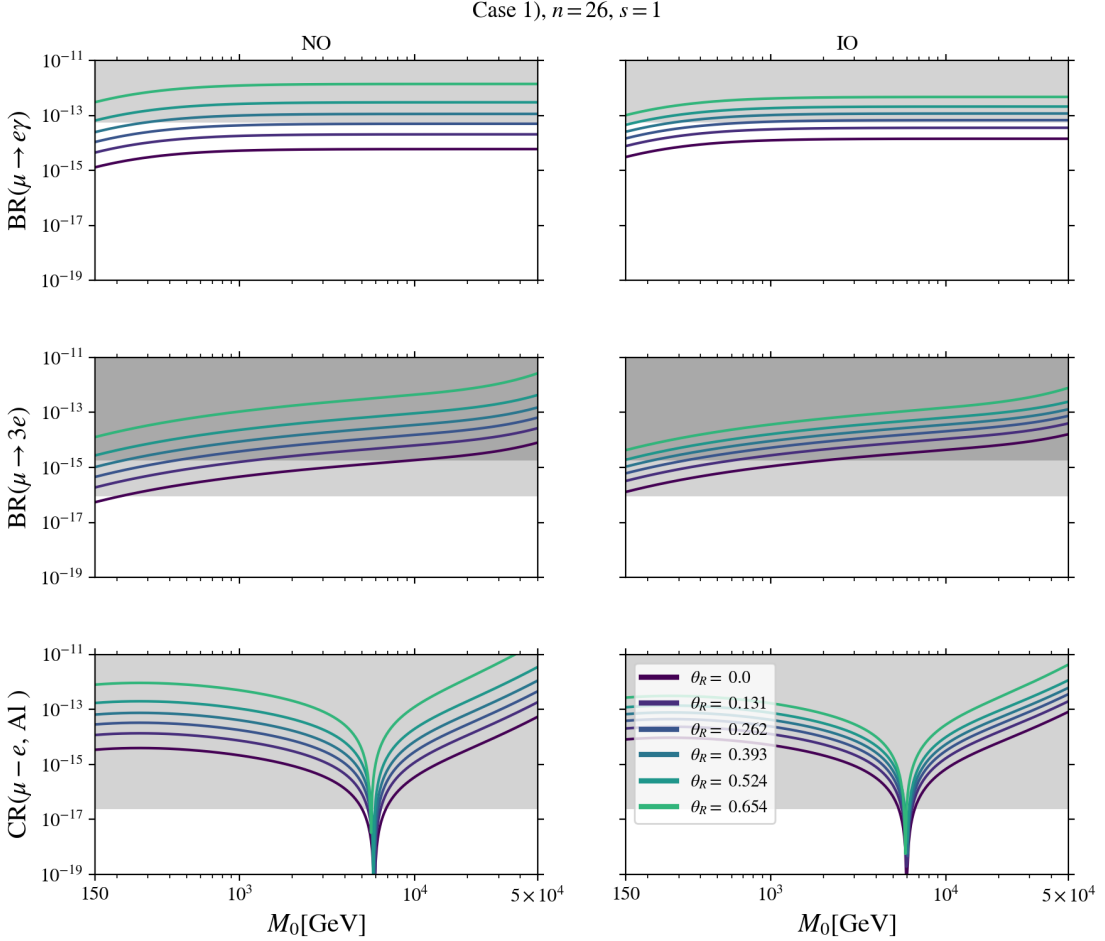


Figure 2: **Case 1).** Predictions for $\text{BR}(\mu \rightarrow e\gamma)$, $\text{BR}(\mu \rightarrow 3e)$ and $\text{CR}(\mu - e, \text{Al})$ as a function of M_0 in the upper, middle and lower row. Note that the range of the scale M_0 is larger in these plots, $150 \text{ GeV} \lesssim M_0 \lesssim 50 \text{ TeV}$, than in the numerical scans. For the group theoretical parameters and light neutrino mass orderings compare fig. 1. The parameter μ_0 is set to $\mu_0 = 1 \text{ keV}$ and θ_L to its best-fitting value for the lepton mixing angles. Six different values of θ_R between 0 and $\frac{\pi}{4}$ are explored, see different colours. The grey regions indicate exclusions of future experiments, see fig. 1.

from Phase 1 of Mu3E reduces the available parameter space for all θ_R to $M_0 \lesssim 10$ (3) TeV for light neutrino masses with NO (IO). Imposing the prospective bound of Mu3E Phase 2 on $\text{BR}(\mu \rightarrow 3e)$ leaves for $\mu_0 = 1 \text{ keV}$ only small values of M_0 , $M_0 \lesssim 200 \text{ GeV}$, for light neutrino masses with NO unconstrained, if $\theta_R = 0$. In contrast to this, the forecasts from COMET and Mu2e clearly exclude this possibility and would only allow for viable parameter space close to $M_0 \approx 6.5 \text{ TeV}$, where the cancellation occurs.

To comprehensively analyse the parameter space that we have scanned, we display in fig. 3 the results for the BRs and CR either as function of the scale M_0 , μ_0 or the free angle θ_R . The different colour-coding indicates, on the one hand, which experimental constraint can/does exclude a data point, i.e. for grey points at least one of the prospective bounds on $\text{BR}(\mu \rightarrow e\gamma)$, $\text{BR}(\mu \rightarrow 3e)$ and $\text{CR}(\mu - e, \text{Al})$ is violated as well as the current limit on at least one of the elements of the matrix η , see eq. (50), while the orange points correspond to the situation in which at least one of the prospective bounds is violated, but all current constraints on the magnitude of the matrix elements $\eta_{\alpha\beta}$ are fulfilled and red points, eventually, represent data points that are excluded by the current

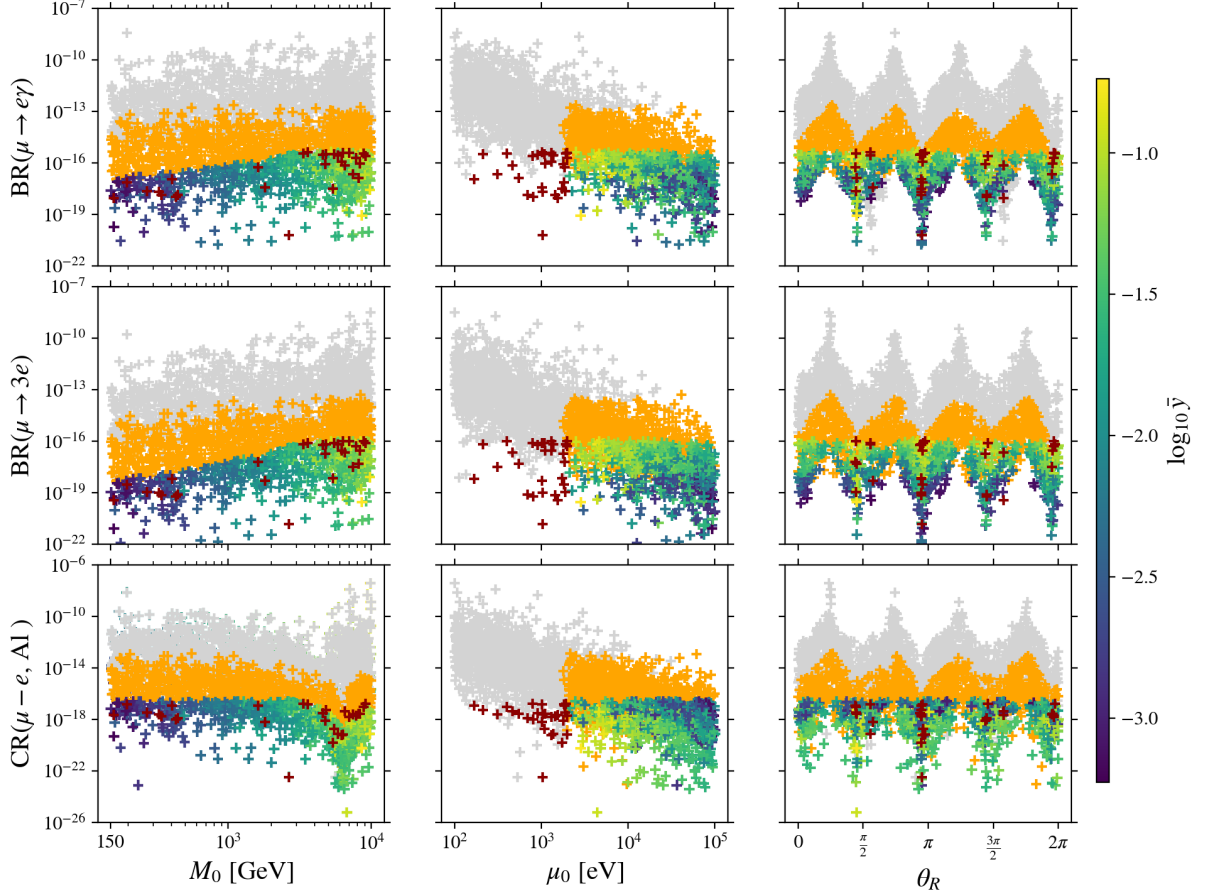


Figure 3: **Case 1).** Results of numerical scan for $\text{BR}(\mu \rightarrow e\gamma)$, $\text{BR}(\mu \rightarrow 3e)$ and $\text{CR}(\mu - e, \text{Al})$ varying M_0 , μ_0 and θ_R in the ranges in eqs. (58), (57) and (56), respectively. The parameters n and s are the same as in figs. 1 and 2. Lepton mixing angles are always accommodated well. The light neutrino mass ordering is fixed to NO and m_0 to $m_0 = 0.03$ eV. The average Yukawa coupling \bar{y} is defined in eq. (71). Points in grey, orange and red are excluded by different (current/future) experimental bounds, see text for details. Points in other colours correspond to a certain value of \bar{y} , see colour bar, and pass all the imposed limits.

limits on η , but not by the future bounds on the three studied $\mu - e$ transitions.¹⁰ On the other hand, the different colours which can be read off from the colour bar signal the average value of the Yukawa coupling, \bar{y} , which is defined as

$$\bar{y} = \frac{1}{3} (y_1 + y_2 + y_3) \quad (71)$$

for each viable data point that satisfies both the expected limits on the mentioned cLFV processes and the current bounds on $\eta_{\alpha\beta}$.¹¹ We clearly see that a minimum value of μ_0 around 2 keV is required in order to pass all bounds, while values of M_0 in the entire studied range, see eq. (58), can lead to viable points (with corresponding size of \bar{y}). As mentioned, the behaviour of $\eta_{e\mu}$ and, thus, of the BRs and CR with respect to θ_R is determined by the behaviour of the Yukawa couplings. In

¹⁰We remark that not in all scans data points corresponding to red points are found.

¹¹Note that first the grey points, then the orange ones, then the viable points which are coloured according to the colour bar and eventually the red points are plotted. We notice that the areas of the grey and the orange points can overlap, whereas the areas occupied by the viable points and by the grey and orange points usually hardly have an overlap.

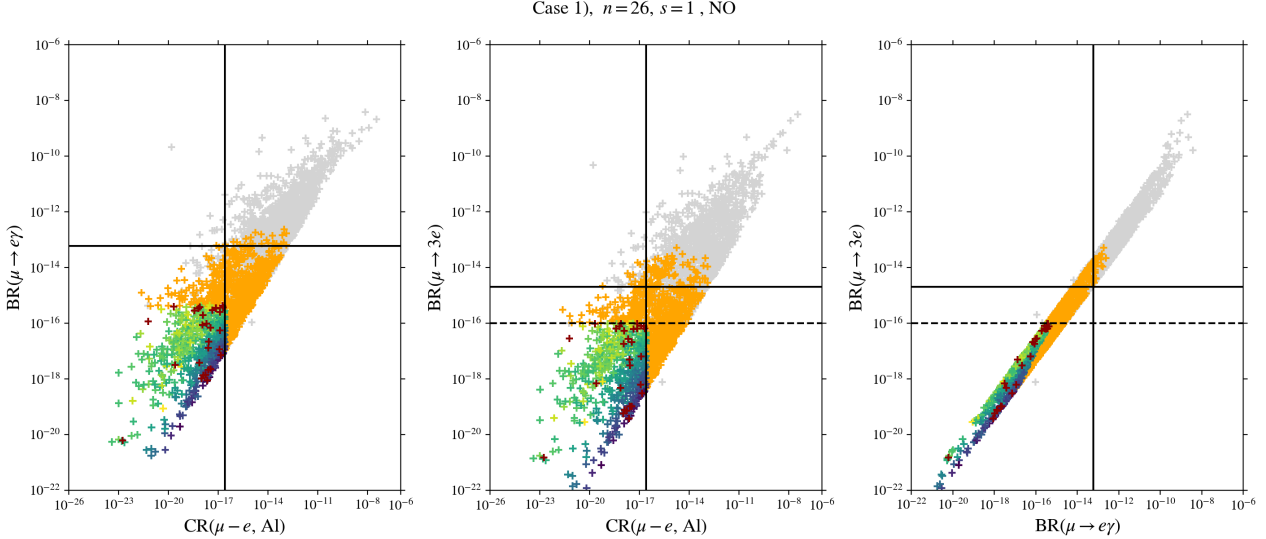


Figure 4: **Case 1).** Comparison of results for $\text{BR}(\mu \rightarrow e\gamma)$, $\text{BR}(\mu \rightarrow 3e)$ and $\text{CR}(\mu - e, \text{Al})$ for $n = 26$, $s = 1$ and light neutrino masses with NO and $m_0 = 0.03 \text{ eV}$. The colour-coding is the same as in fig. 3. For $\text{BR}(\mu \rightarrow e\gamma)$ the black line indicates the future bound from MEG II, for $\text{BR}(\mu \rightarrow 3e)$ the solid (dashed) black line corresponds to the expected limit from Mu3E Phase 1 (2) and for $\text{CR}(\mu - e, \text{Al})$ the black line represents the prospective bound from COMET.

particular, we observe enhanced values of the cLFV signals for $\cos 2\theta_R$ being close to zero, since it entails at least one large Yukawa coupling, which can easiest be seen from eqs. (35) and (36). Smaller values of these signals are obtained, if the magnitude of $\cos 2\theta_R$ is maximised, as this allows for smaller Yukawa couplings. As we see, the prospective bounds on $\text{BR}(\mu \rightarrow 3e)$ and $\text{CR}(\mu - e, \text{Al})$ are both effective, whereas all viable points correspond to $\text{BR}(\mu \rightarrow e\gamma) \lesssim 6 \times 10^{-16}$, which is two orders of magnitude smaller than the future limit, see eq. (54). The results in fig. 3 are for light neutrino masses with NO and $m_0 = 0.03 \text{ eV}$. Those obtained for smaller m_0 (in particular, $m_0 = 0$) and the same light neutrino mass ordering look similar. Also light neutrino masses with IO and larger values of m_0 , i.e. the benchmark value $m_0 = 0.015 \text{ eV}$, exhibit the same behaviour. However, if m_0 is sufficiently small (we have checked $m_0 = 0$ and $m_0 = 10^{-5} \text{ eV}$ numerically), the dependence of the BRs and CR on θ_R differs, since a cancellation among the terms of $\eta_{e\mu}$ becomes possible for certain values of θ_R . Nevertheless, the expected size of the BRs and CR is the same as for larger m_0 and light neutrino masses with NO.

Lastly, we display possible correlations among $\text{BR}(\mu \rightarrow e\gamma)$, $\text{BR}(\mu \rightarrow 3e)$ and $\text{CR}(\mu - e, \text{Al})$ in fig. 4. Since all three observables mainly depend on $|\eta_{e\mu}|^2$, see section 4.2, we expect them to be proportional to each other. This is to a certain extent also visible in fig. 4. The shown results confirm the exclusion potential of the future experiments for the three different observables: limited for $\text{BR}(\mu \rightarrow e\gamma)$ alone, considerable for $\text{BR}(\mu \rightarrow 3e)$ and strongest for $\text{CR}(\mu - e, \text{Al})$. In particular, we see that more data points still compatible with the prospective limit on $\text{BR}(\mu \rightarrow 3e)$ from Mu3E Phase 2 can be excluded by the bound expected from $\mu - e$ conversion in aluminium than vice versa, compare plot in the middle of fig. 4.

4.4 Results for Case 2)

In the discussion of the results for Case 2), it is decisive whether t is odd (equivalent to u odd, see eq. (45)) or even (meaning u even), since for t odd the matrix combination in square brackets in eq. (22) is not automatically diagonal and the light neutrino masses depend on the angle θ_R . Indeed, the formulae for them are the same as those in eqs. (34)-(36) for Case 1) with $\cos 2\theta_R$ being replaced by $\sin 2\theta_R$. Consequently, we in general observe a dependence of the flavour observables on this angle if t is odd, while this does not happen for t even, because the mentioned matrix combination is

then always diagonal and the light neutrino masses do not depend on θ_R , see eq. (26). As expected and observed in the numerical analysis, the results do not depend on whether s is even or odd.

Before focussing on values of u (or equivalently of the combination $2s - t$) that allow for a good fit of the experimental data on the lepton mixing angles, see comment below eq. (45), we study the general dependence of the results for the three different $\mu - e$ transitions on the parameters of this scenario. We first remark that, similar to the parameter s for Case 1), see eq. (67), the parameter v for Case 2) does not appear in the expression for η as given in eq. (24), since the matrix $U_0(\theta)$ can be written as

$$U_0(\theta) = U_0(\theta, v = 0) \text{diag}(e^{i\phi_v/6}, e^{-i\phi_v/3}, e^{i\phi_v/6}), \quad (72)$$

where $U_0(\theta, v = 0)$ refers to the matrix $U_0(\theta)$ with $v = 0$. Here we have used the form of $\Omega(3)$ shown in eq. (99) in appendix B and that the relevant rotation occurs in the (13)-plane.

We, then, display for the choice t even (u even) the results for $\text{BR}(\mu \rightarrow e\gamma)$, $\text{BR}(\mu \rightarrow 3e)$ and $\text{CR}(\mu - e, \text{Al})$ in the $\frac{u}{n} - \theta_L$ -plane¹² for a fixed value of μ_0 and M_0 , $\mu_0 = 1 \text{ keV}$ and $M_0 = 3 \text{ TeV}$, and light neutrino masses with NO (IO) and non-zero m_0 , see eq. (46), in the left (right) of fig. 5. As mentioned, the angle θ_R is irrelevant and thus not specified. For $\text{BR}(\mu \rightarrow e\gamma)$, shown in the upper row, the dark (light) blue regions indicate the parameter space in which the prospective bound from the experiment MEG II is passed at the 1σ (3σ) level, see eq. (54). As one can see, the impact of this future limit is mild on the considered parameter space, while being slightly stronger for light neutrino masses with IO. Similarly, for $\text{BR}(\mu \rightarrow 3e)$, see plots in the middle row, the dark (light) blue regions indicate the parameter space compatible with the expected bound from Mu3E Phase 1 at the 1σ (3σ) level, see eq. (54). We observe that about half of the parameter space in the shown plane can be disfavoured; again, for light neutrino masses with IO the exclusion reach is slightly larger. The impact of the prospective limit from Mu3E Phase 2 at the 1σ (3σ) level on the parameter space is displayed with the dark (light) red regions. We clearly see that the viable parameter space is considerably reduced. The lower row of fig. 5 contains the corresponding plots for $\text{CR}(\mu - e, \text{Al})$. As expected, the future bounds from COMET and Mu2e, respectively, see eq. (55), can only be passed in small regions of the parameter space. These are shown in dark (light) blue for the bound from COMET at the 1σ (3σ) level and in dark (light) red for Mu2e at the same σ levels. Since these bounds are very similar, the regions are largely super-imposed. As explained in section 3, the ratio $\frac{u}{n}$ and the free angle θ_L are also constrained by the requirement to accommodate the lepton mixing angles well. For this reason, we show in the plots for $\text{CR}(\mu - e, \text{Al})$ in dark (light) grey the parameter space which leads to $\chi^2 \leq 100$ (300), when using the χ^2 -function as defined in eq. (111) in appendix C. These large values are chosen in order to ensure the visibility of the corresponding parameter space in the $\frac{u}{n} - \theta_L$ -plane. In the insets the regions with $\chi^2 \leq 27$ are displayed in grey. While compatible with the future bound from MEG II and mostly with the one from Mu3E Phase 1, this part of the parameter space will be excluded by Mu3E Phase 2 and the upcoming searches for $\mu - e$ conversion in aluminium for the chosen values of the two scales μ_0 and M_0 .

In fig. 6 the corresponding results for t odd (u odd) are displayed for several fixed values of θ_R . Again, μ_0 and M_0 are set to $\mu_0 = 1 \text{ keV}$ and $M_0 = 3 \text{ TeV}$. As for t even, we study the three different $\mu - e$ transitions for both light neutrino mass orderings, see left and right plots, respectively. In the upper row the parameter space which is compatible with the prospective bound on $\text{BR}(\mu \rightarrow e\gamma)$ from MEG II at the 1σ level is shown in different colours corresponding to the six different values of θ_R . As we can see, the smaller the shown value of θ_R is, the smaller the allowed parameter space in the $\frac{u}{n} - \theta_L$ -plane is. Furthermore, the viable parameter space for light neutrino masses with IO is slightly reduced compared to the one for NO. The same observations can be made when analysing the parameter space allowed by the future limit on $\text{BR}(\mu \rightarrow 3e)$ from Mu3E Phase 1 at the 1σ level. We note that, as expected, the resulting allowed portion of parameter space is considerably smaller than in the case of $\text{BR}(\mu \rightarrow e\gamma)$. Applying the prospective bound on $\mu - e$ conversion in aluminium from COMET at the 1σ level to the parameter space, we find that only tiny regions remain allowed

¹²According to the definition of u in eq. (45) it varies between $-(n-1)$ and $2(n-1)$ and should be an integer. In this analysis, we treat $\frac{u}{n}$ as continuous parameter in the interval $-1 \leq \frac{u}{n} \leq 2$.

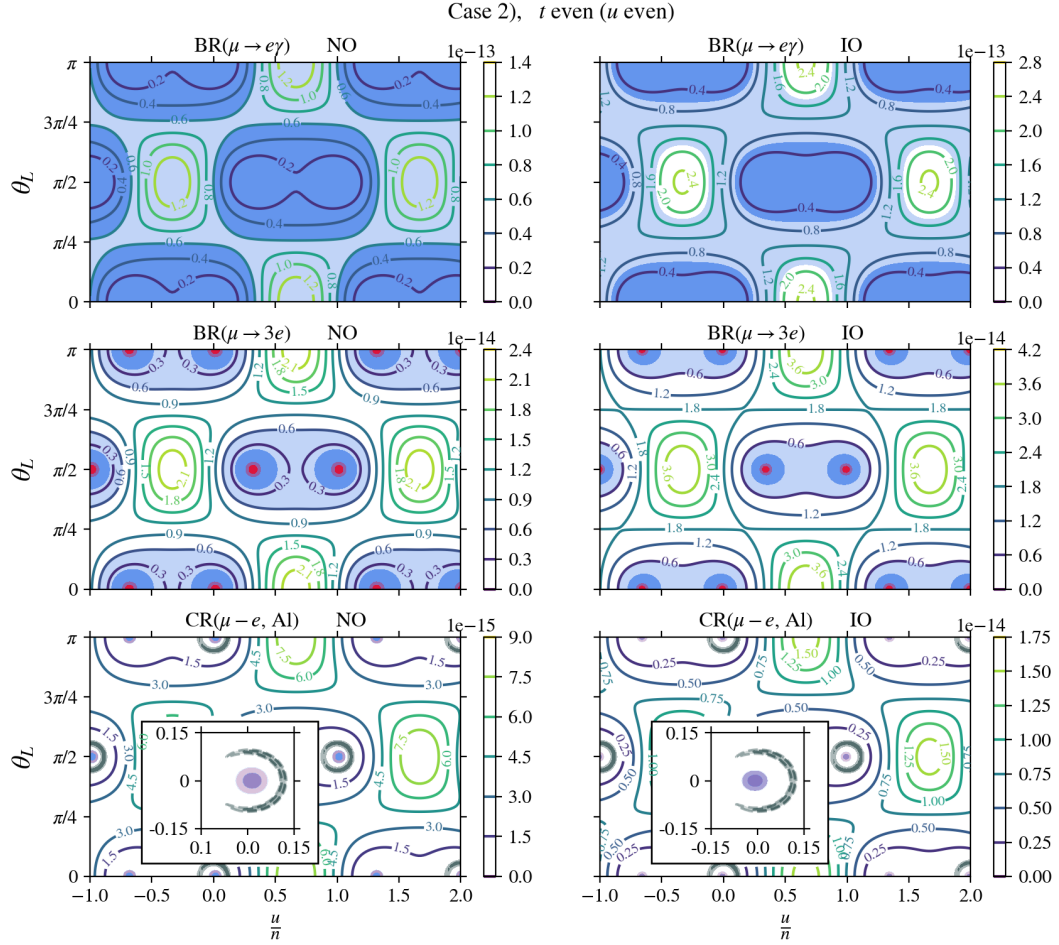


Figure 5: **Case 2), t even (u even).** Predictions for $\text{BR}(\mu \rightarrow e\gamma)$, $\text{BR}(\mu \rightarrow 3e)$ and $\text{CR}(\mu - e, \text{Al})$ in the $\frac{u}{n} - \theta_L$ -plane in the upper, middle and lower row. Left (right) plots are for light neutrino masses with NO (IO) and $m_0 = 0.03$ (0.015) eV. The scales μ_0 and M_0 are set to $\mu_0 = 1$ keV and $M_0 = 3$ TeV, respectively. Dark (light) blue and red regions indicate the regions of parameter space compatible at the 1σ (3σ) level with different prospective bounds on the BRs and CR, see text for details. In the plots for $\text{CR}(\mu - e, \text{Al})$ grey regions indicate the parameter space in which the lepton mixing angles can be accommodated, i.e. dark (light) grey for $\chi^2 \leq 100$ (300) and in the insets $\chi^2 \leq 27$.

in the $\frac{u}{n} - \theta_L$ -plane, see plots in the lower row in fig. 6. In these plots, we also display the areas in which the lepton mixing angles are accommodated to a certain degree, i.e. $\chi^2 \leq 100$, see eq. (111) in appendix C, in different light colours (and with dashed contours) depending on the value of θ_R .¹³ In the insets, instead the parameter space with $\chi^2 \leq 27$ is displayed. Overall, we see that it is very challenging, if not impossible, for all shown values of θ_R to reconcile the requirement to fit the lepton mixing angles well with passing the expected strong bounds on $\mu - e$ conversion in aluminium. We remark that for $\theta_R \approx \frac{\pi}{4}$ we obtain areas very similar those for t even. This is consistent, since in this case the matrix combination in square brackets in eq. (22) is (nearly) diagonal and the light neutrino masses are (almost) proportional to the square of the Yukawa couplings, see eq. (26), as it always happens for t even.

In order to further study the results for Case 2), we specify the values of n and u , corresponding to certain combinations of s and t , such that the lepton mixing angles can be accommodated well.

¹³Again, a larger value of χ^2 is used in order to increase visibility.

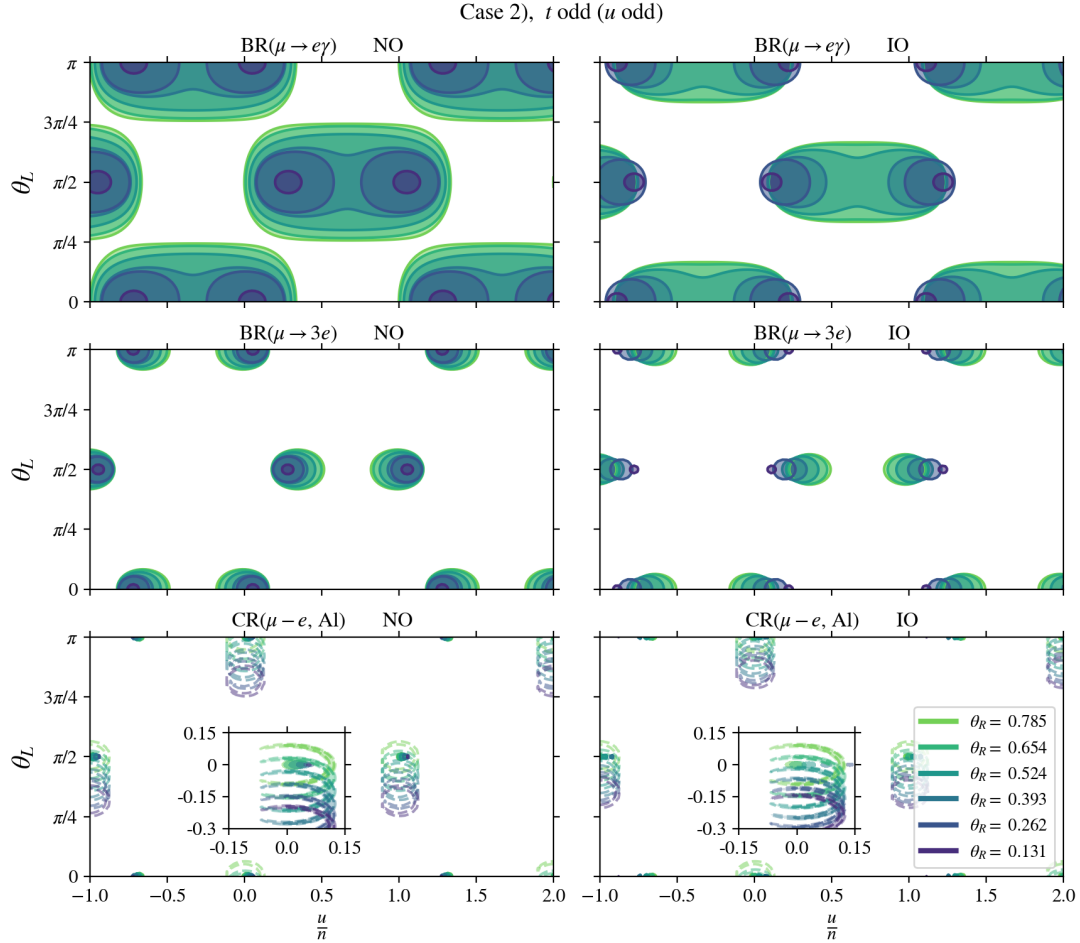


Figure 6: **Case 2), t odd (u odd).** Predictions for $\text{BR}(\mu \rightarrow e\gamma)$, $\text{BR}(\mu \rightarrow 3e)$ and $\text{CR}(\mu - e, \text{Al})$ in the $\frac{u}{n} - \theta_L$ -plane in the upper, middle and lower row. Light neutrino masses, μ_0 and M_0 are chosen as in fig. 5. For six different values of θ_R , the parameter space that is compatible at the 1σ level with the future bound on $\text{BR}(\mu \rightarrow e\gamma)$ from MEG II, on $\text{BR}(\mu \rightarrow 3e)$ from Mu3E Phase 1 and on $\text{CR}(\mu - e, \text{Al})$ from COMET, respectively, is displayed. In the plots for $\text{CR}(\mu - e, \text{Al})$, different light-coloured regions (with dashed contours) indicate the parameter space in which the lepton mixing angles can be accommodated (corresponding to $\chi^2 \leq 100$ and in the insets to $\chi^2 \leq 27$).

As has been shown in [33, 45, 47], a viable choice is

$$n = 14 \quad \text{together with} \quad u = -1, 0, 1, \quad (73)$$

since then $\frac{u}{n}$ is small enough. In terms of the parameters s and t , see eq. (45), the mentioned values of u correspond to e.g. $s = 0$ and $t = 0$ as well as $s = 1$ and $t = 2$ for $u = 0$, $s = 0$ and $t = 1$ for $u = -1$ and $s = 1$ and $t = 1$ for $u = 1$.¹⁴ In the following, we numerically explore these combinations of s and t . As is known [33], two different values of the free angle lead to a good fit of the lepton mixing parameters and we consider both of these. Like for Case 1), we first analyse the behaviour of the BRs and CR for varying M_0 , while fixing μ_0 to $\mu_0 = 1 \text{ keV}$, and either assuming light neutrino masses with NO or IO.

For t even, we take $s = 1$ and $t = 2$ (leading to $u = 0$), as shown in fig. 7. This leads to $\sin^2 \theta_{13} \approx 0.022$, $\sin^2 \theta_{12} \approx 0.34$ and $\sin^2 \theta_{23} = 0.5$, in agreement with [33, 45, 47]. Clearly, there is no dependence on the angle θ_R . Also the two different values of θ_L that permit a good fit to lepton

¹⁴The choice $s = 0$ and $t = 0$ leads to trivial Majorana phases, since I_1 and I_2 are zero, see e.g. [33].

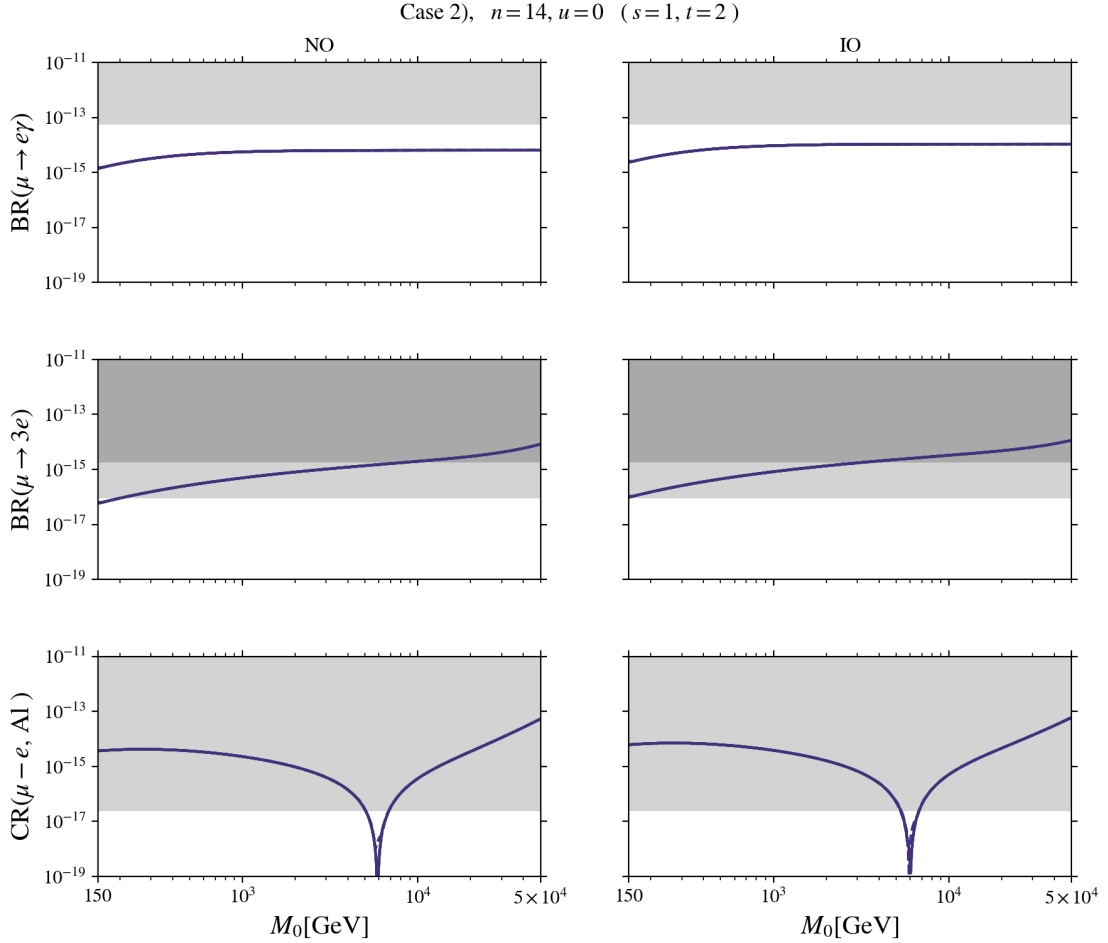


Figure 7: **Case 2), t even (u even).** Predictions for $\text{BR}(\mu \rightarrow e\gamma)$, $\text{BR}(\mu \rightarrow 3e)$ and $\text{CR}(\mu - e, \text{Al})$ as a function of M_0 in the upper, middle and lower row. The group theory parameters are chosen as $n = 14$, $s = 1$ and $t = 2$, leading to $u = 0$. Light neutrino masses with NO (IO) correspond to the plots in the left (right). Solid and dashed lines (almost always super-imposed) refer to the two different values of the angle θ_L that allow for best-fitting the lepton mixing angles. For the range of M_0 , the value of μ_0 and the grey regions, see fig. 2 of Case 1).

mixing data lead to nearly identical results, since the solid and dashed curves are almost always super-imposed. Here the solid curve represents the results for the smaller value of the angle θ_L , while the dashed curve corresponds to those obtained for the larger value of θ_L ; explicit values of θ_L can be found in e.g. [33, 47]. In fig. 7 we display the same experimental constraints for the BRs of $\mu \rightarrow e\gamma$ and $\mu \rightarrow 3e$ and $\text{CR}(\mu - e, \text{Al})$ as in fig. 2 for Case 1). The conclusions which can be drawn regarding the parameter space compatible with these future limits are very similar to those found for Case 1) and $\theta_R = 0$, namely the future bound on $\text{BR}(\mu \rightarrow e\gamma)$ is passed for the shown interval of M_0 , while the prospective limit from Mu3E Phase 1 can only constrain larger masses, i.e. $M_0 \gtrsim 10$ (3) TeV, for light neutrino masses with NO (IO). In contrast to this, Mu3E Phase 2 is expected to reduce the allowed parameter space to $M_0 \lesssim 200$ GeV for light neutrino masses with NO and the future bound on $\text{CR}(\mu - e, \text{Al})$ forces M_0 to lie in the interval $5 \text{ TeV} \lesssim M_0 \lesssim 7 \text{ TeV}$ for both light neutrino mass orderings – close to the value of M_0 which leads to a (complete) cancellation in the CR, see eq. (65).

For t odd, we employ as example $s = 1$ and $t = 1$ which give rise to $u = 1$. For this value of u and $n = 14$, the lepton mixing angles read $\sin^2 \theta_{13} \approx 0.022$, $\sin^2 \theta_{12} \approx 0.34$ and $\sin^2 \theta_{23} \approx 0.56$, see also [33, 45, 47]. Using the same conventions as in figs. 2 and 7, we display the results in fig. 8 for six different values of the angle θ_R in different colours. While for t even, we hardly see any difference

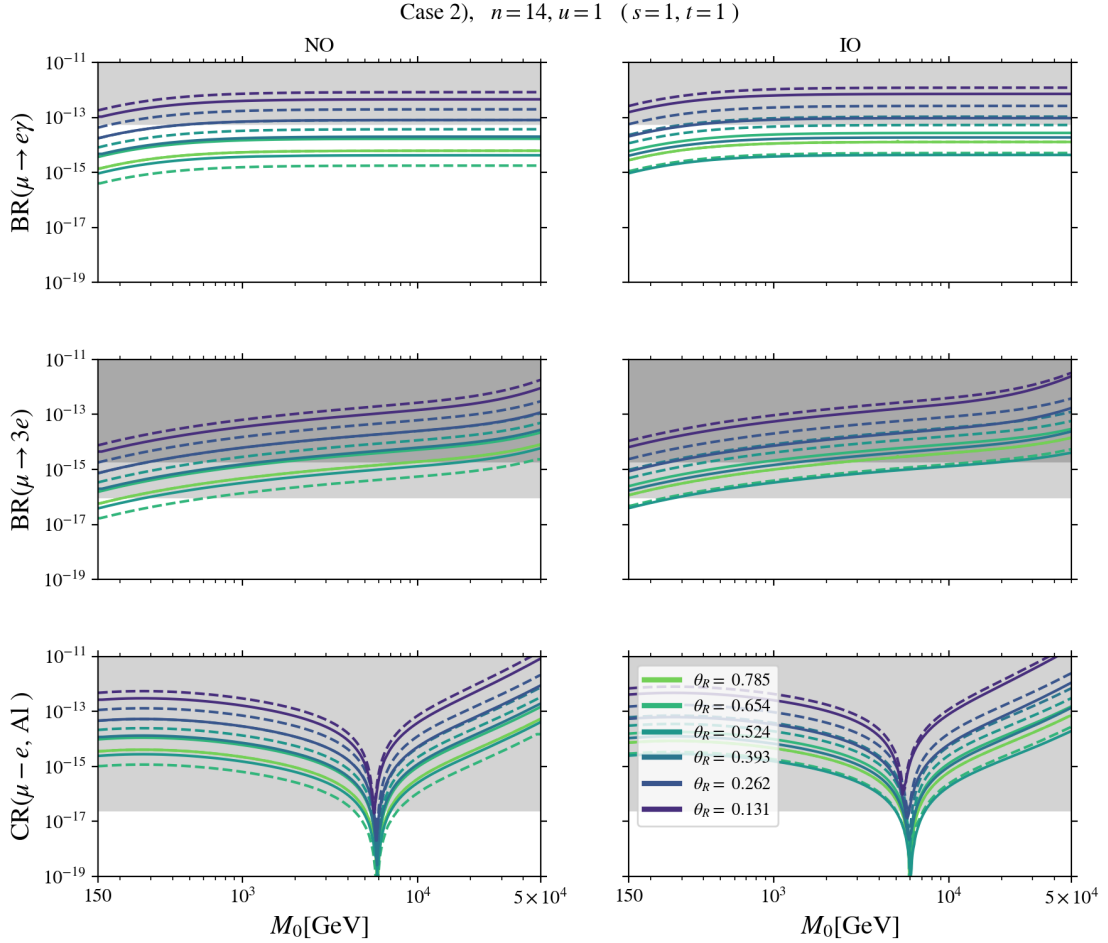


Figure 8: **Case 2), t odd (u odd).** Predictions for $\text{BR}(\mu \rightarrow e\gamma)$, $\text{BR}(\mu \rightarrow 3e)$ and $\text{CR}(\mu - e, \text{Al})$ as a function of M_0 in the upper, middle and lower row. The group theory parameters are chosen as $n = 14$, $s = 1$ and $t = 1$, corresponding to $u = 1$. The conventions in these plots are the same as in figs. 2 and 7.

in the results for the two different values of θ_L that lead to a good fit of the lepton mixing angles, the solid and dashed curves can be clearly distinguished in fig. 8. We also observe that the larger of the shown values of θ_R result in smaller values of the BRs and CR, except for $\theta_R = \frac{\pi}{4}$. For $\theta_R = \frac{\pi}{4}$ we instead find very similar results as for the combination $s = 1, t = 2$ ($u = 0$), see fig. 7. This is expected, since for $\theta_R = \frac{\pi}{4}$ the matrix combination in square brackets in eq. (22) is automatically diagonal and the light neutrino masses are proportional to the squares of the Yukawa couplings even for t odd. Comparing the results for light neutrino masses with NO and IO, they appear to be very similar, compare plots in the left and the right in fig. 8. For the larger values of θ_R that we show the prospective bound on $\text{BR}(\mu \rightarrow e\gamma)$ is passed, while the expected limit from Mu3E Phase 1 is more constraining, especially for larger values of M_0 . The future bound from Mu3E Phase 2 can exclude all parameter space for $\mu_0 = 1 \text{ keV}$, unless $M_0 \lesssim 600$ (300) GeV for light neutrino masses with NO (IO) and certain larger values of θ_R are chosen. The limit expected from COMET (and also Mu2e), on the other hand, restricts the allowed parameter space to values of M_0 close to $M_0 \approx 6.5 \text{ TeV}$, for which a cancellation occurs in the CR. Furthermore, we note that the choice $s = 0$ and $t = 1$, corresponding to $u = -1$, leads to similar results as shown in fig. 8.¹⁵

Before moving on to the results of the numerical scans, we estimate the size of the BRs and CR

¹⁵For this value of u and $n = 14$, the atmospheric mixing angle is best-fitted to $\sin^2 \theta_{23} \approx 0.44$, while the reactor and the solar mixing angles are like for $u = 0$ and $u = 1$.

Case 2), $n=14$, $s=1$, $t=2$ ($u=0$), NO

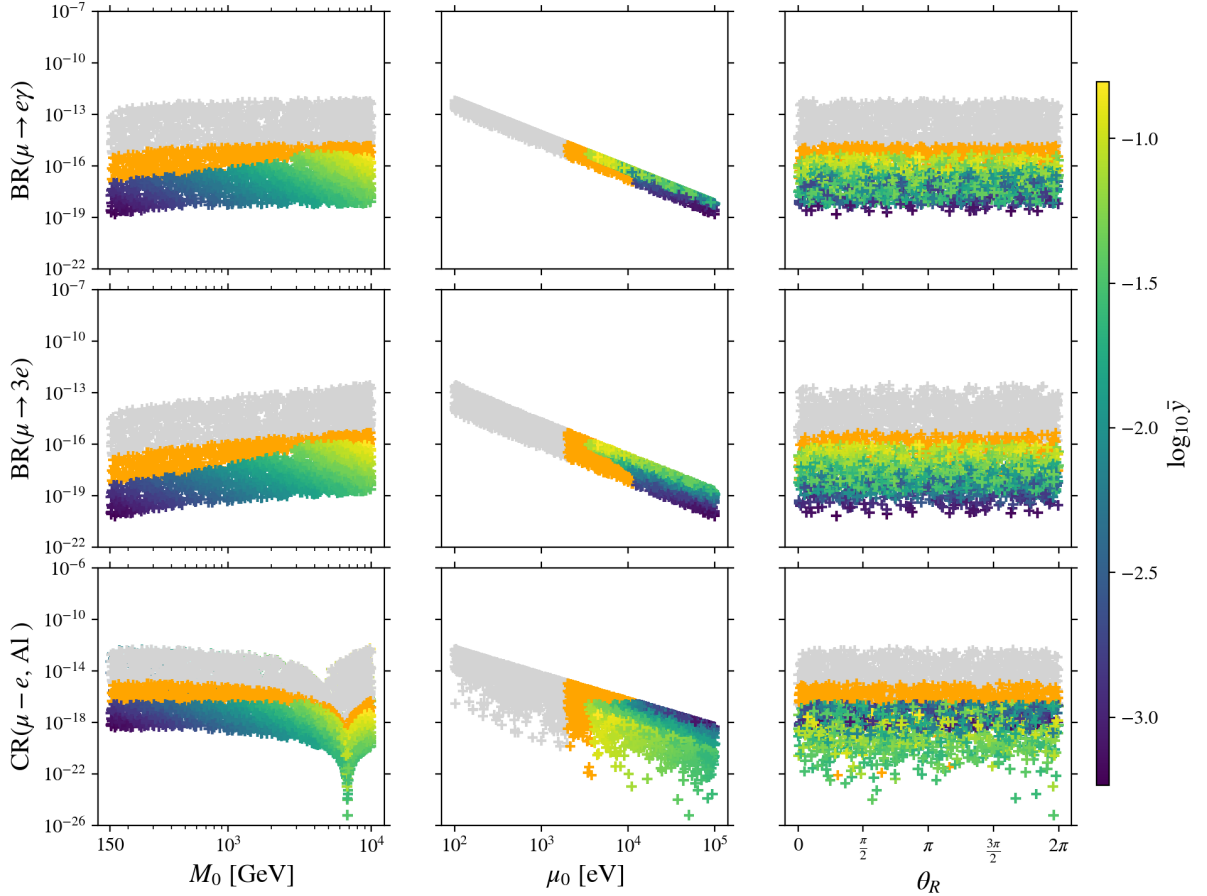


Figure 9: **Case 2), t even (u even).** Results of numerical scan for $\text{BR}(\mu \rightarrow e\gamma)$, $\text{BR}(\mu \rightarrow 3e)$ and $\text{CR}(\mu - e, \text{Al})$ varying M_0 , μ_0 and θ_R in the ranges in eqs. (58), (57) and (56), respectively. As example of the group theory parameters $n = 14$, $s = 1$ and $t = 2$, corresponding to $u = 0$, is chosen. For conventions, see fig. 3.

with the help of the analytic approximations, found in section 4.2. Similar to Case 1), see eq. (68), we first express the most relevant element of the matrix η , $\eta_{e\mu}$, in terms of Δy_{ij}^2 and lepton mixing observables which replace the combinations of θ_L and $\frac{u}{n}$ that show up

$$\eta_{e\mu} = \frac{\eta'_0}{6} (2 \Delta y_{21}^2 + 3 (1 - 2 (\sin^2 \theta_{13} + \sin^2 \theta_{23} - \sin^2 \theta_{13} \sin^2 \theta_{23}) - 6 i J_{\text{CP}}) \Delta y_{31}^2) . \quad (74)$$

This formula holds for t even as well as t odd and $\theta_R = \frac{\pi}{4}$. Then, fixing $\mu_0 = 1 \text{ keV}$ and $M_0 = 3 \text{ TeV}$, we find for $u = 0$ ($u = 1$) and light neutrino masses with NO and $m_0 = 0.03 \text{ eV}$

$$\text{BR}(\mu \rightarrow e\gamma) \approx 6.2 (5.7) \times 10^{-15} , \quad \text{BR}(\mu \rightarrow 3e) \approx 9.9 (9.1) \times 10^{-16} , \quad \text{CR}(\mu - e, \text{Al}) \approx 4.3 (4.0) \times 10^{-16} \quad (75)$$

as well as for IO light neutrino masses and $m_0 = 0.015 \text{ eV}$

$$\text{BR}(\mu \rightarrow e\gamma) \approx 1.1 (1.2) \times 10^{-14} , \quad \text{BR}(\mu \rightarrow 3e) \approx 1.7 (1.9) \times 10^{-15} , \quad \text{CR}(\mu - e, \text{Al}) \approx 7.4 (8.4) \times 10^{-16} . \quad (76)$$

These estimates are consistent with the results displayed in figs. 7 and 8.

In figs. 9 and 10 we provide results of the numerical scans for t even corresponding to u even ($s = 1$, $t = 2$ and thus $u = 0$) and for t odd/ u odd ($s = 1$, $t = 1$, meaning $u = 1$), respectively. The colour-coding is the same as in fig. 3 and the definition of the quantity \bar{y} can be found in eq. (71). We

Case 2), $n=14$, $s=1$, $t=1$ ($u=1$), NO

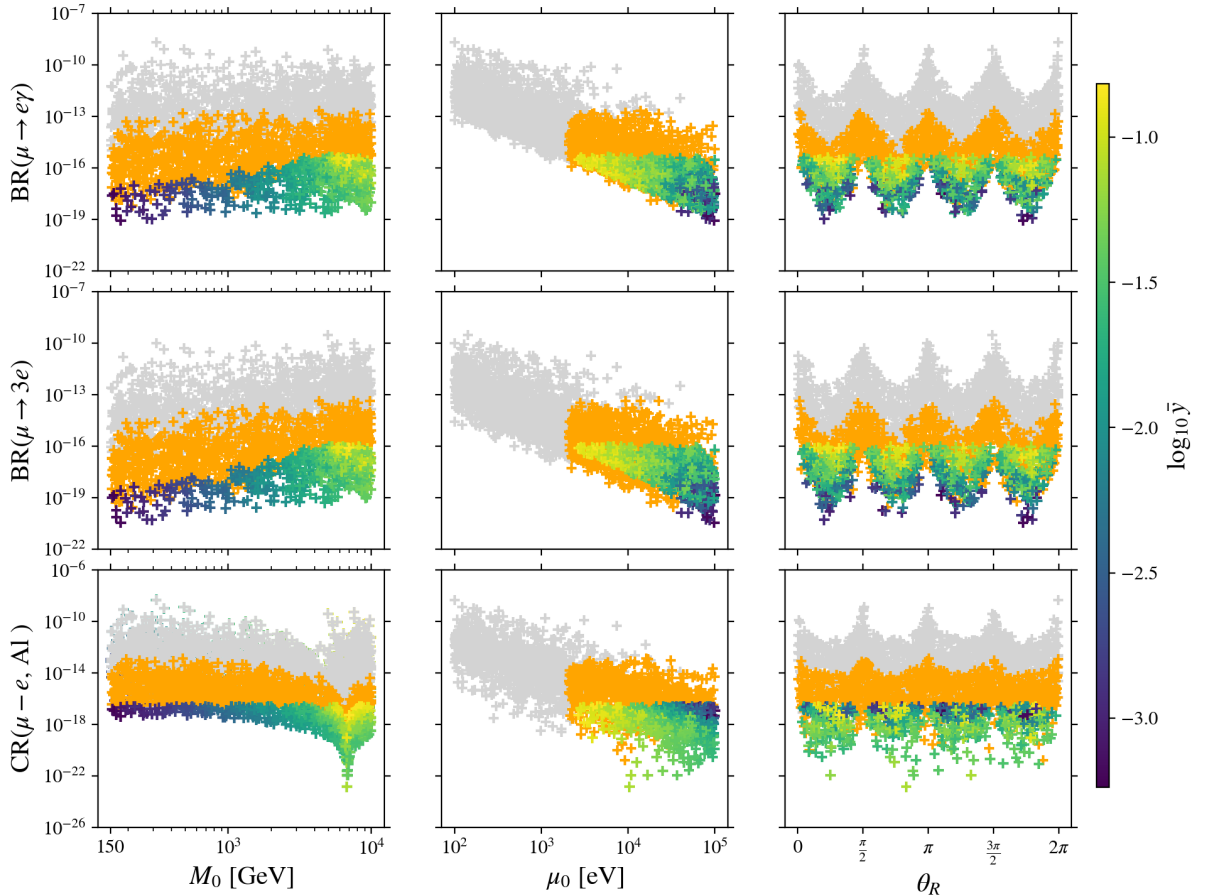


Figure 10: **Case 2), t odd (u odd).** Results of numerical scan for $\text{BR}(\mu \rightarrow e\gamma)$, $\text{BR}(\mu \rightarrow 3e)$ and $\text{CR}(\mu - e, \text{Al})$ varying M_0 , μ_0 and θ_R in the ranges in eqs. (58), (57) and (56), respectively. As example of the group theory parameters $n = 14$, $s = 1$ and $t = 1$, meaning $u = 1$, is chosen. For conventions, see fig. 3.

see that the same orders of magnitude for the BRs and CR are predicted as in Case 1) and that also for Case 2) the prospective limits for both processes $\mu \rightarrow 3e$ and $\mu - e$ conversion in aluminium can be reached, while $\text{BR}(\mu \rightarrow e\gamma)$ is expected to be smaller than 6×10^{-16} in the portion of parameter space that is allowed. Furthermore, this part of the parameter space is characterised by μ_0 being larger than 2 keV, whereas the scanned intervals of M_0 and θ_R are not constrained. Nevertheless, we also observe certain differences compared to the results for Case 1). In particular, both BRs reveal lower limits, $\text{BR}(\mu \rightarrow e\gamma) \gtrsim 10^{-19}$ and $\text{BR}(\mu \rightarrow 3e) \gtrsim 10^{-21}$, and the CR is predicted to be larger than 5×10^{-22} for values of M_0 which are not too close to $M_0 \approx 6.5$ TeV, where the cancellation occurs.¹⁶ As expected, for t even, see fig. 9, no dependence of the flavour observables on the angle θ_R is seen. Consequently, we observe less spread in the data points. For t odd, see fig. 10, a clear dependence on θ_R is observed. In contrast to the results for Case 1), the BRs and CR are now enhanced for $\sin 2\theta_R$ close to zero, since then at least one Yukawa coupling becomes large (compare the results found in [47]), while for $|\sin 2\theta_R|$ being maximal the Yukawa couplings and, hence, the size of the cLFV signals are suppressed. This behaviour is very similar for light neutrino masses with IO and $m_0 = 0.015$ eV as well as in situations in which the lightest neutrino mass m_0 is set to zero.

Eventually, we compare the results of the numerical scans for the four different combinations

¹⁶ We actually exclude all values of the CR which are obtained for $4.5 \text{ TeV} \lesssim M_0 \lesssim 7.5 \text{ TeV}$.

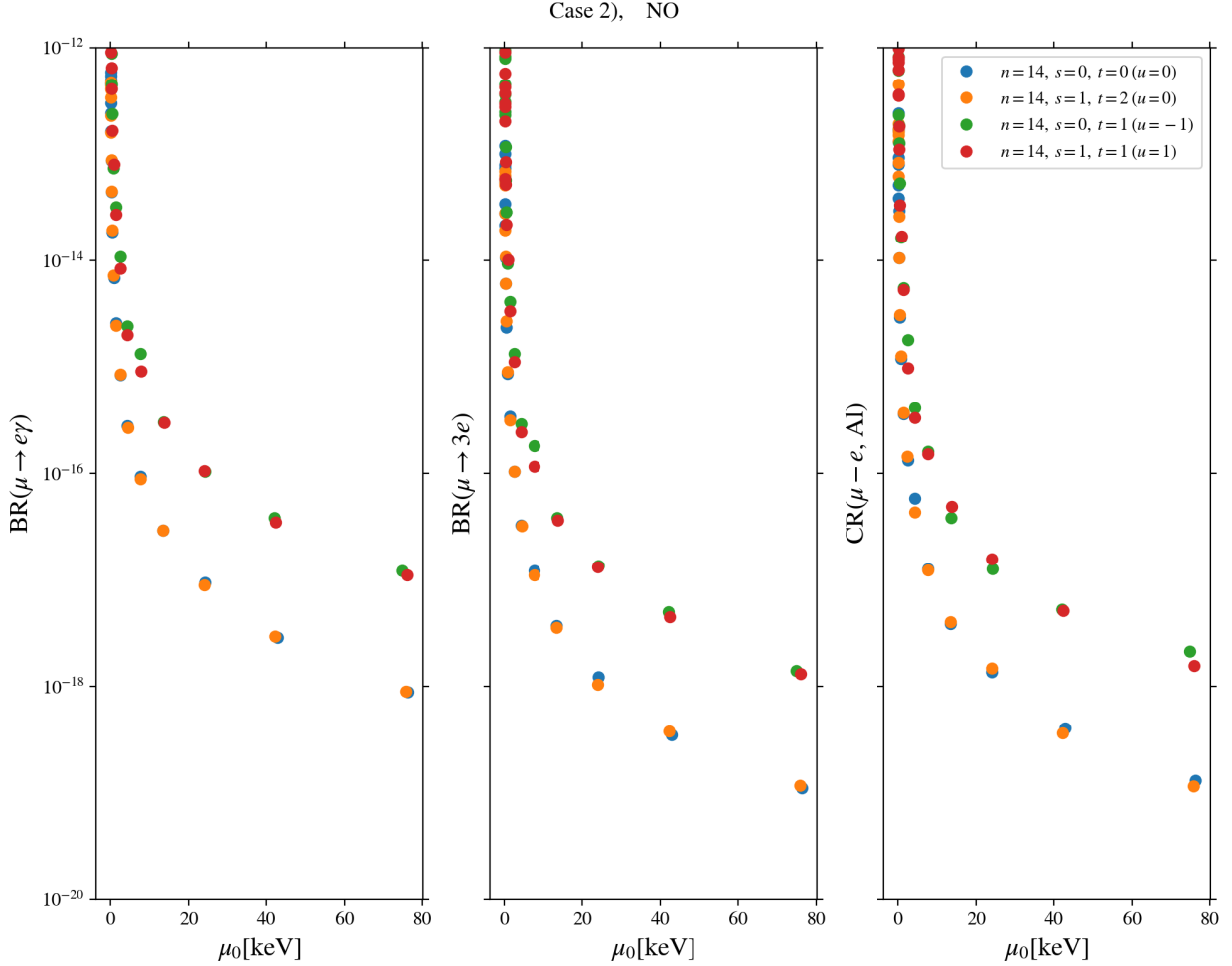


Figure 11: **Case 2).** Comparison of results for $\text{BR}(\mu \rightarrow e\gamma)$, $\text{BR}(\mu \rightarrow 3e)$ and $\text{CR}(\mu - e, \text{Al})$ for different combinations of s and t (choices of u). The group index n is fixed to $n = 14$. Light neutrino masses follow NO and $m_0 = 0.03 \text{ eV}$. The shown averages are made over the results of the scans in logarithmically uniform bins of the scale μ_0 . For details see text.

$\{s = 0, t = 0\}$, $\{s = 1, t = 2\}$ (corresponding to $u = 0$), $\{s = 0, t = 1\}$ ($u = -1$) and $\{s = 1, t = 1\}$ ($u = 1$) in fig. 11. In order to do so, we divide the scanned range of μ_0 in 30 logarithmically uniform bins and also the data points accordingly. Then, we take the average of the results for the two BRs and the CR in each bin and plot it with respect to μ_0 .¹⁷ We see that the two combinations corresponding to $u = 0$ lead to (nearly) the same averages. This is supported by the observation that the matrix element $\eta_{e\mu}$ in eq. (74) can be written in terms of the lepton mixing angles and J_{CP} that all depend on s and t only through u , compare [33]. Furthermore, it can be observed that the resulting averages are smaller by up to a factor 10 to 25, if $u = 0$. We note that also the two combinations corresponding to $u = -1$ and $u = 1$, respectively, lead to very similar results for the cLFV signals. The reason why the results for $u = -1$ and $u = 1$ are larger than those for $u = 0$ (mainly) lies in the fact that the displayed averages also take into account the part of the parameter space in which θ_R fulfills $\sin 2\theta_R \approx 0$, entailing at least one large Yukawa coupling and, thus, larger BRs and CR. This can also explain the similarity of the results for $u = -1$ and $u = 1$. Moreover, we note that the analogue of fig. 11 looks very similar for light neutrino masses with IO and $m_0 = 0.015 \text{ eV}$.

¹⁷In fig. 11, we take as value representing a bin the central value of μ_0 in this bin.

Case 3 a), $n=34$, $m=2$, $s=2$, NO

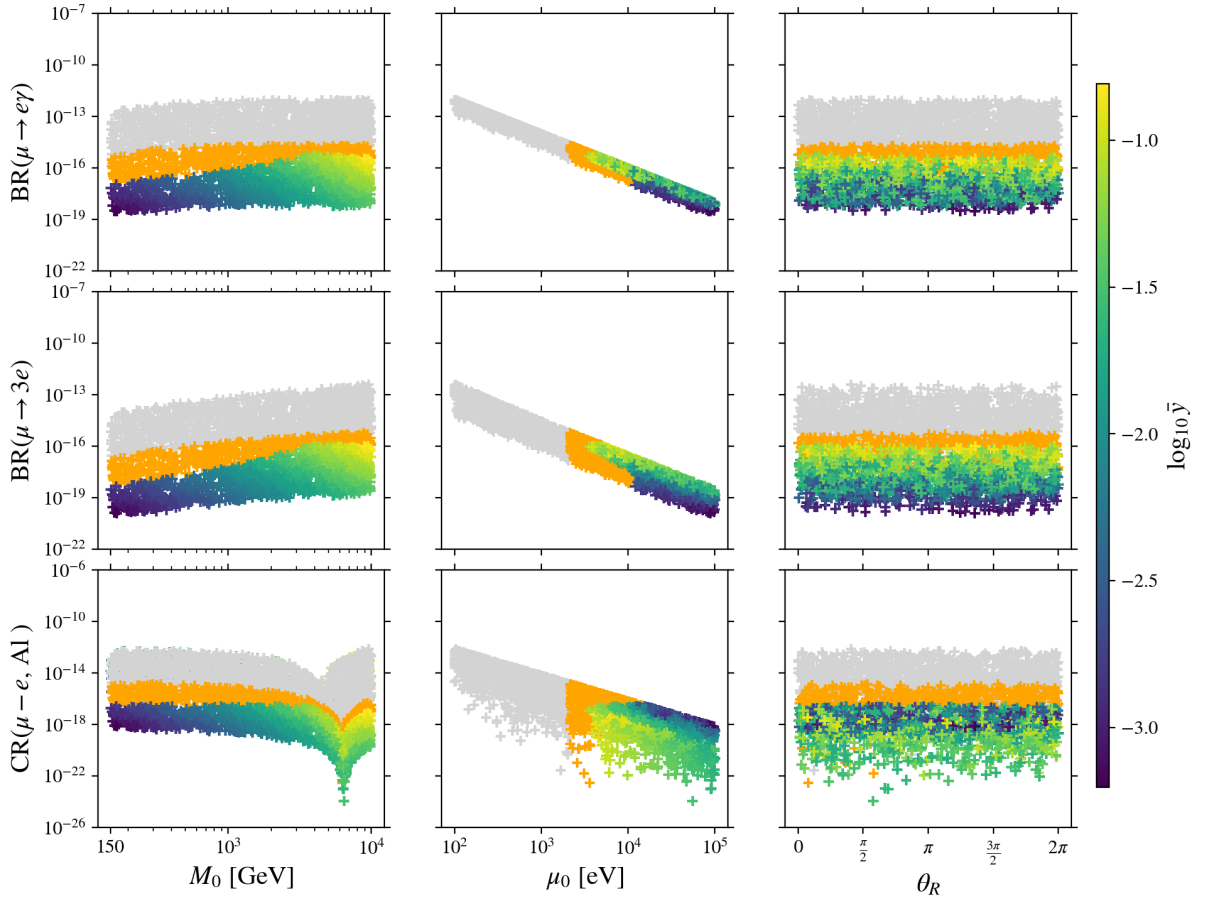


Figure 12: **Case 3 a), m and s both even (or both odd).** Results of numerical scan for $\text{BR}(\mu \rightarrow e\gamma)$, $\text{BR}(\mu \rightarrow 3e)$ and $\text{CR}(\mu - e, \text{Al})$ varying M_0 , μ_0 and θ_R in the ranges in eqs. (58), (57) and (56), respectively. As example of the group theory parameters $n = 34$, $m = 2$ and $s = 2$ is chosen. For conventions, see fig. 3.

4.5 Results for Case 3 a)

Like for Case 2), also for Case 3 a) it is relevant which residual symmetries, encoded in the parameters m and s , are preserved in the neutral lepton sector in order to determine whether the results depend in general on the angle θ_R or not. Concretely, for m and s being both even or being both odd no dependence on θ_R is expected, while for the combination m even and s odd or vice versa such a dependence is anticipated, because the matrix combination in square brackets in eq. (22) is not diagonal and the light neutrino masses depend on θ_R , see section 3. It is, thus, important to consider numerical examples which represent these different possibilities. For this reason, we choose, as in [47], one example with m odd,

$$n = 16 \quad \text{and} \quad m = 1 , \quad (77)$$

leading to $\sin^2 \theta_{13} \approx 0.025$ and $\sin^2 \theta_{23} \approx 0.61$,¹⁸ and another one with m even,

$$n = 34 \quad \text{and} \quad m = 2 , \quad (78)$$

giving rise to $\sin^2 \theta_{13} \approx 0.022$ and $\sin^2 \theta_{23} \approx 0.61$. The solar mixing angle is fixed by the choice of the CP symmetry, i.e. the parameter s , and the free angle and all values of s , $0 \leq s \leq n - 1$, allow

¹⁸We note that the value of the reactor mixing angle is slightly outside the experimentally preferred 3σ range [49].

Case 3 a), $n = 34$, $m = 2$, $s = 1$, NO

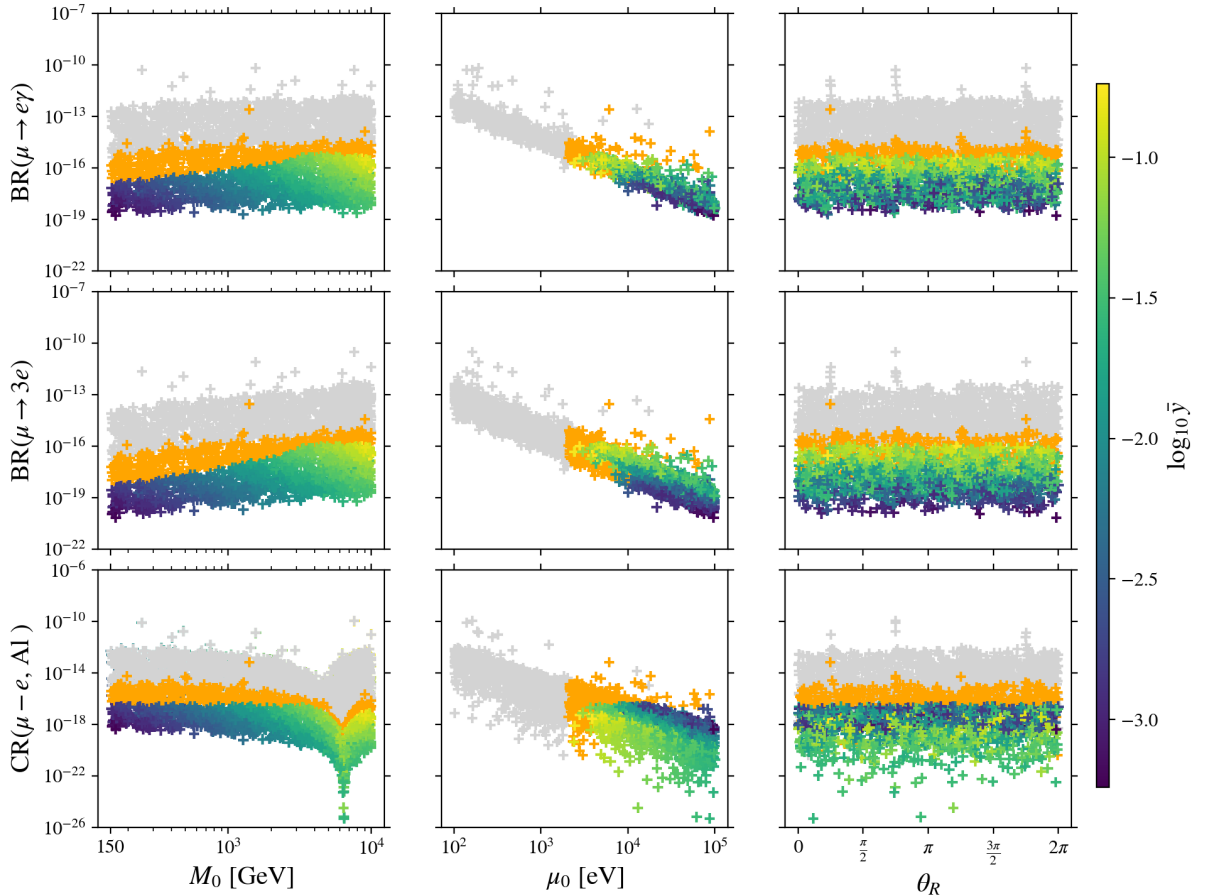


Figure 13: **Case 3 a), m even and s odd (or vice versa).** Results of numerical scan for $\text{BR}(\mu \rightarrow e\gamma)$, $\text{BR}(\mu \rightarrow 3e)$ and $\text{CR}(\mu - e, \text{Al})$ varying M_0 , μ_0 and θ_R in the ranges in eqs. (58), (57) and (56), respectively. As example of the group theory parameters $n = 34$, $m = 2$ and $s = 1$ is chosen. For conventions, see fig. 3.

for a good fit of the lepton mixing angles, usually for two different values of the free angle. For examples of viable fits, see [33] and more recently [47].

With this information, we can study the signal strength of the BRs and CR for n and m given in the $\frac{s}{n} - \theta_L$ -plane (treating $\frac{s}{n}$ as continuous parameter between 0 and 1, but still keeping track of whether s is even or odd). We fix the values of μ_0 and M_0 , e.g. $\mu_0 = 1 \text{ keV}$ and $M_0 = 3 \text{ TeV}$, and the light neutrino mass spectrum. Then, we superimpose the results of the fit to the solar mixing angle, similar to the analysis for Case 2) found in figs. 5 and 6. We find for all possible combinations of m and s being even and odd as well as for light neutrino masses with NO (IO) and $m_0 = 0.03$ (0.015) eV that no constraint on the parameter space arises from the prospective bound on $\mu \rightarrow e\gamma$ from MEG II and on $\mu \rightarrow 3e$ from Mu3E Phase 1 at the 3σ level, while the future limit of Mu3E Phase 2 and the expected reach of the experiments COMET and Mu2e exclude the entire parameter space. Thus, we do not display any corresponding plots.

We instead continue with giving an estimate for m and s both even or both odd as well as for m even and s odd or vice versa for $\theta_R = 0$ (since then the matrix combination in square brackets in eq. (22) is diagonal) that is based on the analytic form of $\eta_{e\mu}$. For this, we replace the terms depending on $\frac{m}{n}$ with the sine of the reactor mixing angle and take the limit θ_L being zero (using $\theta_L \approx \pi$ leads to the same result), compare section 3 and [33]. Then, we have

$$\eta_{e\mu} \approx \frac{\eta'_0}{6} e^{\frac{4\pi i}{3}} \left(2 \Delta y_{21}^2 - 3 (\sqrt{2 - 3 \sin^2 \theta_{13}} + \sin \theta_{13}) \sin \theta_{13} \Delta y_{31}^2 \right). \quad (79)$$

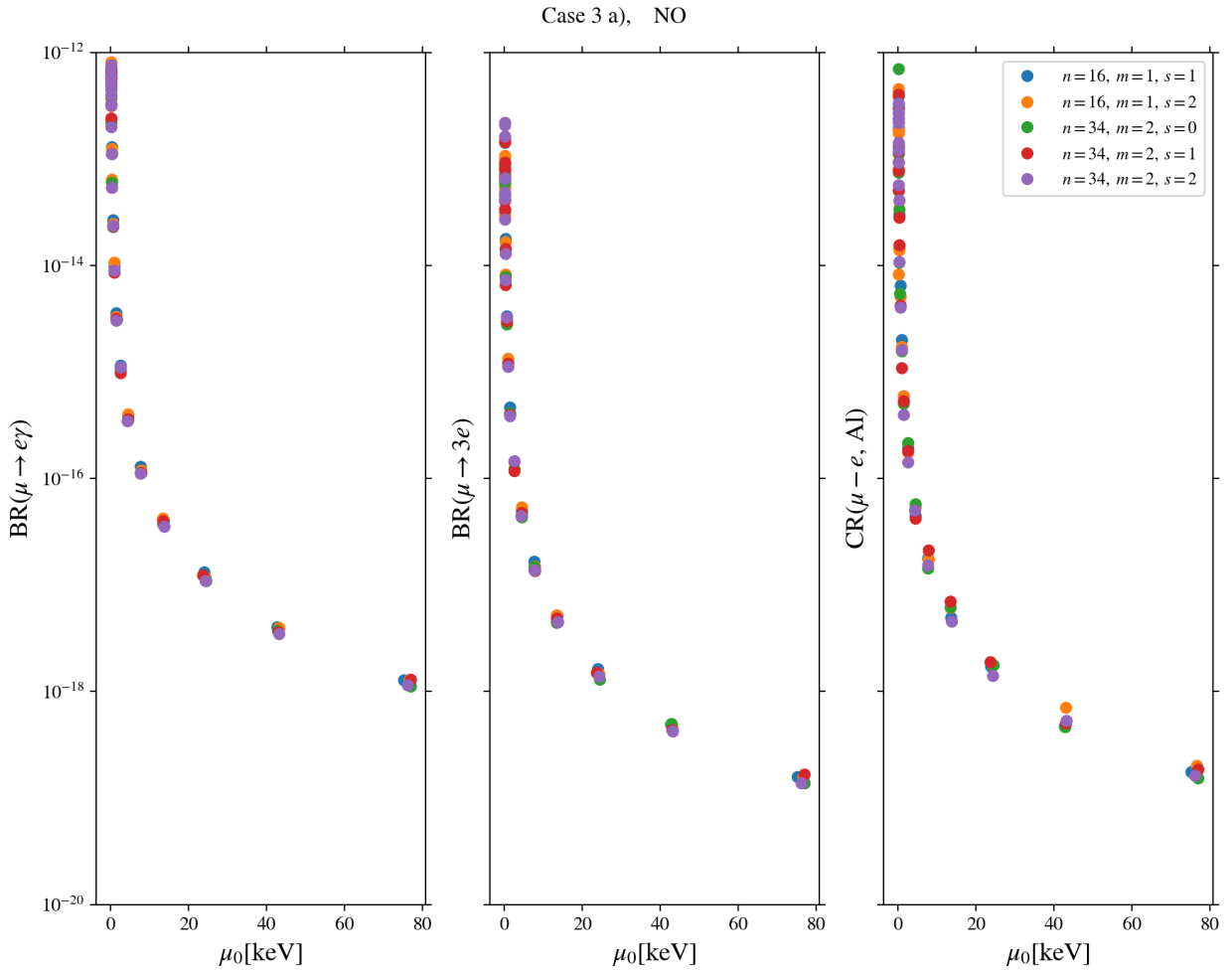


Figure 14: **Case 3 a).** Comparison of results for $\text{BR}(\mu \rightarrow e\gamma)$, $\text{BR}(\mu \rightarrow 3e)$ and $\text{CR}(\mu - e, \text{Al})$ for different combinations of m and s . The group index n is either fixed to $n = 16$ or to $n = 34$. For further conventions and details see fig. 11 for Case 2).

This expression coincides with the one obtained for Case 1), see eq. (68), up to the overall phase. Consequently, we refer to the estimates of the BRs and CR found in eqs. (69) and (70) for light neutrino masses with NO and IO and non-vanishing m_0 , respectively.

We perform numerical scans for the concrete choices $n = 16$, $m = 1$ and $s = 1$ as well as $s = 2$ and for $n = 34$, $m = 2$ and $0 \leq s \leq 2$. The results are presented in figs. 12-14 for light neutrino masses with NO and non-zero m_0 .

As expected, in fig. 12 no dependence on the free angle θ_R is observed. Although these plots assume m and s both even (since we use $n = 34$), the results for m and s both odd (for $n = 16$) look very similar. For light neutrino masses with IO and $m_0 = 0.015$ eV we also find comparable results. We have verified that taking $m_0 = 0$ leads to very similar plots as well. Like for Case 2), t even (u even), the viable data points can be characterised by $\mu_0 \gtrsim 3$ keV, while M_0 and θ_R are not restricted. Furthermore, the future limit on $\text{BR}(\mu \rightarrow 3e)$ as well as on $\text{CR}(\mu - e, \text{Al})$ can be saturated for the viable points, whereas the maximum value of $\text{BR}(\mu \rightarrow e\gamma)$ is around 6×10^{-16} and thus much lower than the prospective bound from MEG II. We also remark that both BRs appear to be bounded from below, $\text{BR}(\mu \rightarrow e\gamma) \gtrsim 10^{-19}$ and $\text{BR}(\mu \rightarrow 3e) \gtrsim 10^{-20}$. The CR of $\mu - e$ conversion in aluminium reveals – for $M_0 \lesssim 4.5$ TeV or $M_0 \lesssim 7.5$ TeV – also a lower limit, $\text{CR}(\mu - e, \text{Al}) \gtrsim 10^{-21}$.

For the choice m even and s odd (for $n = 34$) we expect the results to depend on θ_R and this dependence should be similar to the one found for Case 1), compare [47]. As can be observed in fig. 13, the dependence is much milder (for light neutrino masses with NO and $m_0 = 0.03$ eV) than

in the other studied cases, Case 1) (see fig. 3), Case 2) for t odd (see fig. 10) and Case 3 b.1) for m even and s odd or vice versa (see fig. 19). We have confirmed that for m odd and s even (employing $n = 16$) a very similar result is obtained. Assuming light neutrino masses with IO and $m_0 = 0.015$ eV also leads to plots similar to those shown in fig. 13. For NO light neutrino masses and m_0 being very small ($m_0 = 0$ or $m_0 = 10^{-5}$ eV) we find instead a larger dependence on θ_R like for Case 1) in fig. 3, when considering e.g. $n = 16$, $m = 1$ and $s = 2$. Regarding the experimental prospects to detect cLFV signals involving the muon and the electron for Case 3 a) and m even and s odd or vice versa, these are similar to those for m and s both even or both odd, namely for the studied examples we obtain $4 \times 10^{-21} \lesssim \text{BR}(\mu \rightarrow e\gamma) \lesssim 6 \times 10^{-16}$, $\text{BR}(\mu \rightarrow 3e) \gtrsim 10^{-22}$ and $\text{CR}(\mu - e, \text{Al}) \gtrsim 10^{-21}$, if the cancellation region, see footnote 16, is avoided.

Lastly, we would like to compare the different choices of n , m and s that we have analysed numerically. Like for Case 2), see fig. 11, we make use of averages corresponding to a certain binning of the data in the parameter μ_0 . We find that the results of the BRs and CR are nearly independent of the choice of n , m and s , as can be clearly seen in fig. 14, where we show the results for light neutrino masses with NO and non-zero m_0 . This behaviour can be explained with the fact that no enhancement of the BRs and CR is observed for certain values of the angle θ_R , compare fig. 13. The corresponding plots for light neutrino masses with IO and $m_0 = 0.015$ eV reveal the same features, as expected from the above discussion.

4.6 Results for Case 3 b.1)

The relevant parameters for Case 3 b.1) are the same as for Case 3 a). Given the different assignment of the light neutrino masses, see e.g. eq. (27), the values of the parameters n , m and s that can lead to a good agreement with the experimental data on lepton mixing angles differ for Case 3 b.1) from those for Case 3 a). As mentioned in section 3, see also [33], the parameter m is preferred to be close to $\frac{n}{2}$ in order to correctly accommodate the measured value of the solar mixing angle. Unlike for Case 3 a), the smallest value of the index n that permits a good fit can be small, e.g. even $n = 2$. Nevertheless, we study numerically the example

$$n = 20 \quad \text{and} \quad m = 9, 10, 11, \quad (80)$$

since a larger n allows to analyse, on the one hand, values of m which are not equal to $\frac{n}{2}$ and, on the other hand, several different values of the parameter s (corresponding to different CP symmetries), because s varies between 0 and $n - 1$. Results for the lepton mixing angles can be found in [33, 47]. Like for Case 3 a), we expect that the results for m and s both even or both odd are independent of the angle θ_R , whereas those for m even and s odd or vice versa reveal a dependence on this parameter. This expectation is confirmed in the following.

We begin the analysis of the BRs and CR by evaluating their sizes in the $\frac{s}{n} - \theta_L$ -plane¹⁹ for a fixed ratio of $\frac{m}{n}$, $\frac{m}{n} = \frac{9}{20}$, $\frac{m}{n} = \frac{10}{20}$ and $\frac{m}{n} = \frac{11}{20}$, as well as for fixed values of the two scales μ_0 and M_0 , $\mu_0 = 1$ keV and $M_0 = 3$ TeV, see figs. 15-17. The colour-coding in these figures is the same as in fig. 5 for Case 2). In particular, the dark (light) grey regions in the plots for $\text{CR}(\mu - e, \text{Al})$ indicate the parameter space in which the lepton mixing angles are accommodated to a certain degree, i.e. $\chi^2 \leq 100$ (300). These regions are found to be consistent with those shown in corresponding plots in [33, 47]. The plots in the left in figs. 15-17 assume that light neutrino masses follow NO with $m_0 = 0.03$ eV, while the plots in the right in these figures are based on an IO light neutrino mass spectrum with $m_0 = 0.015$ eV. Fig. 15 represents the combination m and s both even and, thus, no dependence on θ_R is expected, and also observed, while in figs. 16 and 17 m is odd and s even such that the results depend on θ_R . Here, they are shown for $\theta_R = 0$, for which the matrix combination in square brackets in eq. (22) is diagonal. We complete the set of plots by figs. 22-24 in appendix D in which we display for $\frac{m}{n} = \frac{9}{20}$ and $\frac{m}{n} = \frac{11}{20}$ and s even as well as for $\frac{m}{n} = \frac{10}{20}$ and s odd the results for six different values of the angle θ_R in different colours, similar to e.g. fig. 6 for Case 2) and t odd. We note that the results for $\frac{m}{n} = \frac{9}{20}$ ($\frac{m}{n} = \frac{11}{20}$) and s even agree for the choice $\theta_R = 0$ with those for

¹⁹The ratio $\frac{s}{n}$ is taken to be continuous, $0 \leq \frac{s}{n} \leq 1$, and s is either assumed to be even or odd.

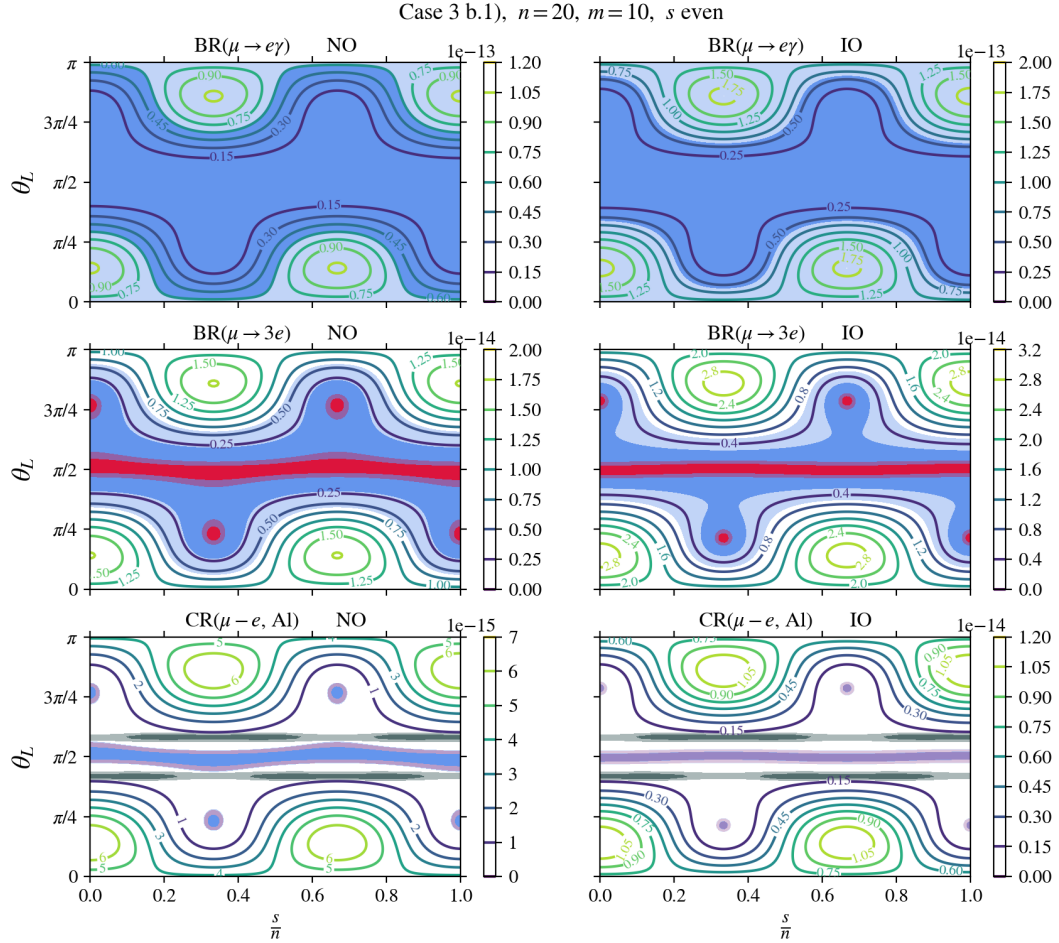


Figure 15: **Case 3 b.1), m and s both even.** Predictions for $\text{BR}(\mu \rightarrow e\gamma)$, $\text{BR}(\mu \rightarrow 3e)$ and $\text{CR}(\mu - e, \text{Al})$ in the $\frac{s}{n} - \theta_L$ -plane in the upper, middle and lower row. The group theory parameters are chosen as $n = 20$ and $m = 10$. The conventions are like in fig. 5 of Case 2) and t even (u even). Plots reflecting the features of examples with m and s both odd can be found in figs. 16 and 17, since these are displayed for the choice $\theta_R = 0$.

$\frac{m}{n} = \frac{9}{20}$ ($\frac{m}{n} = \frac{11}{20}$) and s odd and, similarly, the choice $\frac{m}{n} = \frac{10}{20}$ and s odd with $\theta_R = 0$ reproduces the results of $\frac{m}{n} = \frac{10}{20}$ and s even. Consequently, the results for all possible combinations of m and s even and odd are covered with the six figures, figs. 15-17 and figs. 22-24. We see for m and s both even or both odd as well as for m even and s odd or vice versa and $\theta_R = 0$ that in most situations the prospective bound on $\text{BR}(\mu \rightarrow e\gamma)$ is passed in the entire parameter space – at least at the 3σ level, whereas the limit expected from Mu3E Phase 1 excludes about half of the parameter space at the 3σ level and the future bound from Mu3E Phase 2 considerably reduces the viable regions of parameter space. Employing the expected limits from COMET and Mu2e only leaves a small portion of parameter space in the $\frac{s}{n} - \theta_L$ -plane allowed, which in general is hardly compatible with the regions preferred by the measured values of the lepton mixing angles. In addition, we observe that the future bounds are slightly more likely to be satisfied for light neutrino masses with NO and $m_0 = 0.03 \text{ eV}$ than in the case of an IO light neutrino mass spectrum with $m_0 = 0.015 \text{ eV}$ (compare plots in the left with those in the right in figs. 15-17). When considering the dependence on θ_R for the combinations m even and s odd or vice versa, see especially figs. 22-24 in appendix D, we note that the shape and size of the parameter space passing a certain future bound depends on the actual value of θ_R and for the larger ones among the shown values it is usually smaller. Furthermore, the regions of parameter space that lead to an agreement of the lepton mixing angles with experimental data shift as function of θ_R . It is, thus, necessary to investigate each value of θ_R separately in

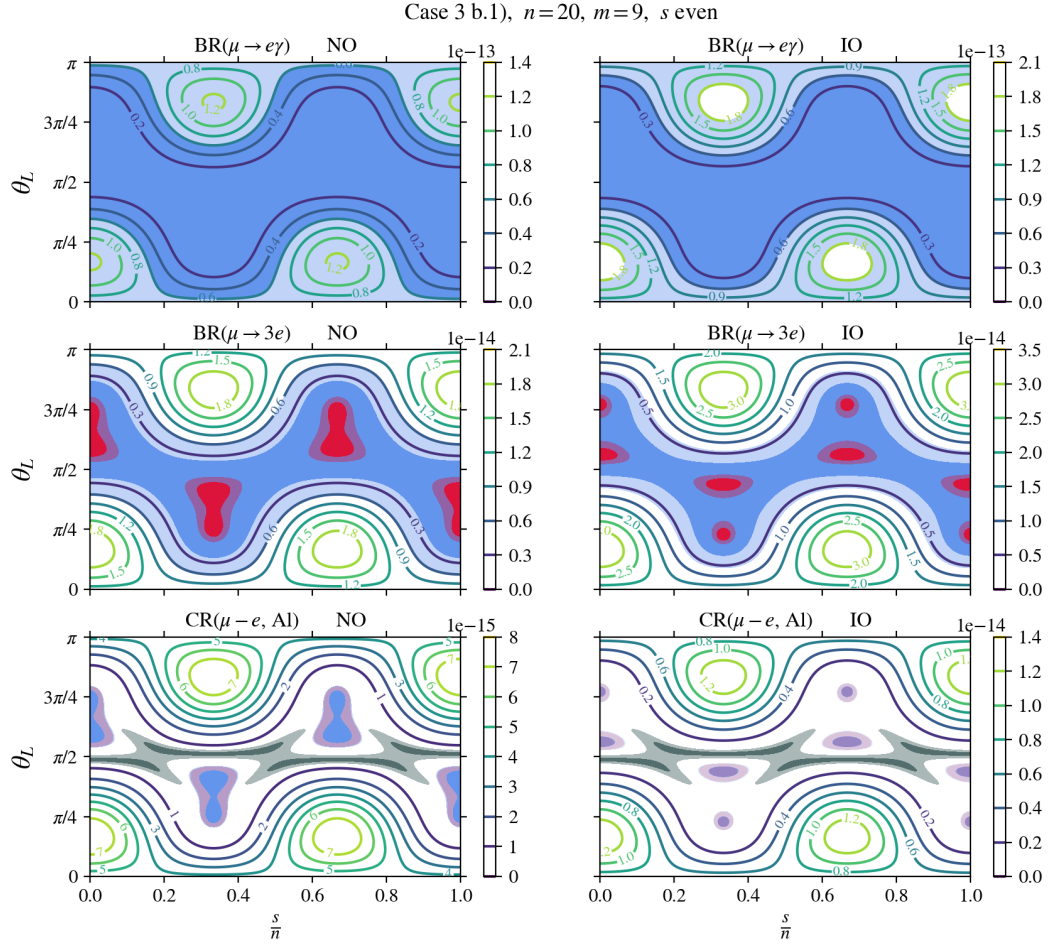


Figure 16: **Case 3 b.1), m odd, s even and $\theta_R = 0$.** Predictions for $\text{BR}(\mu \rightarrow e\gamma)$, $\text{BR}(\mu \rightarrow 3e)$ and $\text{CR}(\mu - e, \text{Al})$ in the $\frac{s}{n} - \theta_L$ -plane in the upper, middle and lower row. The group theory parameters are chosen as $n = 20$ and $m = 9$. For the remaining conventions see fig. 15. The dependence on θ_R is illustrated with six different values of θ_R in different colours in fig. 22 in appendix D. Results for an example of the combination m even and s odd and different values of θ_R are found in fig. 24 in the same appendix.

order to make more quantitative statements about the constraints imposed by the future limits on the different $\mu - e$ transitions and their compatibility with the restrictions coming from fitting the lepton mixing angles well.

To numerically estimate the BRs and CR, we first give an approximate formula for $\eta_{e\mu}$ for m and s both even or both odd or m even and s odd or vice versa, assuming $\theta_R = 0$. For this, we take $m = \frac{n}{2}$, express θ_L in terms of the reactor mixing angle, compare [33, 47], and then arrive at

$$\eta_{e\mu} = \frac{\eta'_0}{3\sqrt{2}} e^{\frac{4\pi i}{3}} \left(3(e^{-3i\phi_s} \sqrt{1 - 3 \sin^2 \theta_{13}} + \sqrt{2} \sin \theta_{13}) \sin \theta_{13} \Delta y_{21}^2 - \sqrt{2} \Delta y_{31}^2 \right), \quad (81)$$

where Δy_{21}^2 and Δy_{31}^2 are related to the light neutrino masses as follows $\Delta y_{21}^2 = \left(\frac{M_0^2}{\mu_0 \langle H \rangle^2} \right) (m_3 - m_2)$ and $\Delta y_{31}^2 = \left(\frac{M_0^2}{\mu_0 \langle H \rangle^2} \right) (m_1 - m_2)$, since the identification of Yukawa couplings and light neutrino masses is altered compared to Case 1) through Case 3 a) due to the permutation, c.f. eq. (27). Using

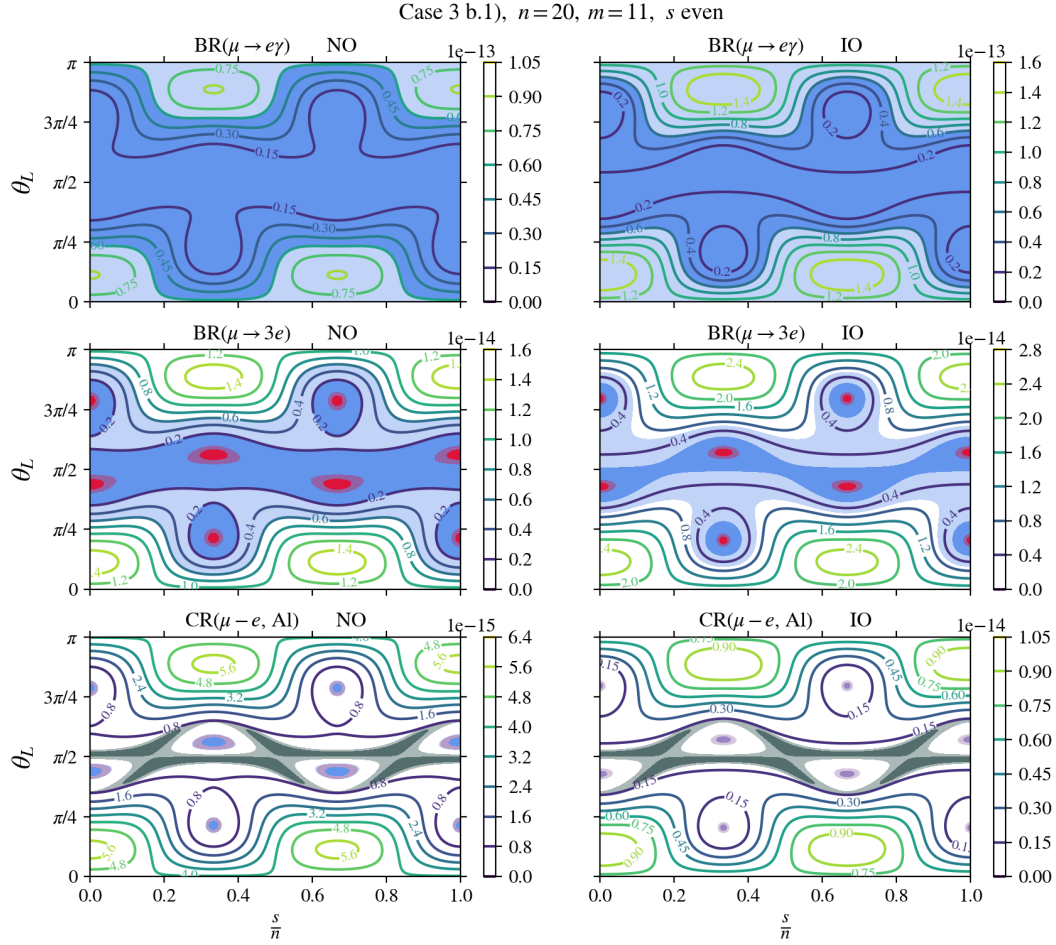


Figure 17: **Case 3 b.1), m odd, s even and $\theta_R = 0$.** Predictions for $\text{BR}(\mu \rightarrow e\gamma)$, $\text{BR}(\mu \rightarrow 3e)$ and $\text{CR}(\mu - e, \text{Al})$ in the $\frac{s}{n} - \theta_L$ -plane in the upper, middle and lower row. The group theory parameters are chosen as $n = 20$ and $m = 11$. For the remaining conventions see fig. 15. The dependence on θ_R is illustrated with six different values of θ_R in different colours in fig. 23 in appendix D. Results for an example of the combination m even and s odd and different values of θ_R are found in fig. 24 in the same appendix.

that $-0.6 \lesssim \cos 3\phi_s \lesssim 0.71$, see [33], we obtain as intervals for the BRs and CR

$$\begin{aligned} 3.9 \times 10^{-15} &\lesssim \text{BR}(\mu \rightarrow e\gamma) &\lesssim 9.3 \times 10^{-15}, \\ 6.3 \times 10^{-16} &\lesssim \text{BR}(\mu \rightarrow 3e) &\lesssim 1.5 \times 10^{-15}, \\ 2.7 \times 10^{-16} &\lesssim \text{CR}(\mu - e, \text{Al}) &\lesssim 6.6 \times 10^{-16} \end{aligned} \quad (82)$$

for light neutrino masses with NO and $m_0 = 0.03 \text{ eV}$, while for IO light neutrino masses with $m_0 = 0.015 \text{ eV}$ we get

$$\begin{aligned} 8.8 \times 10^{-15} &\lesssim \text{BR}(\mu \rightarrow e\gamma) &\lesssim 1.3 \times 10^{-14}, \\ 1.4 \times 10^{-15} &\lesssim \text{BR}(\mu \rightarrow 3e) &\lesssim 2.1 \times 10^{-15}, \\ 6.2 \times 10^{-16} &\lesssim \text{CR}(\mu - e, \text{Al}) &\lesssim 9.1 \times 10^{-16}. \end{aligned} \quad (83)$$

Again, we have fixed the two scales μ_0 and M_0 to $\mu_0 = 1 \text{ keV}$ and $M_0 = 3 \text{ TeV}$, respectively. From these estimates we see that the future bound on $\text{BR}(\mu \rightarrow e\gamma)$ is usually passed as well as the limit on $\text{BR}(\mu \rightarrow 3e)$ expected from Mu3E Phase 1, whereas Mu3E Phase 2 can exclude this scenario and also the experiments COMET and Mu2e have this potential, since $\text{CR}(\mu - e, \text{Al})$ is larger than 2×10^{-16} for the chosen values of the scales μ_0 and M_0 and the assumed light neutrino mass spectra.

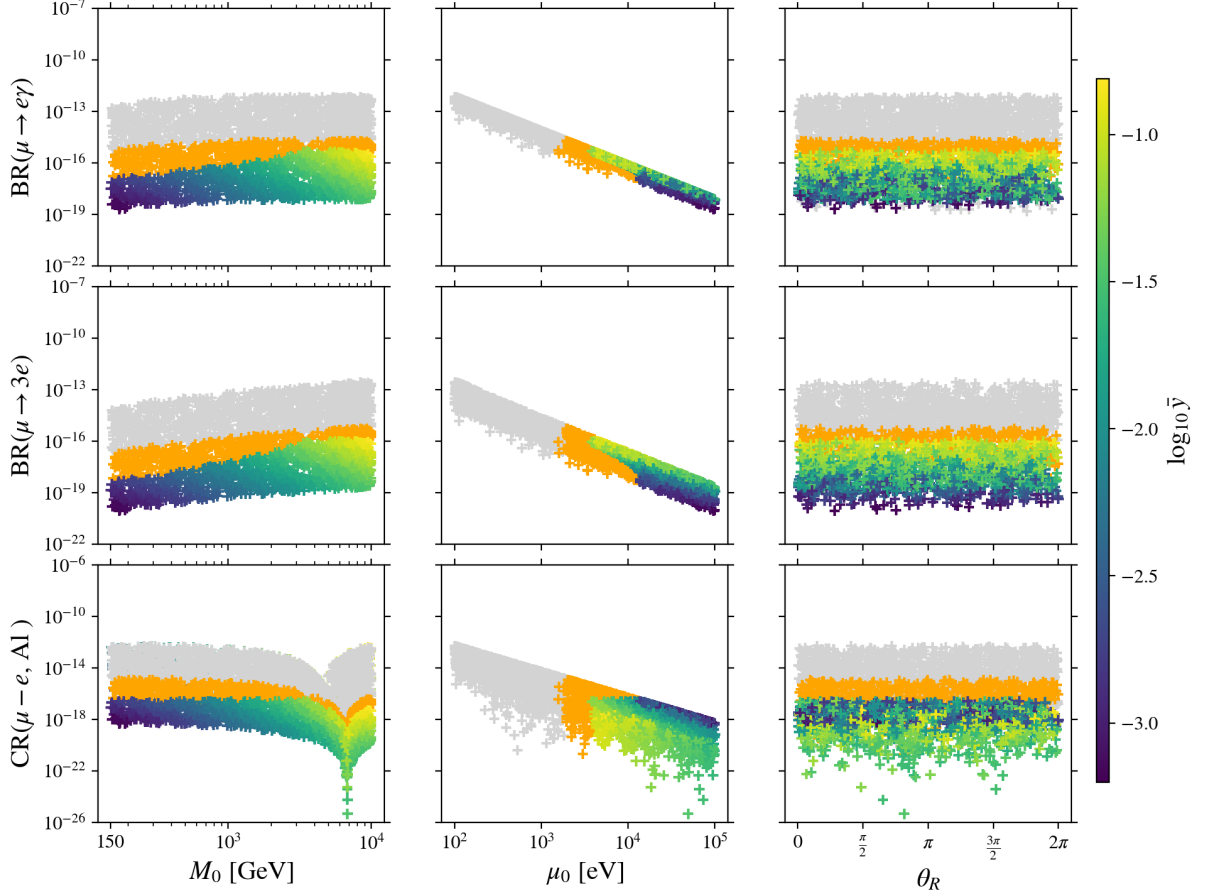


Figure 18: **Case 3 b.1), m and s both odd (or both even).** Results of numerical scan for $\text{BR}(\mu \rightarrow e\gamma)$, $\text{BR}(\mu \rightarrow 3e)$ and $\text{CR}(\mu - e, \text{Al})$ varying M_0 , μ_0 and θ_R in the ranges in eqs. (58), (57) and (56), respectively. As example of the group theory parameters $n = 20$, $m = 9$ and $s = 1$ is chosen. For conventions, see fig. 3.

In a next step, we scrutinise the parameter space by performing numerical scans for different values of m and s : for $m = 10$ we have studied $s = 2$, $s = 3$ and $s = 10$, for $m = 9$ the choices of s are $s = 1$, $s = 2$, $s = 18$ and $s = 19$, while for $m = 11$ we have fixed s to $s = 0$, $s = 1$ and $s = 2$. We show examples of these scans in figs. 18 and 19 for the concrete choices $m = 9$ and $s = 1$ as well as $m = 9$ and $s = 2$, respectively, assuming that light neutrino masses follow NO and $m_0 = 0.03$ eV. Since $m = 9$ and $s = 1$ are both odd, no dependence on θ_R is revealed, while for $m = 9$ and $s = 2$ a clear dependence on θ_R is observed, as expected. Like for Case 1), at least one Yukawa coupling is enhanced for $\cos 2\theta_R \approx 0$ and, consequently, also the BRs and CR, whereas for $|\cos 2\theta_R| \approx 1$ the signal strength of the studied cLFV processes is suppressed, compare [47] for the dependence on θ_R . We have checked that the other choices of m and s both even or both odd as well as light neutrino masses with IO and $m_0 = 0.015$ eV lead to plots that are very similar to those found in fig. 18. This holds analogously for the other choices of m and s with one of them being even and the other one odd and the results displayed in fig. 19. Regarding the ranges of the BRs and CR, we usually find for the viable data points (the ones coloured according to the colour bar in figs. 18 and 19) $10^{-19} \lesssim \text{BR}(\mu \rightarrow e\gamma) \lesssim 6 \times 10^{-16}$, $\text{BR}(\mu \rightarrow 3e) \gtrsim 10^{-21}$ and $\text{CR}(\mu - e, \text{Al}) \gtrsim 10^{-22}$ (excluding $4.5 \text{ TeV} \lesssim M_0 \lesssim 7.5 \text{ TeV}$) with $\text{BR}(\mu \rightarrow 3e)$ and $\text{CR}(\mu - e, \text{Al})$ saturating the expected limits from Mu3E Phase 2 and COMET, respectively.

We summarise and compare the results of all the performed numerical scans for light neutrino masses with NO and non-vanishing m_0 in fig. 20 using the same strategy of binning and averaging

Case 3 b.1), $n=20$, $m=9$, $s=2$, NO

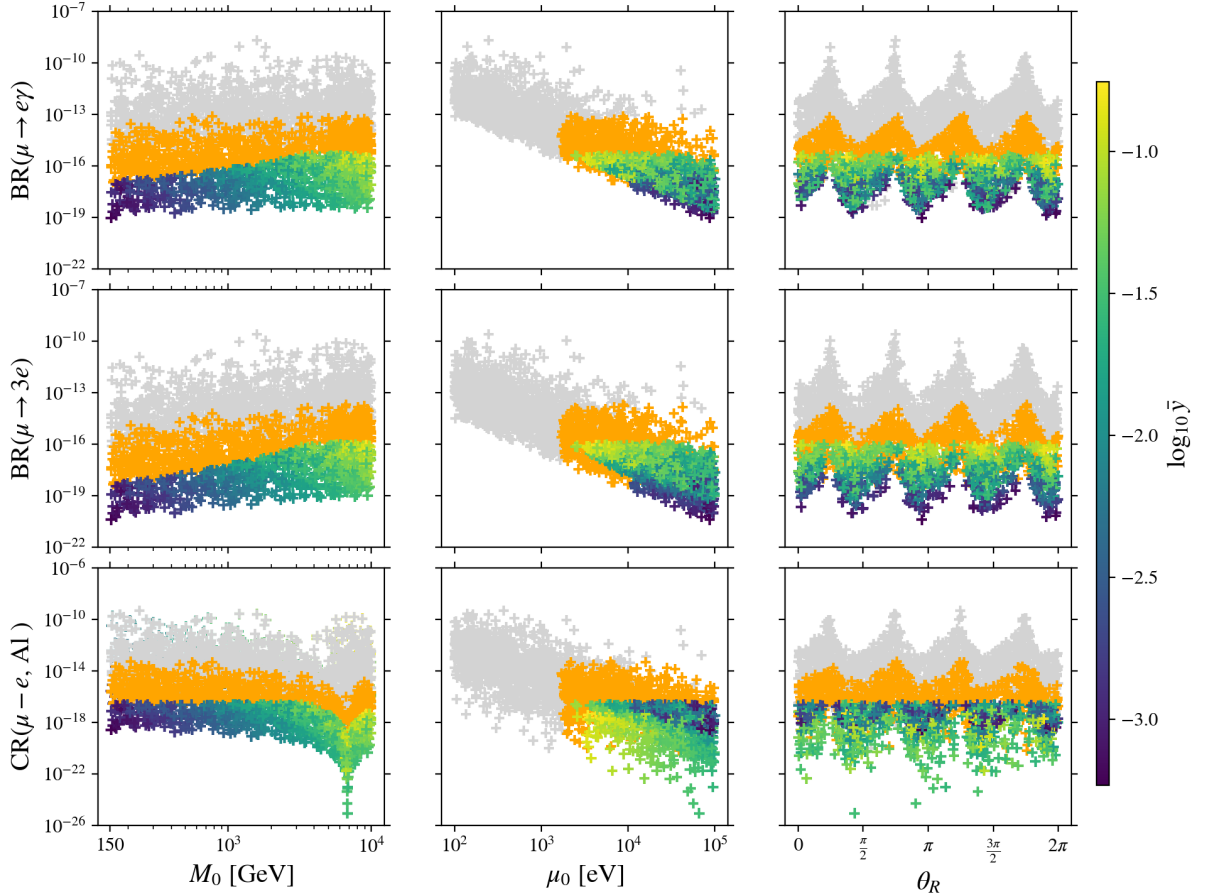


Figure 19: **Case 3 b.1), m odd and s even (or vice versa).** Results of numerical scan for $\text{BR}(\mu \rightarrow e\gamma)$, $\text{BR}(\mu \rightarrow 3e)$ and $\text{CR}(\mu - e, \text{Al})$ varying M_0 , μ_0 and θ_R in the ranges in eqs. (58), (57) and (56), respectively. As example of the group theory parameters $n = 20$, $m = 9$ and $s = 2$ is chosen. For conventions, see fig. 3.

as in fig. 11. We observe that the combinations of m even and s odd or vice versa lead to larger BRs and CR in average (up to a factor 25) than those with m and s both even or both odd. Analogous to Case 2), this is due to the enhancement of the BRs and CR for certain values of the angle θ_R for m even and s odd or vice versa, entailing larger averages, which does not occur for m and s both even or both odd. For light neutrino masses with IO and $m_0 = 0.015 \text{ eV}$ the plots shown in fig. 20 look very similar.

5 Comments on cLFV τ decays

We also consider the following cLFV decays of the tau lepton $\tau \rightarrow \mu\gamma$, $\tau \rightarrow e\gamma$, $\tau \rightarrow 3\mu$ and $\tau \rightarrow 3e$. As current experimental bounds on the BRs of these decays we use (all at 90% C.L.)

$$\begin{aligned} \text{BR}(\tau \rightarrow \mu\gamma) &< 4.2 \times 10^{-8} \quad (\text{Belle [75]}), & \text{BR}(\tau \rightarrow e\gamma) &< 3.3 \times 10^{-8} \quad (\text{Belle [76]}), \\ \text{BR}(\tau \rightarrow 3\mu) &< 1.9 \times 10^{-8} \quad (\text{Belle II [77]}), & \text{BR}(\tau \rightarrow 3e) &< 2.7 \times 10^{-8} \quad (\text{Belle [76]}). \end{aligned} \quad (84)$$

The prospective limits are

$$\begin{aligned} \text{BR}(\tau \rightarrow \mu\gamma) &< 6.9 \times 10^{-9} \quad (\text{Belle II [78]}), & \text{BR}(\tau \rightarrow e\gamma) &< 9 \times 10^{-9} \quad (\text{Belle II [78]}), \\ \text{BR}(\tau \rightarrow 3\mu) &< 3.6 \times 10^{-10} \quad (\text{Belle II [78]}), & \text{BR}(\tau \rightarrow 3e) &< 4.7 \times 10^{-10} \quad (\text{Belle II [78]}). \end{aligned} \quad (85)$$

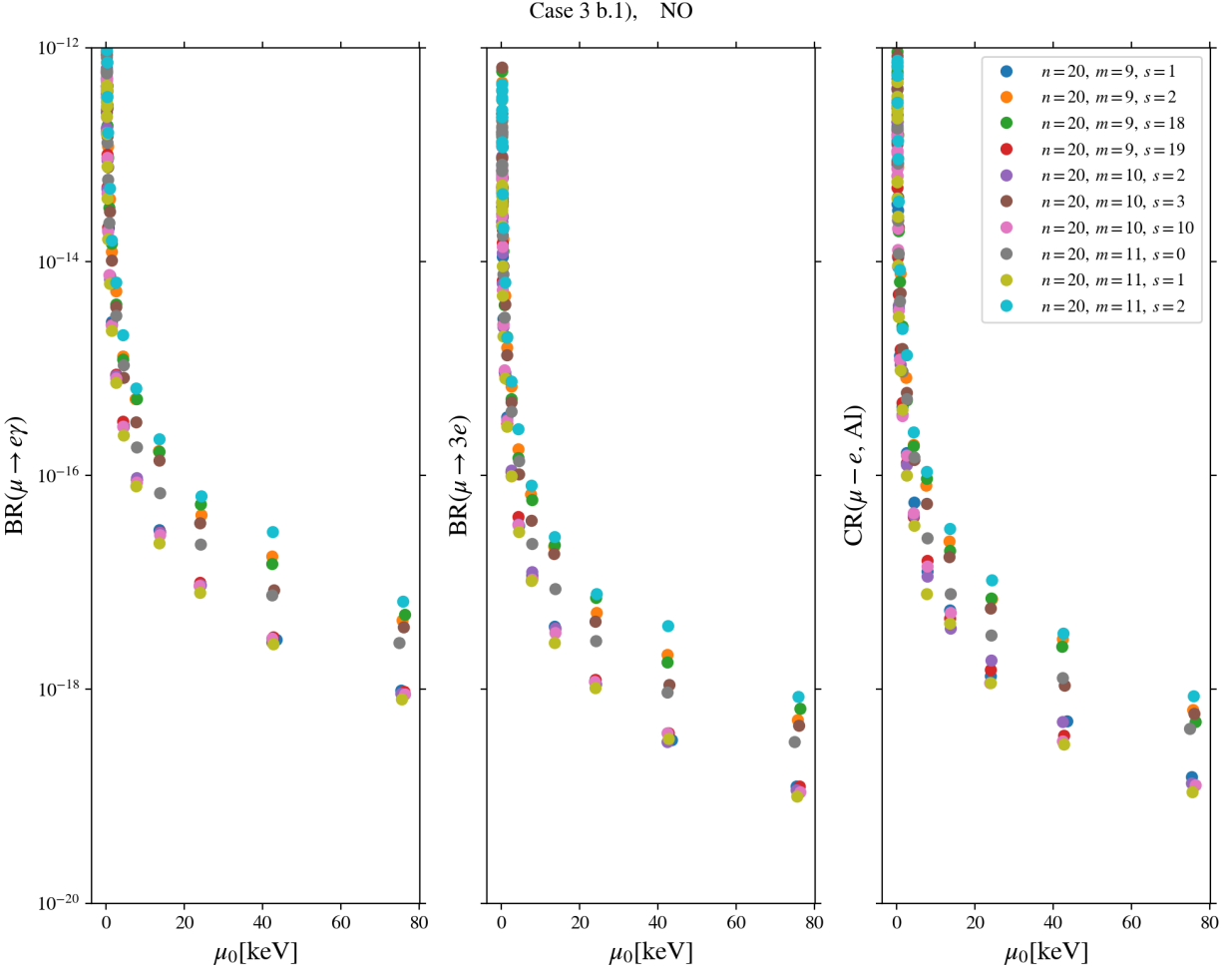


Figure 20: **Case 3 b.1).** Comparison of results for $\text{BR}(\mu \rightarrow e\gamma)$, $\text{BR}(\mu \rightarrow 3e)$ and $\text{CR}(\mu - e, \text{Al})$ for different combinations of m and s . The group index n is set to $n = 20$. For further conventions and details see fig. 11 for Case 2).

Before discussing the results of the numerical scans, we give simple formulae for $\eta_{\mu\tau}$ and $\eta_{e\tau}$ for Case 1) that are relevant for the cLFV decays $\tau \rightarrow \mu\gamma$, $\tau \rightarrow 3\mu$ and $\tau \rightarrow e\gamma$, $\tau \rightarrow 3e$, respectively, similar to $\eta_{e\mu}$ dominating the $\mu - e$ transitions. They read

$$\eta_{\mu\tau} = \frac{\eta'_0}{6} (2 \Delta y_{21}^2 - 3 (1 - 2 \sin^2 \theta_{13}) \Delta y_{31}^2) \quad (86)$$

and

$$\eta_{e\tau} = \frac{\eta'_0}{6} (2 \Delta y_{21}^2 + 3 (\sqrt{2 - 3 \sin^2 \theta_{13}} - \sin \theta_{13}) \sin \theta_{13} \Delta y_{31}^2) , \quad (87)$$

respectively, with Δy_{ij}^2 being defined in the vicinity of eq. (68). We see that, in particular, $\eta_{e\tau}$ has a form similar to $\eta_{e\mu}$. Numerical estimates for the corresponding BRs can be derived with the help of these formulae and the approximations found in section 4.2. For $\mu_0 = 1 \text{ keV}$ and $M_0 = 3 \text{ TeV}$ we get

$$\begin{aligned} \text{BR}(\tau \rightarrow \mu\gamma) &\approx 2.3 \times 10^{-14} , & \text{BR}(\tau \rightarrow 3\mu) &\approx 3.6 \times 10^{-15} , \\ \text{BR}(\tau \rightarrow e\gamma) &\approx 1.2 \times 10^{-15} , & \text{BR}(\tau \rightarrow 3e) &\approx 2.0 \times 10^{-16} \end{aligned} \quad (88)$$

for light neutrino masses with NO and $m_0 = 0.03 \text{ eV}$, while for IO light neutrino masses with $m_0 = 0.015 \text{ eV}$ we find

$$\begin{aligned} \text{BR}(\tau \rightarrow \mu\gamma) &\approx 4.2 \times 10^{-14} , & \text{BR}(\tau \rightarrow 3\mu) &\approx 6.6 \times 10^{-15} , \\ \text{BR}(\tau \rightarrow e\gamma) &\approx 1.4 \times 10^{-15} , & \text{BR}(\tau \rightarrow 3e) &\approx 2.3 \times 10^{-16} . \end{aligned} \quad (89)$$

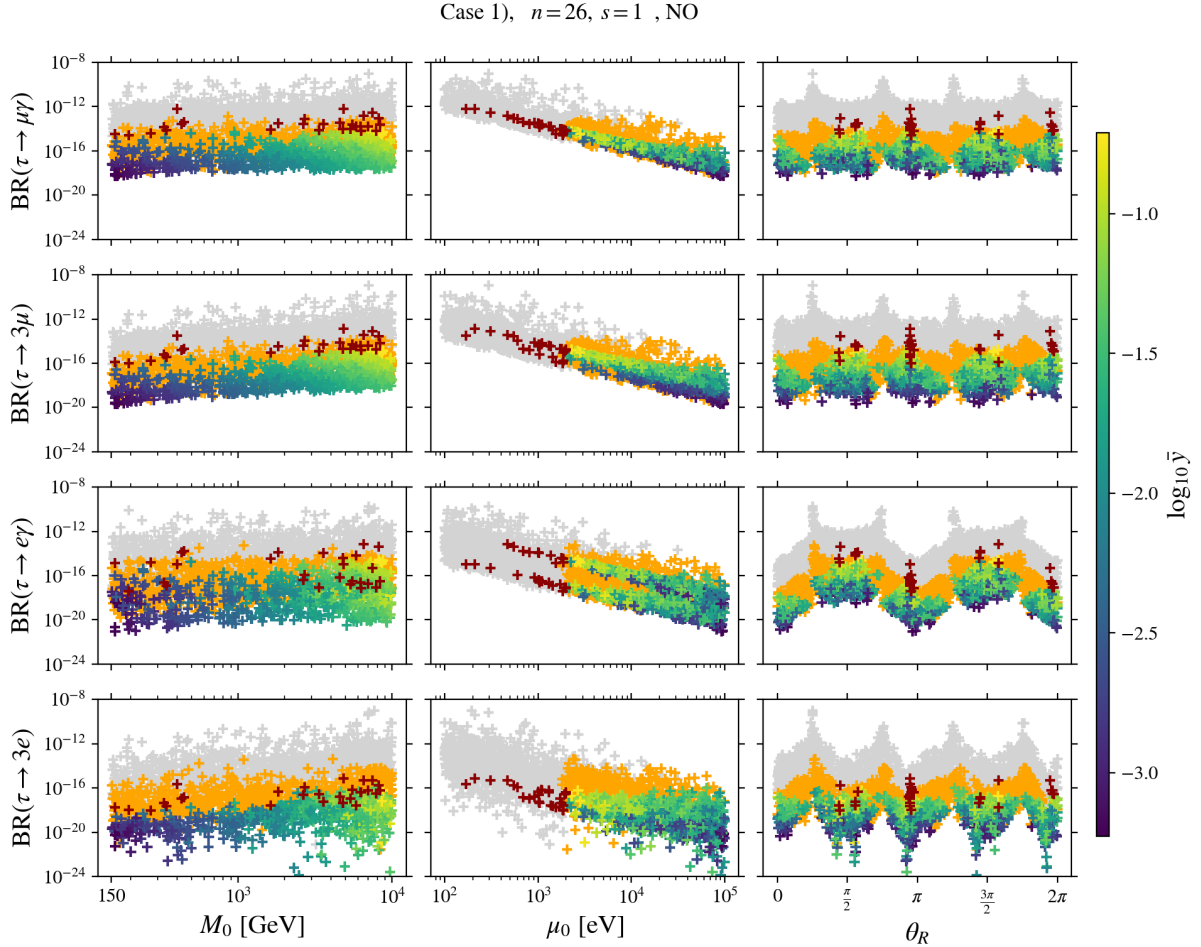


Figure 21: **Case 1).** Results of numerical scan for $\text{BR}(\tau \rightarrow \mu\gamma)$, $\text{BR}(\tau \rightarrow 3\mu)$, $\text{BR}(\tau \rightarrow e\gamma)$ and $\text{BR}(\tau \rightarrow 3e)$ varying M_0 , μ_0 and θ_R in the ranges in eqs. (58), (57) and (56), respectively. The parameters n and s are the same as in fig. 1. For conventions see fig. 3.

These already indicate that the presented scenario is most likely not constrained by the current nor by the prospective limits on the studied cLFV tau lepton decays, see eqs. (84) and (85). This observation is confirmed by the numerical scans that we have performed. As example, the results for $n = 26$, $s = 1$ and light neutrino masses with NO and $m_0 = 0.03$ eV are shown in fig. 21. The colour-coding is the same as in fig. 3 for the corresponding $\mu - e$ transitions. The largest values obtained for the different BRs for the viable data points are

$$\begin{aligned} \text{BR}(\tau \rightarrow \mu\gamma) &\lesssim 7 \times 10^{-15}, & \text{BR}(\tau \rightarrow 3\mu) &\lesssim 2 \times 10^{-15}, \\ \text{BR}(\tau \rightarrow e\gamma) &\lesssim 3 \times 10^{-15}, & \text{BR}(\tau \rightarrow 3e) &\lesssim 2 \times 10^{-16} \end{aligned} \quad (90)$$

and, thus, clearly inaccessible by the mentioned facilities. The observed dependence on the angle θ_R is driven by $\cos 2\theta_R$, like for the $\mu - e$ transitions, and is due to the fact that for $\cos 2\theta_R \approx 0$ at least one Yukawa coupling is large, compare eqs. (34)-(36), while for $|\cos 2\theta_R|$ large smaller values of the Yukawa couplings are accessible and, consequently, also smaller values of the BRs can be obtained. The results for light neutrino masses with IO and $m_0 = 0.015$ eV are similar and the upper limits obtained for the BRs are only slightly larger than those given in eq. (90). We have also performed numerical scans for $m_0 = 0$ and light neutrino masses with NO and IO, respectively, and obtain results that are qualitatively similar to those displayed in fig. 21.

Also for the other cases, Case 2) through Case 3 b.1), the values of the BRs are of similar order as those given in eq. (90) for the viable points in the scans and, thus, cannot be tested by current

and near-future experiments. We have checked that for Case 2) the BRs of the different studied cLFV tau lepton decays do not depend on the angle θ_R for t even that corresponds to u even, whereas the expected dependence on θ_R is found for t odd equivalent to u odd. Furthermore, the exact value of the parameter s is not directly relevant. For Case 3 a), we observe that the BRs of the cLFV tau lepton decays also have similar features as the studied $\mu - e$ transitions, i.e. for m and s being both even or both odd there is no dependence on the angle θ_R , while for m even and s odd or vice versa such a dependence is expected and usually a milder one is found in the numerical scans. Lastly, we have checked that statements analogous to those made for the $\mu - e$ transitions also hold for the cLFV tau lepton decays for Case 3 b.1).

6 Summary

We have studied a scenario in which light neutrino masses are generated via the ISS mechanism and a flavour and CP symmetry determine the flavour structure. The 3+3 gauge singlet fermions form three pairs of pseudo-Dirac states that are (nearly) degenerate in mass, because in the neutral lepton sector only the Dirac neutrino Yukawa matrix breaks G_f and CP to G_ν which is the direct product of a Z_2 symmetry and CP. Among charged leptons the residual symmetry is $G_e = Z_3$ and in the chosen basis the charged lepton mass matrix is diagonal with three free parameters corresponding to the charged lepton masses. There are four cases, Case 1) through Case 3 b.1), that lead to four different types of lepton mixing patterns. In the neutral lepton sector, the parameter space is spanned by the three Yukawa couplings y_f , the two angles θ_L and θ_R , all contained in the Dirac neutrino Yukawa matrix, as well as the two scales M_0 and μ_0 . The couplings y_f are fixed by the light neutrino masses, the angle θ_L is adjusted such that the lepton mixing angles are accommodated well and the two scales M_0 and μ_0 determine the mass of the heavy sterile states and the size of lepton number breaking, respectively. The angle θ_R is a free parameter and varied in its entire range, $0 \leq \theta_R \leq 2\pi$.

We have focussed on the BRs of the cLFV decays $\mu \rightarrow e\gamma$ and $\mu \rightarrow 3e$ and $\mu - e$ conversion in nuclei, both analytically and numerically. To study these processes numerically, we have chosen examples for each of the cases which can accommodate the lepton mixing angles well. While current limits on these processes do not constrain the studied parameter space, future bounds can exclude part of it. In particular, the expected limit on $\mu \rightarrow 3e$ from Mu3E Phase 2 and the prospective bounds on $\mu - e$ conversion in aluminium from COMET and Mu2e set relevant restrictions. If these are passed, the size of $\text{BR}(\mu \rightarrow e\gamma)$ turns out to be about two orders of magnitude smaller than the future limit from MEG II.

We have also analysed the signal strength of four cLFV tau lepton decays, $\tau \rightarrow \mu\gamma$, $\tau \rightarrow e\gamma$, $\tau \rightarrow 3\mu$ and $\tau \rightarrow 3e$. If the lepton mixing angles are accommodated well and the future bounds on the three most relevant $\mu - e$ transitions are passed, the BRs of these decays are rather suppressed, below 10^{-14} , meaning these are much lower than the expected limits from Belle II.

We have observed that the BRs and CR reveal different dependences on the free angle θ_R , depending on the choice of the case, Case 1) through Case 3 b.1), and the parameters determining the residual symmetries: for Case 1) they always have such a dependence, while for Case 2) it is decisive whether the parameter t is even or odd, i.e. for t even there is no such dependence, whereas for t odd a dependence is observed. For Case 3 a) and Case 3 b.1) we have found that for the parameters m and s both even or both odd no dependence exists, while for one of them being even and the other one odd a dependence similar to the one observed for Case 1) is seen. Nevertheless, it is usually milder for Case 3 a) than for the other cases.

The phenomenology of this option, option 2, is very different from that of the already studied option 1 [45], where only the Majorana mass matrix μ_S of the gauge singlets S_j , $j = 1, 2, 3$, carries non-trivial flavour structure in the neutral lepton sector, since in the case of option 1 all cLFV signals are highly suppressed. For this reason, it can be interesting to consider further options and variants of this scenario.

Acknowledgements

We thank Miguel G. Folgado for help with the local computer cluster. This work is supported by the Spanish MINECO through the Ramón y Cajal programme RYC2018-024529-I, the FPI fellowship PRE2021-098730, by the national grant PID2020-113644GB-I00, by the Generalitat Valenciana through PROMETEO/2021/083 as well as by the European Union's Horizon 2020 research and innovation programme under the Marie Skłodowska-Curie grant agreement No. 860881 (HIDDeV network) and under the Marie Skłodowska-Curie Staff Exchange grant agreement No. 101086085 (ASYMMETRY).

A Basics of group theory of $\Delta(3n^2)$ and $\Delta(6n^2)$

For completeness, the basics of the discrete groups $\Delta(3n^2)$ and $\Delta(6n^2)$ are presented. The groups $\Delta(3n^2)$, $n \geq 2$ integer, can be described with three generators a , c and d that satisfy the relations

$$a^3 = e, \quad c^n = e, \quad d^n = e, \quad cd = dc, \quad aca^{-1} = c^{-1}d^{-1}, \quad ada^{-1} = c, \quad (91)$$

where e is the neutral element of the group [31]. As detailed in [32], the groups $\Delta(6n^2)$, $n \geq 2$ integer, can be generated by adding a further generator b . The relations involving this generator read

$$b^2 = e, \quad (ab)^2 = e, \quad bcb^{-1} = d^{-1}, \quad bdb^{-1} = c^{-1}. \quad (92)$$

For the trivial representation **1** all elements of the group are represented by the character 1. The representation matrices of the generators, $a(\mathbf{3})$, $b(\mathbf{3})$, $c(\mathbf{3})$ and $d(\mathbf{3})$, are taken in one irreducible, faithful, complex three-dimensional representation, called **3**, of $\Delta(6n^2)$ as²⁰

$$a(\mathbf{3}) = \begin{pmatrix} 1 & 0 & 0 \\ 0 & \omega & 0 \\ 0 & 0 & \omega^2 \end{pmatrix}, \quad b(\mathbf{3}) = \begin{pmatrix} 1 & 0 & 0 \\ 0 & 0 & \omega^2 \\ 0 & \omega & 0 \end{pmatrix}, \quad (93)$$

$$c(\mathbf{3}) = \frac{1}{3} \begin{pmatrix} 1 + 2\cos\phi_n & 1 - \cos\phi_n - \sqrt{3}\sin\phi_n & 1 - \cos\phi_n + \sqrt{3}\sin\phi_n \\ 1 - \cos\phi_n + \sqrt{3}\sin\phi_n & 1 + 2\cos\phi_n & 1 - \cos\phi_n - \sqrt{3}\sin\phi_n \\ 1 - \cos\phi_n - \sqrt{3}\sin\phi_n & 1 - \cos\phi_n + \sqrt{3}\sin\phi_n & 1 + 2\cos\phi_n \end{pmatrix}$$

with $\omega = e^{\frac{2\pi i}{3}}$ and $\phi_n = \frac{2\pi}{n}$. The form of $d(\mathbf{3})$ can be calculated using $d(\mathbf{3}) = a(\mathbf{3})^2c(\mathbf{3})a(\mathbf{3})$. We note that the representation **3** corresponds to **3₁₍₁₎** in the nomenclature of [32].

If the index n of the group $\Delta(6n^2)$ is even, there exists an irreducible, unfaithful, real three-dimensional representation **3'**. The form of the representation matrices $a(\mathbf{3}')$, $b(\mathbf{3}')$ and $c(\mathbf{3}')$ is then

$$a(\mathbf{3}') = a(\mathbf{3}), \quad b(\mathbf{3}') = b(\mathbf{3}), \quad c(\mathbf{3}') = \frac{1}{3} \begin{pmatrix} -1 & 2 & 2 \\ 2 & -1 & 2 \\ 2 & 2 & -1 \end{pmatrix} \quad (94)$$

and $d(\mathbf{3}') = a(\mathbf{3}')^2c(\mathbf{3}')a(\mathbf{3}')$. Note that they do not depend on the index n of the group. The group generated by the representation matrices $g(\mathbf{3}')$ has 24 elements and corresponds to the group $\Delta(24)$. The representation **3'** together with the one generated by the representation matrices $a(\mathbf{3}')$, $c(\mathbf{3}')$, $d(\mathbf{3}')$ and $-b(\mathbf{3}')$ are the only real three-dimensional representations in a generic group $\Delta(6n^2)$ with even n and $3 \nmid n$. They are denoted as **3_{1(n/2)}** and **3_{2(n/2)}** in [32], respectively.

²⁰The similarity transformation $U = \frac{1}{\sqrt{3}} \begin{pmatrix} 1 & 1 & 1 \\ \omega^2 & \omega & 1 \\ \omega & \omega^2 & 1 \end{pmatrix}$ has to be applied to the generators given in eq. (93) in order to obtain the form of the representation matrices as found in [32].

B Relevant matrices $\Omega(\mathbf{3})$, $\Omega(\mathbf{3}')$ and $R_{ij}(\theta)$

As supplementary material the different forms of the matrices $\Omega(\mathbf{3})$ and $\Omega(\mathbf{3}')$ for the cases, Case 1) through Case 3 b.1), as well as the form of the rotation matrices $R_{ij}(\theta_L)$ and $R_{kl}(\theta_R)$ for each combination are collected in this appendix; for further details see [47].

For Case 1) the following form of $\Omega(\mathbf{3})$ and $\Omega(\mathbf{3}')$ is used

$$\Omega(s)(\mathbf{3}) = e^{i\phi_s} U_{\text{TB}} \begin{pmatrix} 1 & 0 & 0 \\ 0 & e^{-3i\phi_s} & 0 \\ 0 & 0 & -1 \end{pmatrix}, \quad (95)$$

$$\Omega(s \text{ even})(\mathbf{3}') = U_{\text{TB}} \text{ and } \Omega(s \text{ odd})(\mathbf{3}') = U_{\text{TB}} \begin{pmatrix} i & 0 & 0 \\ 0 & 1 & 0 \\ 0 & 0 & i \end{pmatrix}, \quad (96)$$

where the matrix U_{TB} encodes tri-bimaximal (TB) mixing,

$$U_{\text{TB}} = \begin{pmatrix} \sqrt{2/3} & \sqrt{1/3} & 0 \\ -\sqrt{1/6} & \sqrt{1/3} & \sqrt{1/2} \\ -\sqrt{1/6} & \sqrt{1/3} & -\sqrt{1/2} \end{pmatrix}, \quad (97)$$

and ϕ_s is defined as $\phi_s = \frac{\pi s}{n}$. The rotation matrices $R_{ij}(\theta_L)$ and $R_{kl}(\theta_R)$ read

$$R_{13}(\theta_L) = \begin{pmatrix} \cos \theta_L & 0 & \sin \theta_L \\ 0 & 1 & 0 \\ -\sin \theta_L & 0 & \cos \theta_L \end{pmatrix} \text{ and } R_{13}(\theta_R) = \begin{pmatrix} \cos \theta_R & 0 & \sin \theta_R \\ 0 & 1 & 0 \\ -\sin \theta_R & 0 & \cos \theta_R \end{pmatrix}. \quad (98)$$

For Case 2) we use as matrices $\Omega(\mathbf{3})$ and $\Omega(\mathbf{3}')$

$$\Omega(s, t)(\mathbf{3}) = \Omega(u, v)(\mathbf{3}) = e^{i\phi_v/6} U_{\text{TB}} R_{13} \left(-\frac{\phi_u}{2} \right) \begin{pmatrix} 1 & 0 & 0 \\ 0 & e^{-i\phi_v/2} & 0 \\ 0 & 0 & -i \end{pmatrix}, \quad (99)$$

$$\Omega(s \text{ even}, t \text{ even})(\mathbf{3}') = U_{\text{TB}} \begin{pmatrix} 1 & 0 & 0 \\ 0 & 1 & 0 \\ 0 & 0 & i \end{pmatrix}, \quad (100)$$

$$\Omega(s \text{ even}, t \text{ odd})(\mathbf{3}') = e^{-i\pi/4} U_{\text{TB}} R_{13} \left(\frac{\pi}{4} \right) \begin{pmatrix} -i & 0 & 0 \\ 0 & e^{-i\pi/4} & 0 \\ 0 & 0 & 1 \end{pmatrix}, \quad (101)$$

$$\Omega(s \text{ odd}, t \text{ even})(\mathbf{3}') = U_{\text{TB}} \begin{pmatrix} i & 0 & 0 \\ 0 & 1 & 0 \\ 0 & 0 & 1 \end{pmatrix}, \quad (102)$$

$$\Omega(s \text{ odd}, t \text{ odd})(\mathbf{3}') = e^{-3i\pi/4} U_{\text{TB}} R_{13} \left(\frac{\pi}{4} \right) \begin{pmatrix} -i & 0 & 0 \\ 0 & e^{i\pi/4} & 0 \\ 0 & 0 & 1 \end{pmatrix}. \quad (103)$$

Here, ϕ_u and ϕ_v are $\phi_u = \frac{\pi u}{n}$ and $\phi_v = \frac{\pi v}{n}$, respectively. The rotation matrices $R_{ij}(\theta_L)$ and $R_{kl}(\theta_R)$ act both in the (13)-plane, see eq. (98).

The matrices $\Omega(\mathbf{3})$ and $\Omega(\mathbf{3}')$ for Case 3 a) and Case 3 b.1) are taken to be of the form

$$\Omega(s, m)(\mathbf{3}) = e^{i\phi_s} \begin{pmatrix} 1 & 0 & 0 \\ 0 & \omega & 0 \\ 0 & 0 & \omega^2 \end{pmatrix} U_{\text{TB}} \begin{pmatrix} 1 & 0 & 0 \\ 0 & e^{-3i\phi_s} & 0 \\ 0 & 0 & -1 \end{pmatrix} R_{13}(\phi_m) , \quad (104)$$

$$\Omega(s \text{ even})(\mathbf{3}') = \begin{pmatrix} 1 & 0 & 0 \\ 0 & \omega & 0 \\ 0 & 0 & \omega^2 \end{pmatrix} U_{\text{TB}} \begin{pmatrix} 1 & 0 & 0 \\ 0 & 1 & 0 \\ 0 & 0 & -1 \end{pmatrix} , \quad (105)$$

$$\Omega(s \text{ odd})(\mathbf{3}') = \begin{pmatrix} 1 & 0 & 0 \\ 0 & \omega & 0 \\ 0 & 0 & \omega^2 \end{pmatrix} U_{\text{TB}} \begin{pmatrix} i & 0 & 0 \\ 0 & -1 & 0 \\ 0 & 0 & -i \end{pmatrix} , \quad (106)$$

where ϕ_s and ϕ_m are given by $\phi_s = \frac{\pi s}{n}$ and $\phi_m = \frac{\pi m}{n}$, respectively, and $\omega = e^{\frac{2\pi i}{3}}$. The rotation matrix $R_{ij}(\theta_L)$ is

$$R_{12}(\theta_L) = \begin{pmatrix} \cos \theta_L & \sin \theta_L & 0 \\ -\sin \theta_L & \cos \theta_L & 0 \\ 0 & 0 & 1 \end{pmatrix} , \quad (107)$$

while the form of $R_{kl}(\theta_R)$ depends on whether m is even or odd. For m even it is given by

$$R_{kl}(\theta_R) = R_{12}(\theta_R) \text{ and } R_{kl}(\theta_R) = R_{23}(\theta_R) = \begin{pmatrix} 1 & 0 & 0 \\ 0 & \cos \theta_R & \sin \theta_R \\ 0 & -\sin \theta_R & \cos \theta_R \end{pmatrix} \quad (108)$$

for m odd. In the latter situation the permutation matrix P_{kl}^{ij} is also needed and it reads

$$P_{23}^{12} = P_{13} = \begin{pmatrix} 0 & 0 & 1 \\ 0 & 1 & 0 \\ 1 & 0 & 0 \end{pmatrix} . \quad (109)$$

C Description of numerical scan

In this appendix, we provide details on the numerical analysis. We use as free parameters the two mass scales μ_0 and M_0 and the angle θ_R . These are varied according to the description found in section 4.1.2. Having generated values for these three, we impose a certain light neutrino mass ordering, NO or IO, and fix the lightest neutrino mass m_0 to one of the benchmark values, m_0^{bm} , mentioned in section 4.1.1. With this information, we determine the three Yukawa couplings y_f using the analytic form of the eigenvalues of the light neutrino mass matrix m_ν at leading order, see eq. (22) and for examples of the eigenvalues eqs. (26) and (34) (we remind that their exact form depends in general on the considered case, the group theory parameters, the choice of the CP symmetry, the light neutrino mass ordering, the value of the lightest neutrino mass m_0 and potentially on the value of θ_R). This is accomplished by minimising the χ^2 -function

$$\chi_m^2(y_f) = \left(\frac{\Delta m_{\text{sol}}^2(y_f) - (\Delta m_{\text{sol}}^2)^{\text{bf}}}{\sigma_{\Delta m_{\text{sol}}^2}} \right)^2 + \left(\frac{\Delta m_{\text{atm}}^2(y_f) - (\Delta m_{\text{atm}}^2)^{\text{bf}}}{\sigma_{\Delta m_{\text{atm}}^2}} \right)^2 + w \left(m_0(y_f) - m_0^{\text{bm}} \right)^2 \quad (110)$$

with $(\Delta m_{\text{sol}}^2)^{\text{bf}}$ and $(\Delta m_{\text{atm}}^2)^{\text{bf}}$ being the best-fit values of the solar and the atmospheric mass squared difference as well as $\sigma_{\Delta m_{\text{sol}}^2}$ and $\sigma_{\Delta m_{\text{atm}}^2}$ being the corresponding 1σ errors [49].²¹ Furthermore, the quantity w is a weighting factor introduced in order to achieve one of the benchmark values of m_0 and, for concreteness, we take $w = 1000$. This minimisation is performed with the function `differential_evolution` of the Python package NumPy. In the next step, we consider the

²¹In case the 1σ errors for e.g. $\Delta m_{\text{sol}}^2(y_f) > (\Delta m_{\text{sol}}^2)^{\text{bf}}$ and for $\Delta m_{\text{sol}}^2(y_f) < (\Delta m_{\text{sol}}^2)^{\text{bf}}$ are different, we use the smaller one of the two.

nine-by-nine mass matrix \mathcal{M}_{Maj} , see eq. (2), with the computed values of the Yukawa couplings and the chosen values of μ_0 , M_0 and θ_R . We fix θ_L such that the χ^2 -function

$$\chi_\theta^2(\theta_L) = \left(\frac{\sin^2 \theta_{12}(\theta_L) - (\sin^2 \theta_{12})^{\text{bf}}}{\sigma_{\sin^2 \theta_{12}}} \right)^2 + \left(\frac{\sin^2 \theta_{13}(\theta_L) - (\sin^2 \theta_{13})^{\text{bf}}}{\sigma_{\sin^2 \theta_{13}}} \right)^2 + \left(\frac{\sin^2 \theta_{23}(\theta_L) - (\sin^2 \theta_{23})^{\text{bf}}}{\sigma_{\sin^2 \theta_{23}}} \right)^2 \quad (111)$$

is minimised. The quantities $(\sin^2 \theta_{ij})^{\text{bf}}$ denote the experimental best-fit values and $\sigma_{\sin^2 \theta_{ij}}$ the corresponding 1σ errors [49]. In the case of the ISS mechanism, i.e. for $|\mu_S| \ll |m_D| \ll |\tilde{M}_{NS}|$ corresponding to $\mu_0 \ll y_f \langle H \rangle \ll M_0$, the eigenvalues of the matrix \mathcal{M}_{Maj} are strongly hierarchical (three are of order sub-eV and six of order sub-TeV to TeV). This requires a high precision in the diagonalisation of this matrix and the extraction of the unitary matrix \mathcal{U} and, consequently, \tilde{U}_ν , see eqs. (3) and (4). It can be achieved by setting the precision to 60 digits using the library `mpmath`.²² The diagonalisation itself is performed with the function `eighe` of this library. We have checked that the resulting light neutrino masses are consistent with the chosen benchmark value of m_0 and the best-fit values of the mass squared differences such that $\chi_m^2(y_f) \lesssim 0.1$. The Yukawa couplings y_f and the angle θ_L could be fixed in one step by diagonalising the matrix \mathcal{M}_{Maj} , extracting the eigenvalues and the matrix \mathcal{U} , and minimising $\chi_{\text{tot}}^2(y_f, \theta_L) = \chi_m^2(y_f, \theta_L) + \chi_\theta^2(y_f, \theta_L)$ with χ_m^2 and χ_θ^2 defined analogously as in eqs. (110) and (111), respectively. However, this requires an increased time of computation and, at the same time, leads to results very similar to those obtained by the described procedure.

After having adjusted y_f and θ_L all parameters of the neutral lepton sector are determined and the BRs and CR are computed with the formulae found in [70, 71].

D Supplementary plots for Case 3 b.1)

Here, we display three further figures that evidence the dependence of the BRs and CR on the free angle θ_R in the $\frac{s}{n} - \theta_L$ -plane for examples of the combinations m odd and s even, see figs. 22 and 23, or vice versa, see fig. 24.

²²Using an even higher precision does not affect the results.

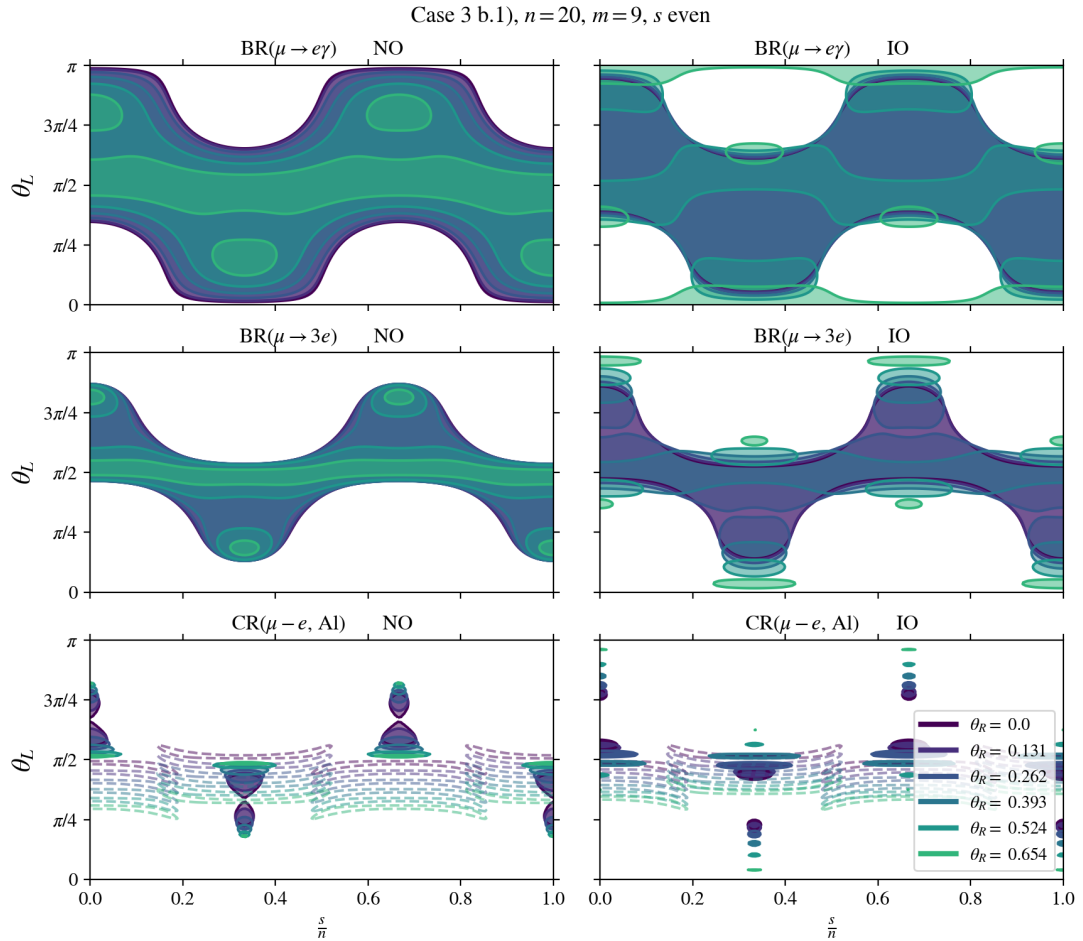


Figure 22: **Case 3 b.1), m odd and s even.** Predictions for $\text{BR}(\mu \rightarrow e\gamma)$, $\text{BR}(\mu \rightarrow 3e)$ and $\text{CR}(\mu - e, \text{Al})$ in the $\frac{s}{n} - \theta_L$ -plane in the upper, middle and lower row for six different values of θ_R . The group theory parameters are chosen as $n = 20$ and $m = 9$. Conventions are analogous as in fig. 6 for Case 2) and t odd (u odd). In fig. 16 in the main text the plots for $\theta_R = 0$ are displayed.

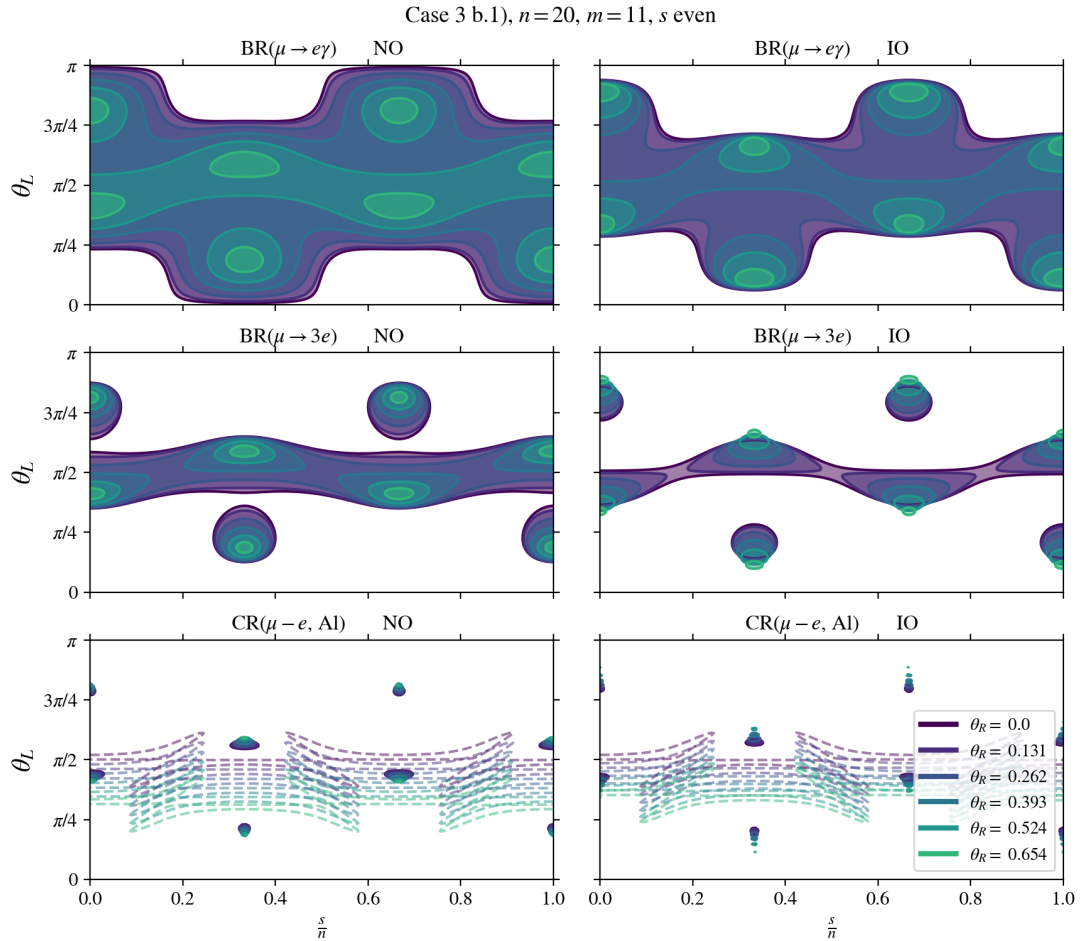


Figure 23: **Case 3 b.1), m odd and s even.** Predictions for $\text{BR}(\mu \rightarrow e\gamma)$, $\text{BR}(\mu \rightarrow 3e)$ and $\text{CR}(\mu - e, \text{Al})$ in the $\frac{s}{n} - \theta_L$ -plane in the upper, middle and lower row for six different values of θ_R . The group theory parameters are chosen as $n = 20$ and $m = 11$. For conventions see fig. 22. In fig. 17 in the main text the plots for $\theta_R = 0$ are displayed.

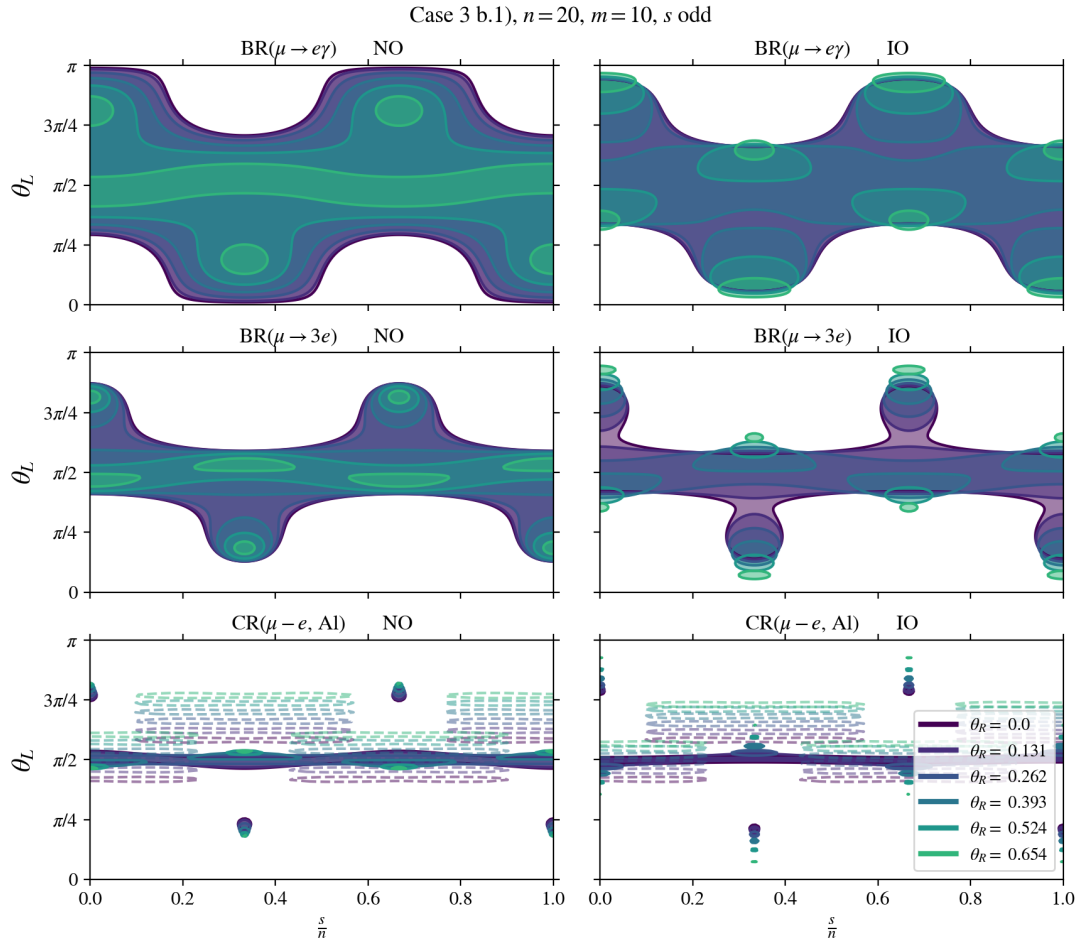


Figure 24: **Case 3 b.1), m even and s odd.** Predictions for $\text{BR}(\mu \rightarrow e\gamma)$, $\text{BR}(\mu \rightarrow 3e)$ and $\text{CR}(\mu - e, \text{Al})$ in the $\frac{s}{n} - \theta_L$ -plane in the upper, middle and lower row for six different values of θ_R . The group theory parameters are chosen as $n = 20$ and $m = 10$. For conventions see fig. 22. The plots shown in fig. 15 in the main text are very similar to the ones obtained for the specific choice $\theta_R = 0$ for $m = 10$ and s odd.

References

- [1] P. Minkowski, Phys. Lett. B **67** (1977), 421-428.
- [2] T. Yanagida, in *Proceedings of the Workshop on the Unified Theory and the Baryon Number in the Universe* (O. Sawada and A. Sugamoto, eds.), KEK Tsukuba, Japan, 1979, p. 95.
- [3] S. L. Glashow, *The future of elementary particle physics*, in *Proceedings of the 1979 Cargèse Summer Institute on Quarks and Leptons* (M. Lévy, J.-L. Basdevant, D. Speiser, J. Weyers, R. Gastmans, and M. Jacob, eds.), Plenum Press, New York, 1980, pp. 687-713.
- [4] M. Gell-Mann, P. Ramond, and R. Slansky, *Complex spinors and unified theories*, in *Supergravity* (P. van Nieuwenhuizen and D. Z. Freedman, eds.), North Holland, Amsterdam, 1979, p. 315.
- [5] R. N. Mohapatra and G. Senjanovic, Phys. Rev. Lett. **44** (1980) 912.
- [6] M. Magg and C. Wetterich, Phys. Lett. B **94** (1980), 61-64.
- [7] J. Schechter and J. W. F. Valle, Phys. Rev. D **22** (1980), 2227.
- [8] T. P. Cheng and L. F. Li, Phys. Rev. D **22** (1980), 2860.
- [9] G. Lazarides, Q. Shafi and C. Wetterich, Nucl. Phys. B **181** (1981), 287-300.
- [10] C. Wetterich, Nucl. Phys. B **187** (1981), 343-375.
- [11] R. N. Mohapatra and G. Senjanovic, Phys. Rev. D **23** (1981), 165.
- [12] R. Foot, H. Lew, X. G. He and G. C. Joshi, Z. Phys. C **44** (1989), 441.
- [13] R. N. Mohapatra and J. W. F. Valle, Phys. Rev. D **34** (1986), 1642.
- [14] R. N. Mohapatra, Phys. Rev. Lett. **56** (1986), 561-563.
- [15] J. Bernabeu, A. Santamaria, J. Vidal, A. Mendez and J. W. F. Valle, Phys. Lett. B **187** (1987), 303-308.
- [16] M. C. Gonzalez-Garcia and J. W. F. Valle, Phys. Lett. B **216** (1989), 360-366.
- [17] F. Feruglio, C. Hagedorn and R. Ziegler, JHEP **1307** (2013) 027 [arXiv:1211.5560 [hep-ph]].
- [18] M. Holthausen, M. Lindner and M. A. Schmidt, JHEP **1304** (2013) 122 [arXiv:1211.6953 [hep-ph]].
- [19] M.-C. Chen, M. Fallbacher, K. T. Mahanthappa, M. Ratz and A. Trautner, Nucl. Phys. B **883** (2014) 267 [arXiv:1402.0507 [hep-ph]].
- [20] G. Ecker, W. Grimus and H. Neufeld, Nucl. Phys. B **247** (1984) 70.
- [21] G. Ecker, W. Grimus and H. Neufeld, J. Phys. A **20** (1987) L807.
- [22] H. Neufeld, W. Grimus and G. Ecker, Int. J. Mod. Phys. A **3** (1988) 603.
- [23] W. Grimus and M. N. Rebelo, Phys. Rept. **281** (1997) 239 [arXiv:hep-ph/9506272].
- [24] P. F. Harrison and W. G. Scott, Phys. Lett. B **535** (2002) 163 [arXiv:hep-ph/0203209].
- [25] W. Grimus and L. Lavoura, Phys. Lett. B **579** (2004) 113 [arXiv:hep-ph/0305309].
- [26] S. F. King, J. Phys. G **42** (2015), 123001 [arXiv:1510.02091 [hep-ph]].

[27] F. Feruglio and A. Romanino, Rev. Mod. Phys. **93** (2021) no.1, 015007 [arXiv:1912.06028 [hep-ph]].

[28] H. Ishimori, T. Kobayashi, H. Ohki, Y. Shimizu, H. Okada and M. Tanimoto, Prog. Theor. Phys. Suppl. **183** (2010), 1-163 [arXiv:1003.3552 [hep-th]].

[29] T. Kobayashi, H. Ohki, H. Okada, Y. Shimizu and M. Tanimoto, *An Introduction to Non-Abelian Discrete Symmetries for Particle Physicists*, 2022, ISBN 978-3-662-64678-6, 978-3-662-64679-3.

[30] W. Grimus and P. O. Ludl, J. Phys. A **45** (2012) 233001 [arXiv:1110.6376 [hep-ph]].

[31] C. Luhn, S. Nasri and P. Ramond, J. Math. Phys. **48** (2007), 073501 [arXiv:hep-th/0701188 [hep-th]].

[32] J. A. Escobar and C. Luhn, J. Math. Phys. **50** (2009), 013524 [arXiv:0809.0639 [hep-th]].

[33] C. Hagedorn, A. Meroni and E. Molinaro, Nucl. Phys. B **891** (2015), 499-557 [arXiv:1408.7118 [hep-ph]].

[34] G. J. Ding, S. F. King and T. Neder, JHEP **1412** (2014) 007 [arXiv:1409.8005 [hep-ph]].

[35] G. J. Ding and S. F. King, Phys. Rev. D **93** (2016) 025013 [arXiv:1510.03188 [hep-ph]].

[36] S. F. King and T. Neder, Phys. Lett. B **736** (2014) 308 [arXiv:1403.1758 [hep-ph]].

[37] G. J. Ding, S. F. King, C. Luhn and A. J. Stuart, JHEP **1305** (2013) 084 [arXiv:1303.6180 [hep-ph]].

[38] F. Feruglio, C. Hagedorn and R. Ziegler, Eur. Phys. J. C **74** (2014) 2753 [arXiv:1303.7178 [hep-ph]].

[39] G. J. Ding, S. F. King and A. J. Stuart, JHEP **1312** (2013) 006 [arXiv:1307.4212 [hep-ph]].

[40] C. C. Li and G. J. Ding, Nucl. Phys. B **881** (2014) 206 [arXiv:1312.4401 [hep-ph]].

[41] C. C. Li and G. J. Ding, JHEP **1508** (2015) 017 [arXiv:1408.0785 [hep-ph]].

[42] G. J. Ding and Y. L. Zhou, Chin. Phys. C **39** (2015) 2, 021001 [arXiv:1312.5222 [hep-ph]].

[43] G. J. Ding and Y. L. Zhou, JHEP **1406** (2014) 023 [arXiv:1404.0592 [hep-ph]].

[44] G. J. Ding and S. F. King, Phys. Rev. D **89** (2014) 9, 093020 [arXiv:1403.5846 [hep-ph]].

[45] C. Hagedorn, J. Kriewald, J. Orloff and A. M. Teixeira, Eur. Phys. J. C **82** (2022) no.3, 194 [arXiv:2107.07537 [hep-ph]].

[46] H. Hettmansperger, M. Lindner and W. Rodejohann, JHEP **04** (2011), 123 [arXiv:1102.3432 [hep-ph]].

[47] M. Drewes, Y. Georis, C. Hagedorn and J. Klarić, JHEP **12** (2022), 044 [arXiv:2203.08538 [hep-ph]].

[48] M. Blennow, E. Fernández-Martínez, J. Hernández-García, J. López-Pavón, X. Marcano and D. Naredo-Tuero, JHEP **08** (2023), 030 [arXiv:2306.01040 [hep-ph]].

[49] I. Esteban, M. C. Gonzalez-Garcia, M. Maltoni, T. Schwetz and A. Zhou, JHEP **09** (2020), 178 [arXiv:2007.14792 [hep-ph]], NuFIT 5.3 (2024), www.nu-fit.org.

[50] N. Aghanim *et al.* [Planck], Astron. Astrophys. **641** (2020), A6 [erratum: Astron. Astrophys. **652** (2021), C4] [arXiv:1807.06209 [astro-ph.CO]].

- [51] K. Afanaciev *et al.* [MEG II], Eur. Phys. J. C **84** (2024) no.3, 216 [arXiv:2310.12614 [hep-ex]].
- [52] U. Bellgardt *et al.* [SINDRUM], Nucl. Phys. B **299** (1988), 1-6.
- [53] W. H. Bertl *et al.* [SINDRUM II], Eur. Phys. J. C **47** (2006), 337-346.
- [54] P. Wintz, *Prepared for 29th International Conference on High-Energy Physics (ICHEP 98), Vancouver, Canada, 23-29 Jul 1998.*
- [55] A. M. Baldini *et al.* [MEG II], Symmetry **13** (2021) no.9, 1591 [arXiv:2107.10767 [hep-ex]].
- [56] A. Blondel, A. Bravar, M. Pohl, S. Bachmann, N. Berger, M. Kiehn, A. Schonning, D. Wiedner, B. Windelband and P. Eckert, *et al.* [arXiv:1301.6113 [physics.ins-det]].
- [57] R. Abramishvili *et al.* [COMET], PTEP **2020** (2020) no.3, 033C01 [arXiv:1812.09018 [physics.ins-det]].
- [58] L. Bartoszek *et al.* [Mu2e], arXiv:1501.05241 [physics.ins-det].
- [59] L. Allwicher, P. Arnan, D. Barducci and M. Nardecchia, JHEP **10** (2021), 129 [arXiv:2108.00013 [hep-ph]].
- [60] A. Abada and M. Lucente, Nucl. Phys. B **885** (2014), 651-678 [arXiv:1401.1507 [hep-ph]].
- [61] E. Arganda, M. J. Herrero, X. Marcano and C. Weiland, Phys. Rev. D **91** (2015) no.1, 015001 [arXiv:1405.4300 [hep-ph]].
- [62] A. Abada, V. De Romeri and A. M. Teixeira, JHEP **09** (2014), 074 [arXiv:1406.6978 [hep-ph]].
- [63] A. Abada, M. E. Krauss, W. Porod, F. Staub, A. Vicente and C. Weiland, JHEP **11** (2014), 048 [arXiv:1408.0138 [hep-ph]].
- [64] A. Abada, V. De Romeri, S. Monteil, J. Orloff and A. M. Teixeira, JHEP **04** (2015), 051 [arXiv:1412.6322 [hep-ph]].
- [65] E. Arganda, M. J. Herrero, X. Marcano and C. Weiland, Phys. Rev. D **93** (2016) no.5, 055010 [arXiv:1508.04623 [hep-ph]].
- [66] A. Abada, V. De Romeri and A. M. Teixeira, JHEP **02** (2016), 083 [arXiv:1510.06657 [hep-ph]].
- [67] V. De Romeri, M. J. Herrero, X. Marcano and F. Scarella, Phys. Rev. D **95** (2017) no.7, 075028 [arXiv:1607.05257 [hep-ph]].
- [68] S. Antusch, E. Cazzato and O. Fischer, Int. J. Mod. Phys. A **32** (2017) no.14, 1750078 [arXiv:1612.02728 [hep-ph]].
- [69] A. Abada and T. Toma, arXiv:2405.01648 [hep-ph].
- [70] R. Alonso, M. Dhen, M. B. Gavela and T. Hambye, JHEP **01** (2013), 118 [arXiv:1209.2679 [hep-ph]].
- [71] A. Ilakovac and A. Pilaftsis, Nucl. Phys. B **437** (1995), 491 [arXiv:hep-ph/9403398 [hep-ph]].
- [72] A. Abada, D. Das, A. Vicente and C. Weiland, JHEP **09** (2012), 015 [arXiv:1206.6497 [hep-ph]].
- [73] M. Hirsch, F. Staub and A. Vicente, Phys. Rev. D **85** (2012), 113013 [erratum: Phys. Rev. D **91** (2015) no.5, 059902], [arXiv:1202.1825 [hep-ph]].
- [74] R. Kitano, M. Koike and Y. Okada, Phys. Rev. D **66** (2002), 096002 [erratum: Phys. Rev. D **76** (2007), 059902], [arXiv:hep-ph/0203110 [hep-ph]].

- [75] A. Abdesselam *et al.* [Belle], JHEP **10** (2021), 19 [arXiv:2103.12994 [hep-ex]].
- [76] P. A. Zyla *et al.* [Particle Data Group], PTEP **2020** (2020) no.8, 083C01.
- [77] I. Adachi *et al.* [Belle-II], arXiv:2405.07386 [hep-ex].
- [78] S. Banerjee, V. Cirigliano, M. Dam, A. Deshpande, L. Fiorini, K. Fuyuto, C. Gal, T. Husek, E. Mereghetti and K. Monsálvez-Pozo, *et al.* [arXiv:2203.14919 [hep-ph]].